Doctoral Thesis

Molecular pathogenesis underlying muscle wasting and development of diagnosis tool for kidney disease in mice.

TOLULOPE PETER SALIU

Graduate School of Integrated Sciences for Life

Hiroshima University

September 2022

ACKNOWLEDGEMENTS

The ones we have established are due to the fact that we are alive to study, otherwise what would I have studied if I am dead. Shouldn't all praise go to the giver of life? To Jehovah is the glory!

My PhD journey that ends with this thesis is full of many characters. These characters, to whom I will forever be grateful have contributed immensely to developing and strengthening many aspect of my scientific growth and character.

I sincerely thank Prof. Noriyuki Yanaka for his encouragement, guidance, and support all throughout the course of this research work. Words can hardly express how grateful I am. Sir, under your tutelage my potential to leave up to my dream as a frontline researcher have been refined. Thank you for trusting me and granting me enough freedom to explore my way through the PhD candidature with sufficient guidance. Thank you for being a great mentor, lifestyle disease complication guru, and friend all wrapped in one. You are an inspiration to me, and I am incredibly favoured to have had you as a supervisor.

I am grateful to all my co-supervisors Dr. Thanutchaporn Kumrungsee, Prof. Hiroyuki Horiuchi and Prof. Taketo Obitsu for their kind effort and constructive comments during the preparation of my doctoral dissertation. A special thanks to Dr. Thanutchaporn Kumrungsee for your innovative suggestions and unconditional sharing of your immense knowledge and skills. Your enthusiasm and wisdom are inspirational.

To all the Molecular Nutrition Lab members both present and past, especially Hashimoto, Yazawa, Miyata, Amal, Hu, Chen, Key it has been my pleasure to work with you all. You all have made the life in the laboratory easier and more enjoyable. Thank you for your friendship.

I am glad to express sincere gratitude to the amazing Graduate School of Integrated Sciences for Life student support staff, especially Himiko Koi for her diligence and support during my study.

To my dear friends, especially Dr. Adesina Adedayo and Dr. Adetunji Adedeji thank you for all the support and tolerance through all these years, I am indeed grateful.

My warmest gratitude goes to my parents Late Mr Oseni Saliu of blessed memory and Mrs Modupe Saliu. Thank you for teaching me and guiding me into who I am today. I could not have asked for more. To my siblings, Damilola, Oluwafemi and Gbenga I so much appreciate your supports, prayers, help and love.

To my wife, Blessing, you are the endless love, undying optimism, and the best friend in my life. Thank you for your patient, and encouragement during stressful time. I specially thank you for making me the best version of myself.

Most importantly, I will forever be grateful to Japan Government for giving me this golden opportunity to be here *ab initio.* I must sincerely say all these intellectual growth and research exploits would not have been possible if not for the MEXT scholarship.

Abbreviations

ADAMs	A disintegrin and metalloproteinases
AIF	Apoptosis-inducing factor
ALS	Autophagy/lysosome system
BUN	Blood urea nitrogen
CDD	Choline-deficient diet
CSA	Cross sectional area
CTX	Cardiotoxin
DAPI	4,6-diamidino-2-phenylindole
DAVID	Database for annotation, visualization, and integrated discovery
DKD	Diabetes kidney disease
DM	Diabetes mellitus
DMEM	Dulbecco's modified eagle medium
DN	Diabetic nephropathy
DSHB	Developmental studies hybridoma bank
ECM	Extracellular matrix
EDL	Extensor digitorum longus
FAO	Fatty acid oxidation
FAPs	Fibro-adipogenic progenitors
FFA	Free fatty acid
FITC	Fluorescein isothiocyanate
GAS	Gastrocnemius
GCs	Glucocorticoids
GR	Glucocorticoid receptor
H&E	Hematoxylin and eosin
HFD	High fat diet
IGF-1	Insulin-like growth factor-1
IR	Insulin resistant
LDHA	Lactate dehydrogenase A-subunit

Luc	Luciferase
miRNA	Micro RNA
MMPs	Matrix metalloproteinases
mTOR	Mammalian target of rapamycin
NAFLD	Non-alcoholic fatty liver disease
NASH	Non-alcoholic steatohepatitis
OCT	Optimum cutting temperature
OXPHOS	Oxidative phosphorylation
PBS	Phosphate-buffered saline
PVDF	Polyvinylidene difluoride
qPCR	Quantitative polymerase chain reaction
Quad	Quadriceps
RAGE	Receptor for advanced glycation end product
ROS	Reactive oxygen species
RT	Room temperature
Saa3	Serum amyloid A3
SC	Satellite cell
SE	Standard error
SOL	Soleus
STZ	Streptozotocin
TA	Tibialis anterior
UPS	Ubiquitin proteosome system
WISP1	WNT 1 inducible signaling pathway protein 1
WT	Wild type

Table of Contents

List of Tables

List of Figures

Chapter 1

General Introduction

1.0 Background

Skeletal muscle wasting also known as muscle atrophy is a devastating condition that increases both morbidity and mortality (Powers et al., 2016; Li et al., 2018; Ng et al., 2020). Unfortunately, muscle wasting happens to everyone with age. In fact, from the age of 35 years, approximately 0.4-1.0% of muscle mass is lost yearly (Mitchell et al., 2012). What is even more sobering is that chronic diseases (e.g diabetes, cancer, obesity renal failure, and cardiac failure etc.) which is most common among the elderly also contribute to loss of muscle mass which eventually lead to poor quality of life and worse survival (Yoshida. and Delafontaine, 2015; Ebner et al., 2015). As if that is not enough, muscle loss is also largely accelerated by inactivity (muscle disuse) (Howard et al., 2020). For instance, in older men about 5% muscle mass could be lost after 14 days of immobilization by bed rest (Suetta et al., 2009). Sport injury and accident is another frequently occurring event that could subject both young and old to immobilization of the joint, usually by a plaster cast or a brace (Howard et al., 2020). Depending on how severe the injury is, on average the recovery time for two-thirds of the sport injuries is within 7 days (Tranaeus et al., 2017; Swain et al., 2016). Such a short period of muscle disuse (≤7 days) has been shown to result in substantial decline in muscle mass (0.5-1.0% per day) (Dirks et al., 2014). Additionally, sedentary lifestyle which has even been made worse by current COVID-19 restrictions is another major factor that is silently fueling loss of muscle mass among all age group (Kirwan et al., 2020). As many people worldwide engage in sedentary lifestyles and as life expectancy increases, muscle wasting and his impact on quality and longevity of life is becoming a more and more important public health problem. Although, several studies have been done in the field of skeletal muscle biology, however, our current understanding of the molecular pathogenesis of muscle wasting is limited, no wonder there is currently no effective therapies to treat muscle wasting.

Two chronic metabolic disease state that have severely contribute to muscle wasting are non-alcoholic fatty liver disease (NAFLD) and diabetes mellitus (DM) (Rubio-Ruiz et al.,

2019; Nishikawa et al., 2021). Coincidentally, the prevalence of these diseases increases with ageing, sedentary lifestyle and chronic overnutrition. Unfortunately, there is currently no therapy that can completely normalize the metabolic alterations that characterized NAFLD and DM. Thus, in the absence of true cure, treating complications of these diseases remain the only source of hope.

Skeletal muscle wasting associated with NAFLD, and DM is a significant complication that could define the overall health status and survival of affected patients. This is because muscle atrophy can contribute to the progression of additional secondary complications such as chronic kidney disease, and cardiovascular disease (Mantovani et al., 2020; Targher et al., 2021; Ferguson and Finck, 2021; Mantovani et al., 2020). These additional complications in turn can also exacerbates muscle wasting. Importantly, several studies have shown that chronic kidney disease can repress muscle regeneration as well as induce muscle protein metabolism imbalance (Zhang et al., 2020; Sabatino et al., 2021). Thus, failure to detect and treat this complication at early stage may blunt any gains made in restoring muscle mass. Regrettably, unlike muscle atrophy, early detection of renal injury in both NAFLD and DM is difficult. No wonder most patient with NAFLD and DM do suffer from end stage renal failure which have no cure. With the alarming rate at which NAFLD and DM is increasing globally, a better understanding of the molecular pathogenesis underlying their complications (especially muscle atrophy and chronic kidney disease) as well as development of diagnostic tool to monitor these complications is greatly needed.

1.1. The objective of this study

The objective of this thesis is to (1) develop a relevant animal model that can be used to study muscle wasting associated with NAFLD and DM; (2) gain a better understanding of the molecular mechanisms involved in the pathogenesis of skeletal muscle atrophy in NAFLD and two different Streptozotocin- (STZ-) induced DM model, and (3) develop a novel diagnostic tool that can be used to detect diabetic nephropathy at early stage. This information will open up new avenues of investigation into the causes and treatment of NAFLD and DM

associated muscle wasting. At the same time allow researchers to longitudinally monitor disease or drug induced kidney injury in real time.

Chapter 2

Literature Review

Scientific interest in loss of skeletal muscle mass associated with aging and chronic metabolic diseases has gained a lot of attention during the last few decades. The considerable interest and research efforts have been seen in this field because loss of muscle mass has been associated with increased risk of both morbidity, mortality, and low quality of life. These research efforts have improved our understanding of skeletal muscle structure and function, in health and disease. This chapter reviews the most important discoveries in recent years, as well as the current challenges, open questions, and fierce debate within the field of muscle biology. The review begins with a brief overview of molecular mechanisms underlying muscle tissue development (myogenesis), with special focus on primary muscle stem cells (termed satellite cells) and muscle regeneration. Next, the general pathophysiological mechanisms governing loss of muscle mass were highlighted. Importantly, the relationship between skeletal muscle mass and metabolic diseases, including non-alcoholic fatty liver disease (NAFLD) and diabetes mellitus (DM) were described. Finally, the impact of other secondary complications associated with NAFLD and DM on muscle atrophy was emphasized.

2.0 Basic Function and Structure of Skeletal Muscle

Skeletal muscle is the most dynamic and adaptive tissues of the human body. Typically, skeletal muscle account for more than 40% total body weight (Kim et al., 2002). Muscle composed primarily of water (75 %), protein (20 %), and other substances such as inorganic salts, minerals, fat, and carbohydrates (5 %) (Frontera and Ochala, 2015). The primary function of skeletal muscle is to convert chemical energy into mechanical energy to generate force and power (Frontera and Ochala, 2015). The generated force is used to maintain an upright body posture, and to produce movement that influences activity, functional independence, and overall wellbeing (Foldvari et al., 2000; Frontera and Ochala, 2015; Santos et al., 2017). Furthermore, skeletal muscles also play significant roles in several other physiological processes, including breathing (Gransee et al., 2012), metabolism

(Baskin et al., 2015), thermogenesis (Rowland et al., 2015), and the secretion of numerous myokines which allow for communication between muscle and other organs as well as communication within muscle itself (Severinsen and Pedersen, 2020). Skeletal muscles are attached to bones throughout the body via tendons (a tough bands of connective tissues). This attachments ensured proper positioning of bones and their movement through voluntary contraction (VanDusen Larkin, 2015).

Skeletal muscle has a unique architecture design that is characterized by bundles of elongated, cylindrical, multinucleated myofibers (also termed fascicles) arranged in a striated pattern (Fig 1A and B) (Frontera and Ochala, 2015). The myofibers are covered by a layer of connective tissue called the endomysium, and they are surrounded by several types of interstitial cells including macrophages, pericytes, fibroblasts, and fibro-adipogenic progenitors (FAPs) (Figure 1A). In between the endomysium and the plasma membrane of the myofibers are important group of called primary muscle stem cells or satellite cells (Figure 1A and C) (Jorgenson et al., 2020). A single muscle fiber (which is typically 100 μm in diameter and 1 cm in length) is surrounded by a plasma membrane (also termed sarcolemma). The gelatinous material that resides underneath the sarcolemma is called sarcoplasm. Approximately 80% of the sarcoplasm is made up of complex rod-like structure called myofibrils (Seiden,1976; Toth et al., 2012; Jorgenson et al., 2020). Basically, the myofibrils are composed of a long in-series array of force-generating elements called sarcomeres. These sarcomeres are connected by a dense protein material, called the Z-Disc and they are surrounded by sarcoplasmic reticulum. The main function the sarcoplasmic reticulum is to store calcium ions (Ca^{2+}) which are required for contraction. The sarcomeres within the myofibrils elicit their function via the active sliding of thin (actin and associated proteins) and thick (myosin and associated proteins) myofilaments. Alteration of any of these proteins can result in loss of muscle mass and other severe consequences. For instance, partial or complete loss of the protein dystrophin could lead to neuromuscular disorders such as Duchenne and Becker muscular dystrophies (Frontera and Ochala, 2015).

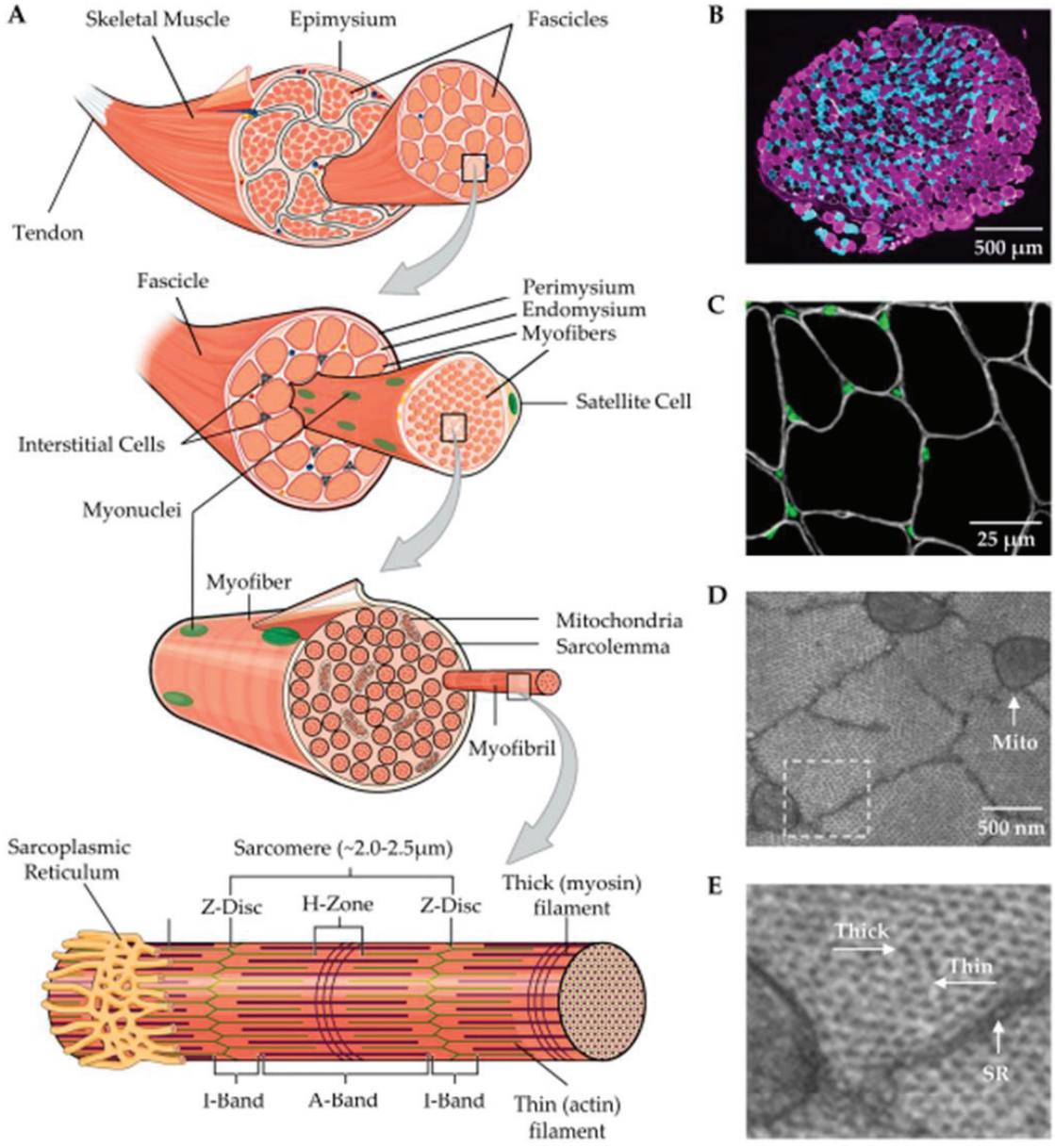

Figure 1. Basic structure of skeletal muscle (Source: Jorgenson et al., 2020)

All myofibers are not created equal, for example some myofibers heavily relied on oxidative metabolism which enable them to exhibit a slow contractile speed (i.e., generate suboptimal force) and are resistant to fatigue. Meanwhile, other myofibers relied on anaerobic glycolytic metabolism, which enables them to exhibit a fast contractile speed (i.e., generate near optimal

force) and fatigue quickly when stimulated to contract (Billeter and Hoppeler, 1992). Skeletal muscle fiber can be grouped into different isoforms base on the myosin heavy chain that they expressed these include Type I (slow oxidative), Type IIA (fast oxidative), and Type IIB (fast glycolytic) fibers (Jorgenson et al., 2020). However, it is important to note that humans do not express the Type IIB myosin isoform, but rather express a very similar (yet slightly slower) Type IIX myosin isoform. Since this differentiation was only established in 1990′s (Hilber et al., 1999; Smerdu et al., 1994; Ennion et al., 1995), it is essential to keep in mind that some older studies with human subjects used Type IIB classification.

2.1. Satellite Cells and Muscle Regeneration

Skeletal muscle has s a robust regenerative capacity, in response to traumatic injury. This process is significantly governed by resident muscle stem cells, also called “satellite cells” (SCs) due to their unique anatomical position between the sarcolemma and the basal lamina of the myofibers (Scharner & Zammit, 2011; Relaix and Zammit, 2012). Satellite cells typically exist in a quiescent (inactive) state in healthy adult muscle but may become activated in response to stimulation, such as muscle damage. Upon activation, SCs will migrate to damage site and undergo extensive proliferation. Majority of SCs progeny termed myoblasts undergo myogenic differentiation to produce new myonuclei to support muscle repair, and if the damage is extensive the myoblast may undergo differentiation and fusion to generate new muscle fiber (Ono et al., 2015). Meanwhile the remaining activated SCs will return to quiescent state to self-renew and replenish the stem cell pool for future needs (Ono et al., 2015; Relaix et al., 2021) (Figure 2). Several transcription factors have been identified as key regulators of SCs activation, expansion, differentiation/fusion as well as return of SCs to the quiescent state during skeletal muscle regeneration (Relaix et al., 2021). Among them, the paired box transcription factor Pax7 and Pax3 as well as myogenic regulatory factors (MRFs: MyoD, Myf5, Myogenin, and MRF4) stands out for the critical role they play in muscle growth, specification, homeostasis, and regeneration (Relaix and Zammit, 2012; Relaix et al., 2021).

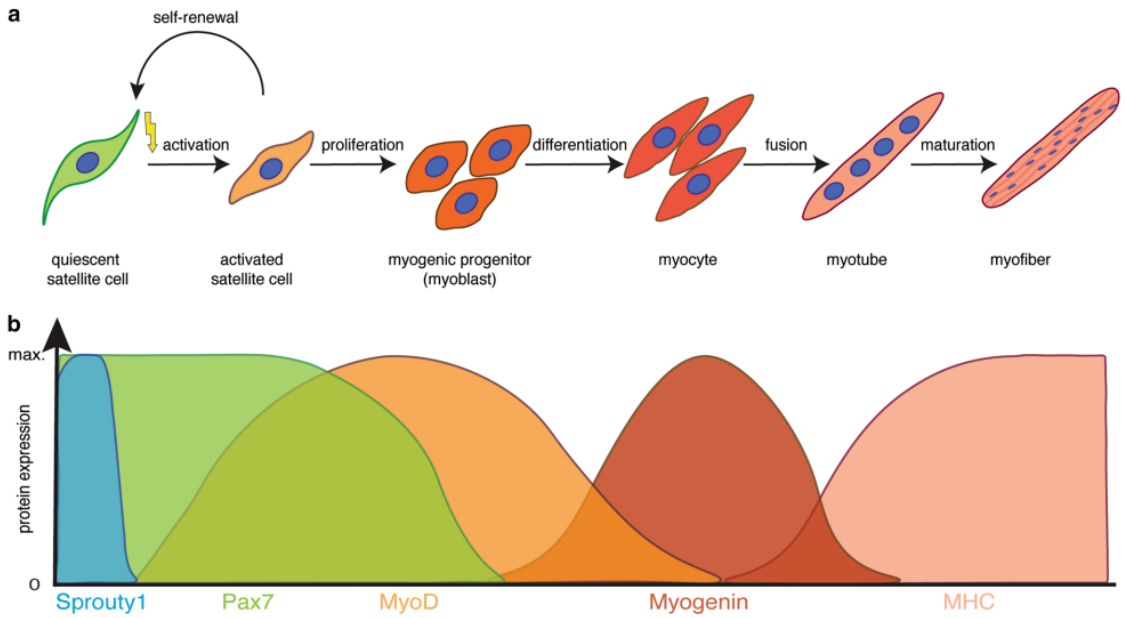

Figure 2. Satellite cell myogenic lineage progression and expression profile of key transcriptional factor regulating the process (Source: Schmidt et al., 2019)

PAX7 is expressed in all muscle SCs no wonder it is commonly used as a marker of SCs. Pax7 is essential for postnatal maintenance and repair of skeletal muscle (Schmidt et al., 2019). Upon activation, the MRFs are rapidly induced in almost all SCs (Zammit et al., 2002). The MRFs is required to regulate SCs progression towards myogenic specification, differentiation, and fusion to form mature multinucleated myofibers (Relaix et al., 2021).

Earlier study in the area of SC behavior indicated that the tight balance between quiescence and activated state of SC plays a critical role in SC renewal. This tightly controlled event was initially taught to be regulated solely by changes in transcriptional factors. For instance, the co-expression of Pax7 and MyoD is a marker of SC proliferation. Immediately after proliferation most of the cells retain MyoD expression but downregulate Pax7 expression. This event triggers the commitment of SCs to differentiate into myocytes via activation of myogenin (Relaix and Zammit, 2012). Meanwhile, other myoblast maintains Pax7 expression but downregulate MyoD expression, this eventually leads to their withdrawal from cell cycle, thereby regaining markers that characterized quiescence state

(Day et al., 2007; Relaix and Zammit, 2012). Moreover, recent studies have indicated that the molecular cues regulating the tight balance between quiescence and activated state of SC goes beyond transcriptional factors. Other factors such as metabolic status and SC niche plays a critical role in determining SC fate (Relaix et al., 2021).

a) Regulation of SC behavior by metabolic status

The metabolic flexibility (i.e., ability to efficiently adapt and use whatever fuel or substrate available to it) of SC has been shown to induce genetic reprogramming that could regulate SC fate. At quiescent state SCs depend solely on fatty acid oxidation (FAO) and oxidative phosphorylation (OXPHOS). This dependence on FAO help increases NAD+ levels which in turn induce SIRT1-dependent deacetylation of its target histone H4 lysine 16. This epigenetic modification preserves SCs in quiescence state by repressing myogenic transcription signals (Figure 3) (Ryall et al., 2015). This is further substantiated through the use of FAO inducers (such as caloric restriction) or elevation of NAD+. Increasing NAD+ levels in aged mice enhances SC quiescence and muscle regenerative potential (Zhang et al., 20-16). Furthermore, the dependence of SC in quiescent state on FAO and downregulation of glycolytic pathway favors the reduction of acetyl-CoA, which in turn prevent histone acetylation that is associated with myogenic program (Wellen et al., 2009). However, since SCs isolation promote the exit of quiescence, the characterization of quiescent SC metabolism in situ remains to be investigated due to lack of technology to isolate SC without activating it. Proliferating SCs on the other hand is associated with a shift toward anaerobic glycolysis. Resent work by Theret et al., (2017) showed that anaerobic glycolytic inhibition decreases SC proliferation and self-renewal, while the induction of anaerobic glycolytic via overexpression of lactate dehydrogenase A- subunit (LDHA) enhanced SC expansion. This metabolic shift towards anaerobic glycolysis induces anabolism processes that support SC growth and proliferation. As for the differentiating SCs, they depend mostly on OXPHOS. This shift towards OXPHOS triggers a burst of ROS that act as secondary messengers to strengthen differentiation. Notably, the sharp outburst of ROS is compensated by elevation in the expression of antioxidant genes (such as PITX2 and PITX3). The deletion of these

antioxidant genes has been shown to induce premature differentiation and impair muscle regeneration capacity (Relaix et al., 2021).

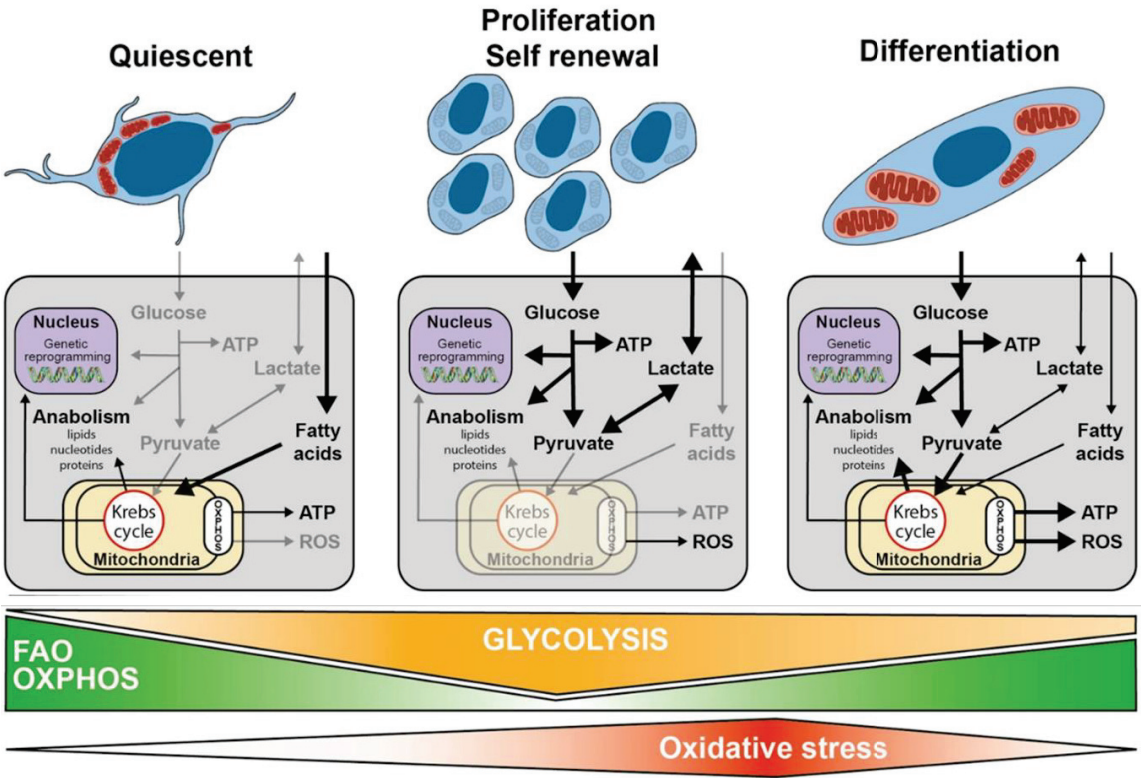

Figure 3. Interplay between metabolic status and SC fate during myogenesis (Source: Relaix et al., 2021).

b) *Regulation of SC behavior by SC niche*

SC are surrounded by a variety of cell types such as endothelial cells, macrophages, fibro adipogenic progenitors (FAPs), pericytes (Mashinchian et al., 2018) and a complex mesh of extracellular matrix (ECM) proteins. The molecular cue generated by these surrounding cells along with the dynamic network of proteins in the ECM plays a critical role in guiding muscle SC behavior, homeostasis, and regeneration. For instance, Baghdadi and colleagues recently demonstrated that culturing Collagen V with SC impaired SC differentiation and SC-specific deletion of Collagen Vα1, resulted in rapid depletion of SC pool (Figure 4) (Baghdadi et al.,

2018). ECM proteins are not only responsible for pro-quiescence maintenance of SC, other ECM proteins such as laminin α1 and laminin α5 were also recently found to be involve in SC activation and differentiation (Rayagiri et al., 2018).

The myofiber itself can serve as another source of molecular signal regulating SC behavior. This molecular interaction is mediated in part by NOTCH. Elegant work by Low and colleagues demonstrated that NOTCH1 and NOTCH3 were found in SCs, while their ligands DLL1 and DLL4 are mainly localized to the myofibers (Figure 4) (Low et al., 2018). This suggests that the interaction between NOTCH ligands and their receptors contributes to maintenance SC quiescent state, and prevention of SC activation and differentiation in an uninjured muscle. Cells in SC niche are also known to interact with SCs and regulate their quiescence and activation via a number of membrane-bound (exosomes) and secreted factors. Du and coworkers recently showed that macrophages support SC activation through the secretion of a metalloproteinase called ADAMTS1 (Du et al., 2017). Adamts1 elicit is activating effect by suppressing the expression of the quiescence regulator NOTCH1 in SCs. In addition, macrophage secreted GDF3 and WNT1 Inducible Signaling Pathway Protein 1 (WISP1) secreted from FAPs are essential factors that stimulate SC differentiation and myoblast fusion (Figure 4) (Varga et al., 2016; Lukjanenko et al., 2019). Although only little is still known about the dynamic signals contained in the exosome release by cells of SC niche and SC itself. The current dissection of this signals at single-cell level using scRNA-seq and mass cytometry will improve our understanding of how SC niche regulate SC fate (De Micheli et al., 2020; Petrilli, et al., 2020).

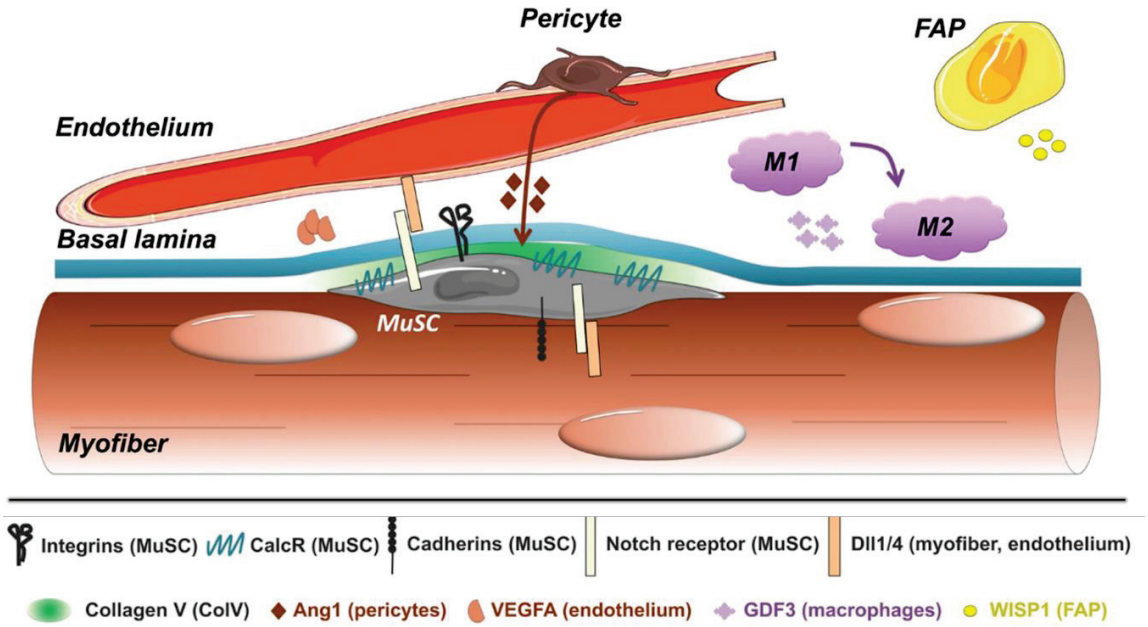

Figure 4. SC microenvironment provides molecular cue that regulate and SC fate (Source: Relaix et al., 2021).

2.2. Muscle wasting and their molecular mechanism

Skeletal muscle wasting also known as muscle atrophy is defined as a decrease in muscle mass due to malnutrition, lack of use (muscle disuse), aging, injury, and several chronic diseases (Ebert et al., 2019; McKinnell and Rudnicki, 2004). The etiology of muscle atrophy is diverse as clearly indicated in the definition above. Muscle atrophy that results from muscle disuse is generally refer to as acute atrophy, such atrophy is generally reversible following exercise. Muscle wasting in aging otherwise known as sarcopenia is a chronic atrophy because it involves a slow and progressive loss of muscle mass without any underlying disease (McKinnell and Rudnicki, 2004; Wood et al., 2021). Cachexia is defined as: "a multifactorial syndrome resulting from chronic diseases (such as renal and cardiac failure, sepsis, diabetes, AIDS, cancer) and characterized by an ongoing loss of muscle mass (with or without loss of fat mass) which cannot be fully reversed by conventional nutritional aids (Ebner et al., 2015; Wood et al., 2021). Since loss of muscle mass is a common endpoint of

diverse atrophic conditions one would expect that molecular cues triggering muscle atrophy in all conditions are similar. Unfortunately, that is not the case, in fact different atrophic condition has distinct pathways that triggers the atrophic process. Although, much is still not known regarding the molecular mechanism governing muscle atrophy, however, some important facts have been established and will be briefly discussed in the following sections.

2.2.1. Abnormal muscle protein metabolism

The accelerated degradation of both myofibrils (which constitute more than 70% of muscle proteins) and soluble proteins together with decrease in protein synthesis is the fundamental cause of muscle wasting, weakness, and physical disability (Cohen et al., 2015). The two major proteolytic systems that are implicated in protein degradation are the ubiquitin-proteosome system (UPS) and autophagy/lysosome system (ALS) (Bonaldo and Sandri, 2013). Meanwhile, downregulation of insulin-like growth factor-1(IGF-1)-Akt-Mammalian Target of Rapamycin (mTOR) signaling pathway is primarily responsible for decrease in protein synthesis in atrophic muscle (Bodine et al., 2001; Rommel et al., 2001). Notably, the IGF-1/Akt/mTOR Signaling Pathway also plays a critical role in regulating the activation of the UPS and the ALS at the transcriptional level a process mediated by inhibition of the forkhead box protein O (FoxO) family transcription factors (Stitt et al., 2004; Mammucari et al., 2007; Zhao, J., et al., 2007). Therefore, the increase in protein breakdown and decrease in protein synthesis seen in wasting muscles cannot be viewed as independent events; rather they are series of coordinated and interlinked adaptations that eventually result in rapid loss of skeletal muscle mass. It is important to note that the two proteolytic machineries (UPS and the ALS) play an important regulatory role in removing un-wanted or defective proteins and maintaining homeostasis in healthy skeletal muscle (Cohen., et al., 2015). Although, we do not fully understand how the UPS recognizes misfolded or defective proteins, however, what is clear is that this regulatory mechanisms are disrupted in muscle atrophy, thereby resulting in accelerated protein catabolism which affect all muscle cell components (Lecker et al., 2006; Bonaldo and Sandri, 2013; Kitajima et al., 2020). Signaling pathways that control the activity of proteolytic machineries as well as orchestrate the downregulation of the protein

synthesis pathway (IGF-1/PI3K/Akt/mTOR Signaling Pathway) in atrophic muscle are continuously emerging. This section will unravel some of such signaling events.

1. The ubiquitin-proteosome system

The UPS is responsible for the breakdown of most muscle sarcomeric proteins, (Cohen et al., 2012) and the induction of this pathway is regulated by the FoxO family transcription factors (Accili and Arden, 2004.). FOXO induced UPS-mediated protein degradation through the induction of muscle-specific E3-ubiquitin ligases, such as Atrogin1/MAFbx and MuRF1/Trim63 (Sandri et al., 2004; Waddell et al., 2008). During atrophy, FOXO-induced E3-ubiquitin ligase MURF1/Trim63 catalyses the degradation of Myosin Heavy Chains, Myosin Light Chain-1/2 (Foletta et al., 2011). Another TRIM protein, known as TRIM32, catalyses the ubiquitylation and degradation of actin, desmin, tropomyosin and other myofibrillar apparatus (Cohen et al., 2012). Whereas Atrogin-1/MAFbx. catalyses the degradation of MyoD, myogenin as well as proteins (such as elongation initiation factor 3 subunit f (eIF3-f)) that promote protein synthesis (Figure 5) (Foletta et al., 2011). Pharmacological strategy to specifically inhibit MuRF1/Trim63 have been pursued, however, this approach fails to prevent atrophy because actin, desmin, tropomyosin and other components of the thin filaments and the cytoskeletal network will still be targeted for degradation by TRIM32. Unlike MuRF1/Trim63 which is muscle specific, TRIM32 is found in almost all cell types. The ubiquitous nature of TRIM32 makes its delicate to target for inhibition. In fact, loss of TRIM32 in mice have been shown to results in considerable neurological defects and myopathy (Kudryashova et al., 2009).

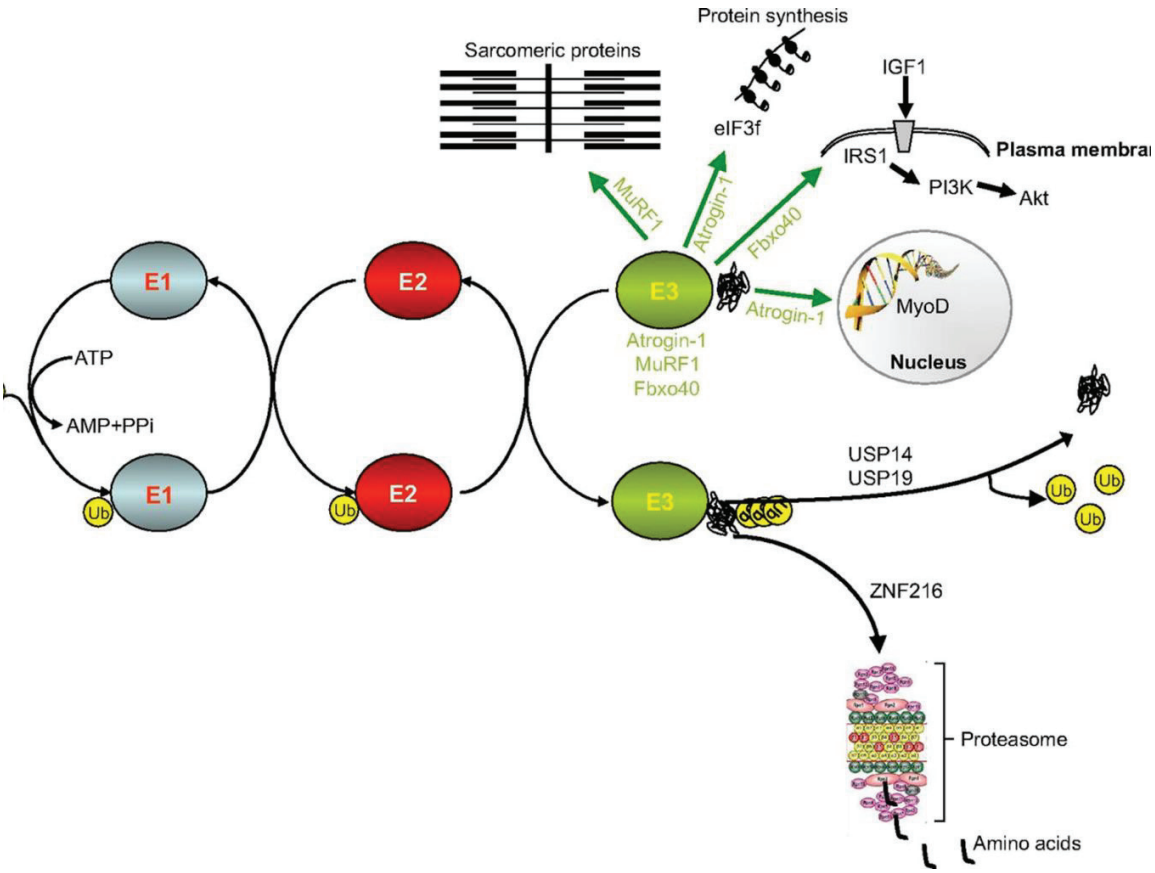

Figure 5. Signals regulating ubiquitin-proteasome systems in muscle atrophy (Source: Bonaldo and Sandri, 2013)

2. *The* autophagy/lysosome system

Under normal condition, autophagy/lysosome system (ALS) plays a critical role in energy generation/consumption and macromolecule turnover events in skeletal muscles (Xia et al., 2012). However, deregulation of this process in muscle promotes ALS-mediated proteolytic degradation of mitochondria (and other cell organelles), no wonder atrophied muscle have decreased endurance capacity (Sandri, 2013; Cohen et al., 2015; Bonaldo and Sandri, 2013). Similar to UPS, transcription factor Forkhead box O3a (FoxO3a) mediate the induction of ALS by activating the transcription of autophagy genes *ATG4, ATG8B, ATG12, LC3, BECLIN1, BNIP3, VPS34, ULK1*, and *ULK2* in skeletal muscle (Mammucari et al., 2007; Zhao et al., 2007; Sanchez et al., 2012; Di Malta et al., 2019). Hyperactivation of FoxO transcription factors have been found to contribute to muscle loss in diverse pathological

conditions, including cancer cachexia, sepsis, diabetes mellitus, chronic kidney disease, critical illness, cirrhosis, among others (Sartori et al., 2021; Oyabu et al., 2022). Given the central role of FoxO transcription factors in mediating both UPS an ALS related proteolysis, it is essential to develop therapeutic strategies that can fine-tuned FoxO activity in other to avoid accelerated muscle protein degradation.

3. IGF-1/PI3K/Akt/mTOR Signaling Pathway

The IGF-1/PI3K/Akt/mTOR Signaling pathway exerts its effect on muscle protein balance by regulating both protein synthesis and degradation pathways (Figure 6) (Cohen., et al., 2015). This signaling cascade stimulate protein synthesis primarily through upregulation of mTOR kinase and inhibition of FoxO family transcription factors. AKT block FoxO activity by phosphorylating FoxO proteins (FoxO1, FoxO3, FoxO4) in the nucleus. The phosphorylation FoxO members results in their export from the nucleus to the cytoplasm (Manning and Cantley, 2007). Several in vivo studies in mice have shown that overproduction of IGF1 or AKT in muscles, promotes muscle hypertrophy and reduce loss of muscle mass (Sacheck et al., 2004; Lai et al., 2004; Bodine et al., 2001). Conversely, downregulation of IGF-1/PI3K/Akt/mTOR signaling pathway which occur in catabolic diseases increases the activation of FoxO family transcription factors which eventually suppress protein synthesis as well as induce muscle protein degradation (Manning and Cantley, 2007). Attenuation of Akt pathway by models of muscle atrophy, elevate nuclear translocation and activity of FoxO members which are required for the upregulation of atrophy-related ubiquitin ligases MuRF1/Trim63 and atrogin-1/MAFbx (Figure 6) (Manning and Cantley, 2007; Sartori et al., 2021). Additionally, activation of FoxO transcription factors also promote protein breakdown by increasing the transcription of autophagy related genes such as LC3 and Bnip3 (Mammucari et al., 2007; Sartori et al., 2021).These findings clearly suggest that activation of AKT kinases could be a valuable strategy to combat muscle wasting. However, such treatments could be dangerous — for example, constant activation of IGF-1/PI3K/Akt/mTOR Signaling cascade have been shown to reduce FOXO activity cancer associated cachexia, but

regrettably, they also have the potential to promote tumour growth (Cohen., et al., 2015; Dong., et al., 2021).

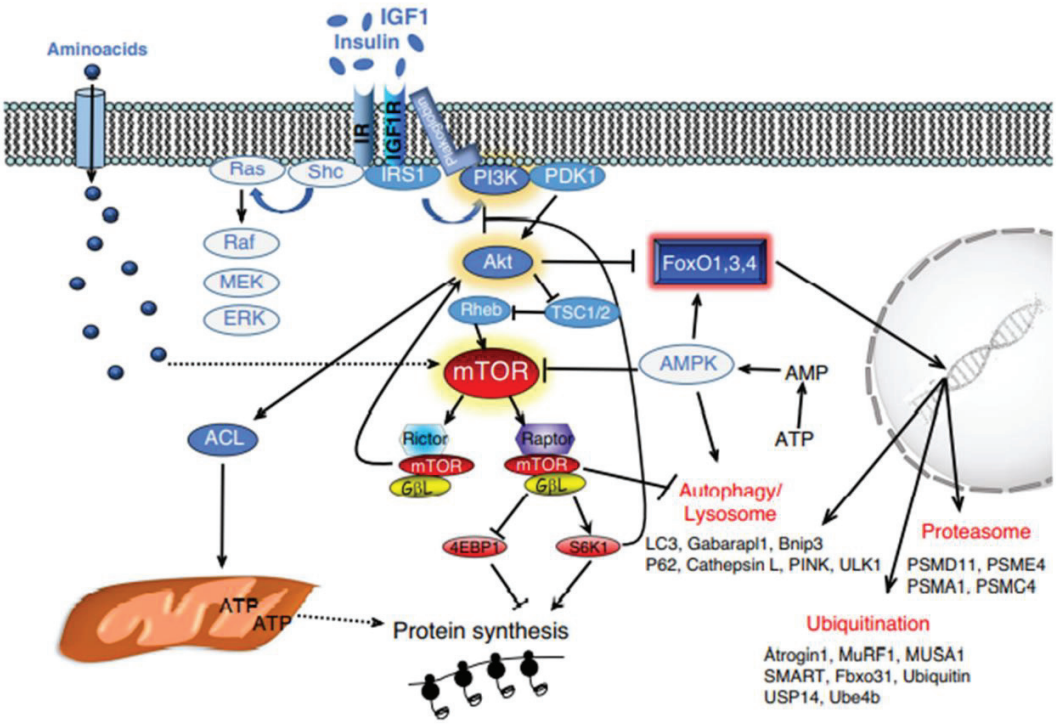

Figure 6. IGF-1/PI3K/Akt/mTOR Signaling pathway (Source: Sartori et al., 2021)

2.2.2. Mitochondrial dysfunction

Defective mitochondrial function has been shown to trigger skeletal muscle wasting via at least three different pathways: (1) increased mitochondrial reactive oxygen species (ROS) production (2) mitochondrial release of proapoptotic factors; and/or (3) low ATP production resulting from mitochondrial damage (Figure 7) (Hyatt and Powers, 2021; Powers et al., 2012).

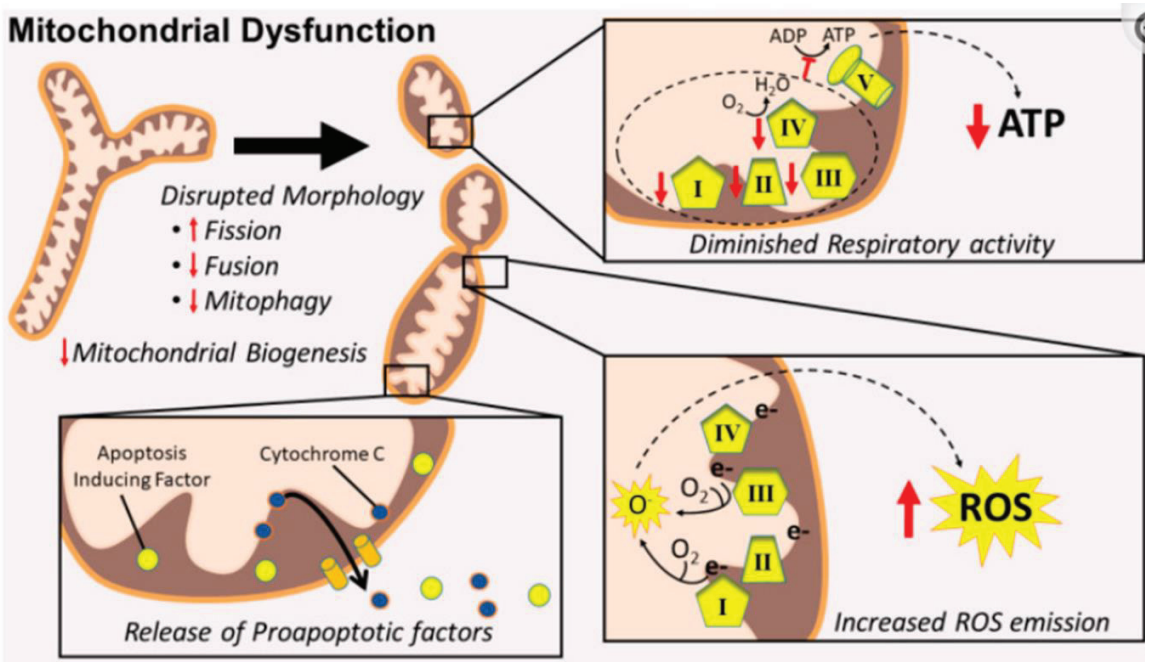

Figure 7. Three major way mitochondrial dysfunction contribute to muscle wasting (Source: Hyatt and Powers, 2021)

1) Increased mitochondrial ROS production.

Several preclinical studies have demonstrated that increases in mitochondria ROS production promote muscle wasting in several conditions including aging, chronic diseases, and prolonged muscle disuse (Hyatt et al., 2019; Hyatt and Powers, 2021; Powers et al., 2012; Shally and McDonagh, 2020; Smuder et al., 2020). Chronic increase in mitochondrial ROS production can induce muscle wasting by suppressing muscle protein synthesis and accelerating muscle protein degradation (Hyatt and Powers, 2021; Powers et al., 2012). Oxidative stress accelerates muscle protein degradation via three independent pathways including, induction of genes responsible for protein degradation especially the key ubiquitin E3ligases (Li et al., 2003), elevation of cytosolic calcium which in turn activate both calpain and caspase-3 (Hyatt and Powers, 2020; Hyatt et al., 2021), and finally increase muscle protein oxidation thereby predisposing such protein to enzymatic hydrolysis (Grune et al.,

1997). On the other hand, redox imbalance represses protein synthesis at translational level by inhibiting Akt/mTOR signaling pathway (Powers et al., 2011).

2) Mitochondrial release of proapoptotic factors.

Mitochondrial damage by oxidative stress and elevated cytosolic calcium level can result in the release of proapoptotic factors such cytochrome c and apoptosis-inducing factor (AIF) (Bloemberg and Quadrilatero, 2019). The release of cytochrome *c* from the mitochondria mediate muscle wasting by activating caspase-3 that subsequently stimulate muscle protein degradation. On the other hand, the released cytochrome c can also induce myonuclei apoptosis (Smuder et al., 2010; Bloemberg and Quadrilatero, 2019). Theoretically, the depletion of myonuclei within skeletal muscle fibers may contribute to the suppression of protein synthesis by reducing the transcriptional capacity of muscle fibers (Powers et al., 2012).

3) Mitochondrial damage result in low ATP production.

Low ATP production resulting from mitochondrial damage have been shown to contribute to muscle wasting by suppressing muscle protein synthesis and accelerating muscle protein degradation (Hyatt and Powers, 2021). Since energy is required for any anabolic process in this case protein synthesis therefore any alteration in energy level in muscle would no doubt impact muscle protein synthesis negatively. Additionally, depletion of muscle energy level can directly or indirectly induce protein degradation via the AMP-kinase activity (Thomson, 2018). Specifically, AMPK is a crucial cellular energy sensor, and once activated, AMPK promote FoxO3 action independently of Akt (Greer et al., 2007). The activation of the transcriptional activating factor FoxO3, upregulate the expression of both UPS an ALS related proteolytic genes such as atrogin-1, MuRF-1, LC3, and Bnip3 which in turn accelerate muscle protein degradation (Romanello and Sandri, 2010; Romanello et al., 2010).

2.2.3. Impairment of satellite cell activity

As described earlier, the remarkable regenerative potential of muscle depends absolutely on small population of muscle cells called satellite cells (SCs). Decrease in SC number and function have been shown to diminish the regenerative capacity of skeletal muscle in both humans and mice (Joseph and Doles, 2021; Relaix et al., 2021). Mechanistically, the process underlying SC dysfunction in muscle atrophy is diverse and new concept is constantly emerging. Although, our knowledge is still limited, however, here are some fact that have been established. For example, deregulation of SC self-renewal pathways has been shown to impaired SC function in both aging and disease state. One of such pathways is Notch signaling pathway. Downregulation of Notch signaling activities in SCs favors rapid myogenic differentiation, without an intervening phase of cell division (Bjornson et al., 2012; Mourikis et al., 2012). This loss of self-renewing ability of SC, result in the depletion of SC pool which ultimately affect muscle regeneration (Fukada et al., 2011).

Cellular senescence, a state of irreversible cell cycle arrest, is another mechanism that often contribute to impairment of SC (Jejurikar and Kuzon, 2003; Saito and Chikenji, 2021). Although this mechanism does not seem relevant to sarcopenia because SC isolated from aged muscle retain their proliferative potential (Renault et al. 2000). However, senescence of muscle SC often impairs muscle regeneration in chronic disease state (Saito and Chikenji, 2021).

Furthermore, age-induced impairment of SC number and activity have also been associated to changes in SC environment (Conboy et al. 2005; Cosgrove et al., 2014; Bernet et al., 2014). This changes disrupt quiescence and subsequent myogenic progression of SC which eventually alters SC maintenance and muscle regenerative capacity (Bentzinger et al., 2013; Sousa-Victor et al., 2014). Interestingly, several reports have shown that exposure of old SC to young systemic environment is capable of restoring the regenerative capacity of aged muscle (Conboy et al. 2005; Cosgrove et al., 2014; Bernet et al., 2014). Circulating factors such as oxidative stress, hormone, inflammatory cytokine and exosome containing non-coding RNA, including microRNAs (miRNAs) are key molecular cues that differentiate old systemic environment from that of the young (Collins et al., 2019; Szentesi et al., 2019;

Papanikolaou et al., 2019; Fochi et al., 2020). The signaling pathways that these circulating agents' triggers is what contribute to SC apoptosis and overall muscle degeneration. Similarly chronic disease also deteriorates muscle SC niche. In fact, evidence suggest that changes in the circulatory factors in SC environment during chronic disease can contribute to decrease in SC pool as well as alters their fate (Bentzinger et al., 2013).

2.2.4. Extracellular matrix remodelling

The ECM is the non-cellular three-dimensional network of macromolecules such as collagen, elastin, proteoglycan, and glycoproteins that not only provides mechanical support for muscle fibers, nerves and blood vessels but also initiates essential biochemical and biophysical dialogue with other cellular components including epithelial cells, fibroblast, myoblast, and or macrophages (Csapo et al., 2020). Although little is known about the role of ECM structure on muscle growth and development. However, recent study has shown that structural modification of ECM (i.e., degradation or thickening) also termed ECM remodeling could influence critical events that control muscle SC proliferation and differentiation, which in turn can influence skeletal muscle health (Stearns-Reider et al., 2017; Zhang et al., 2021). For instance, study has shown that abnormal accumulation of ECM can inhibit SC myogenic differentiation ability during muscle regeneration (Lacraz et al., 2015). Research has also indicated that excessive accumulation of Type 1 collagen one of the protein components in ECM can significantly inhibit myogenic differentiation (Alexakis et al., 2007). Meanwhile, the depletion of Type I collagen could prevent myoblast proliferation and migration (Liu et al., 2020). ECM modification requires tight regulation in other to prevent over degradation or overproduction of ECM (Csapo et al., 2020). Several factors are responsible for aberrant ECM remodelling, for instance, upregulation of TGFβ has been shown to induce the translocation of the transcription factors complex SMAD2–SMAD3 into the nucleus, where it directly stimulates the expression of ECM genes such as *COL1A1, COL3A1* and *TIMP1* (Bonnans et al., 2014). On the other hand, overexpression of enzymes responsible for ECM degradation such as Matrix metalloproteinases (MMPs) and ADAMs (a disintegrin and metalloproteinases) can trigger excessive ECM degradation

(Bonnans et al., 2014). For example, upregulation of heart specific MMP1 have been reported to increase collagen degradation which eventually led to cardiomyopathy (Kim et al., 2000).

2.3. Animal models for studying skeletal muscle atrophy

Although muscle wasting is a common complication associated with several clinical conditions (such as diabetes, liver cirrhosis, cancer, cardiovascular disease, renal failure etc.) muscle disuse, and aging (Yoshida. and Delafontaine, 2015; Mitchell et al., 2012; Howard et al., 2020; Morley et al., 2006; Peng et al., 2007; Tan and Fearon, 2008). However, the molecular and biochemical process that promote this complication are distinct (Holecek, 2012). Thus, to understand the pathogenesis and develop an effective therapeutic strategies to treat muscle wasting, there is need to use clinically relevant model in muscle wasting studies. Interestingly, muscle wasting has been well characterized in different animal models by administering various mediators of muscle wasting (such as cytokine, ROS), hindlimb suspension, microbial infection, denervation, disease induction by specific toxic agent/drug or genetic manipulation (Holecek, 2012; Kottaisamy et al., 2021). For example, muscle wasting associated with cancer has been studied in animal by transplanting tumour cells into the animal or by administering large amounts of potent carcinogens (Holecek, 2012). Recently genetically engineered mouse models have also been used (Holecek, 2012). Similarly, diabetes induced-muscle wasting has been studied by utilizing genetically modified mouse or administration of chemical agents such as Streptozotocin (STZ), alloxan (Kottaisamy et al., 2021). Despite all the advantages animal models offer for investigating and developing novel drug for muscle wasting, there is no single animal model that can totally mimic all the perturbation underlying muscle wasting associated with several disease, aging and inactivity in human. However, since each muscle wasting experimental animal model have a unique pathophysiological mechanism driving them, studying muscle wasting in several muscle wasting animal models is essential. This is because the knowledge gain in each model can be translated to clinical practice to solve the diverse complications of muscle wasting in human patients. Thus, in this study two disease induced animal models were

employed to study muscle wasting including non-alcoholic fatty liver disease (NAFLD), and diabetes mellitus (DM).

2.4. NAFLD and diabetic epidemiology, etiology, and pathogenesis

The prevalence of non-alcoholic fatty liver disease (NAFLD), and diabetes mellitus (DM) continues to rise globally. Recent data showed that approximately one-quarter of the global adult population is estimated to have NAFLD (Lazarus et al., 2021). The situation is even worse for diabetes. In 2021 alone diabetes kills approximately 6.7 million people globally, that means one person dies of diabetes every 1 second. In fact, by 2045 about 783 million people are expected to be living with diabetes (Sun et al., 2022).

NAFLD is a challenging disease that is characterized by excess hepatic fat accumulation (nonalcoholic fatty liver (NAFL)), inflammation, hepatocyte injury (nonalcoholic steatohepatitis (NASH)) and fibrosis (Tilg et al., 2021). Many factors (both exogenous and endogenous) contribute to the pathogenesis of NAFLD. These triggers include insulin resistant (IR), obesity, metabolic syndrome, oxidative stress, gut dysbiosis, adipose tissue secreted hormones, intestinal leakage, endocrine disruptors, and particulate matter (Delli Bovi et al., 2021). Furthermore, genetic, and epigenetic factors have also been shown to influence NAFLD pathogenesis and progression (Gjorgjieva et al., 2019; Taliento et al., 2019). Alterations of epigenetic mechanisms such as DNA methylation, histone acetylation/methylation and non-coding RNA-dependent post-transcriptional regulation plays a critical role in reprogramming molecular mechanisms governing hepatic metabolism disorder associated with NAFLD. For instance, impaired glucose/lipid metabolism pathway and deregulated cellular processes (such as autophagy, endoplasmic reticulum-stress) and unfolded protein response) that converge in the aberrant hepatic lipid accumulation in NAFLD are all under the control of miRNAs (Figure 8) (Gjorgjieva et al., 2019).

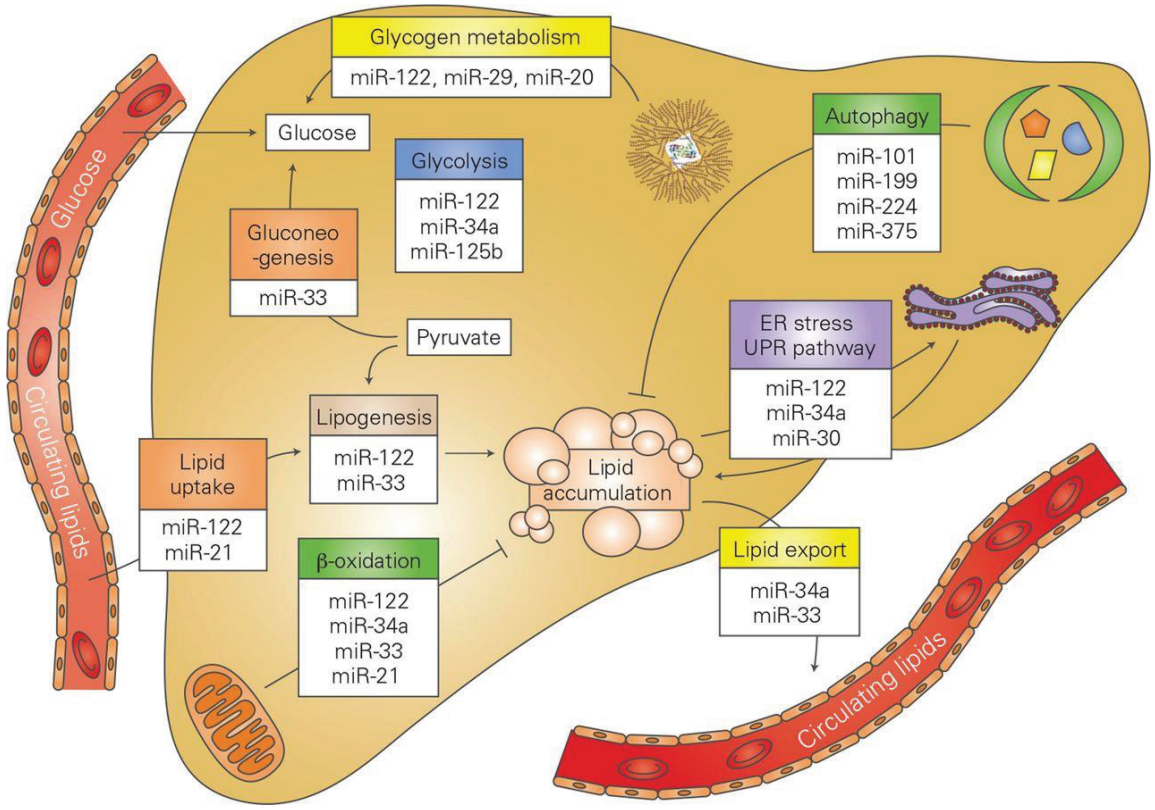

Figure 8. Deregulated miRNAs in NAFLD are an important epigenetic factor that contribute to the reprogramming of glucose/lipid metabolism and stress-induced pathways in NAFLD (Source: Gjorgjieva et al., 2019).

Diabetes mellitus (DM) on the other hand is serious systemic disease that is characterized by hyperglycemia (elevation of blood glucose concentration) due to defect in insulin secretion or insulin action or both. The key mechanism resulting in the two main form of DM (type 1 DM and type 2 DM) is loss of functional pancreatic β-cell mass (Eizirik et al., 2020). Type 1 DM is caused by autoimmune-mediated pancreatic β-cell destruction which lead to an absolute insulin deficiency. The pathogenesis of the disease involves a complex dialog between immune cells (e.g invading or residence macrophage and T cells) and pancreatic β-cell. This pathogenic cross talk is what triggers local inflammation (insulitis) and progressive pancreatic β-cell death mainly via apoptosis (Eizirik et al., 2020). A number of factors shaped this pathogenic dialogue, this includes individual genetic predisposition, age, and

environmental factors such as viral infections and diet, among others (DiMeglio et al., 2018; Nakayasu et al., 2019). The exposure of susceptible individual to this factors can trigger pancreatic β-cell autoimmunity (DiMeglio et al., 2018; Nakayasu et al., 2019). Meanwhile Type 2 DM is characterized by insulin resistance in peripheral tissues specifically the muscle, liver, and adipose tissue (Galicia-Garcia et al., 2020). This condition is usually complicated by progressive failure of pancreatic β-cells to secrete insulin (Galicia-Garcia et al., 2020).

Obesity, is the main driver of type 2 DM. This condition promotes IR via several inflammatory mechanisms such as increased free fatty acid (FFA) release and adipokine deregulation (Chatterjee et al., 2017). Other factors such as genetic, metabolic, sedentary lifestyles, high caloric diets and environmental factors also contribute to the development of Type 2 DM (Chatterjee et al., 2017). In view of the foregoing, it is clear that both NAFLD and DM especially type 2 DM share common pathogenic agent which include obesity, IR, and genetic factors. In fact, recent studies have suggested that a bidirectional relationship exists between NAFLD (or NASH) and type 2 DM (Ferguson and Finck, 2021). Due to this interplay, it is unsurprising then to see that both NAFLD and DM patients almost share common complications such skeletal muscle atrophy, and microvascular disease, especially chronic kidney disease (Mantovani et al., 2020; Targher et al., 2021; Choe et al., 2018; Vignaud et al., 2007).

2.5. Clinical significance of Muscle Wasting in NAFLD and DM

As mentioned earlier, insulin resistance (IR) is a major defect common to both NAFLD and DM (Ferguson and Finck, 2021). Since skeletal muscles is the largest pool of insulin sensitive tissues in human body, it is the major tissue responsible for majority of body's glucose uptake (Son et al., 2017; Wu et al., 2019). No wonder, IR in this tissue significantly results in whole-body metabolic disturbances (Cleasby et al., 2016). This metabolic disturbances subsequently accelerate muscle wasting (Nishikawa et al., 2021). This muscle loss in turn reduces the muscle ability to clear glucose from the blood. This worse glycemic control will eventually promote other secondary complications such as cardiovascular disease, chronic kidney disease, and vision loss, nerve damage, decrease physical performance (Mantovani et al., 2020; Targher et al., 2021; Ferguson and Finck, 2021; Mantovani et al., 2020; Orlando et

al., 2017). These secondary complications can also exacerbate muscle wasting. For example, chronic kidney disease has been shown to worsen muscle wasting by increasing protein degradation and suppressing protein synthesis (Zhang et al., 2020; Sabatino et al., 2021). Interestingly, there are standard treatment available for treating DM and NAFLD associated renal injury, these include glucose and blood pressure control, blockage of renin-angiotensin system and prevention of lipid accumulation (Zoja et al., 2020). Unfortunately, this therapeutic strategies cannot render protection if the renal injury has become chronic a condition called end stage renal disease (ESRD). ESRD is an irreversible damage of kidney that can only be treated by transplantation (Selby and Taal, 2020.). Regrettably most patient with diabetes end up with this end stage renal disease because currently the diagnosis of this disease majorly relies on blood urea nitrogen (BUN), albumin, and cytokines) level (Su et al., 2021). Unfortunately, this parameter has a major problem of low sensitivity thereby missing early injury responses in diabetic kidneys. In addition, these traditional serum/urine biomarkers concentration are often affected by protein diet, intake of certain drugs and other secondary complication of diabetes (Wasung et al., 2015). Other traditional methods such as histological analysis also have a major drawback of invasiveness. Therefore, along with searching for therapeutic strategy to manage muscle wasting there is urgent need to develop non-invasive diagnostic tool for early detection of renal injury in both experimental animal and human patient with DM and NAFLD

Chapter 3

Experiment 1

Satellite cell content and muscle regeneration in a mouse model of NAFLD

3.1. Introduction

Nonalcoholic fatty liver disease (NAFLD), characterized by the accumulation of fat in the liver, is the most common type of liver disease and is widely studied as a leading cause of cirrhosis in developed countries (Cotter and Rinella, 2020). A pathologic relationship between NAFLD and other diseases has been reported previously (VanWagner and Rinella, 2016; Bullón-Vela et al., 2020), and there is increasing evidence that NAFLD is often associated with not only hepatic cirrhosis but also other lifestyle-related diseases such as cardiovascular disease, type 2 diabetes, and cancer (Bullón-Vela et al., 2020). Clinical studies have documented that loss of muscle mass (muscle atrophy) is a major complication associated with NAFLD (Pacifico et al., 2019; Choe et al., 2018). This impairment in the musculoskeletal system has a role in the physical disability, health decline, and increased risk of mortality commonly observed in patients with NAFLD (Cruz et al., 2019). Thus, understanding the cellular and molecular mechanisms that prompt muscle atrophy in NAFLD will lead to identification of novel therapeutic strategies for the treatment of NAFLD. However, the cellular and molecular mechanisms underlying NAFLD-mediated effects on skeletal muscle mass and functions remain unclear because research assessing the pathologic relationship between NAFLD and skeletal muscles at the cellular and molecular level is relatively scarce.

Common mechanisms that cause skeletal muscle atrophy include impaired protein metabolism (increased protein catabolism and decreased protein anabolism), delay in muscle regeneration, and alteration in muscle progenitor cells (also known as satellite cells [SCs]) (Bonaldo and Sandri, 2013; McKenna and Fry, 2017; Muñoz-Cánoves et al., 2020). However, it is not clear whether any of these main mechanisms prompt muscle atrophy in NAFLD. Several studies have indicated that the SC pool and/or function is reduced in a variety of lifestyle-related diseases (such as diabetes, obesity, cancer, and cardiovascular

disease) characterized by loss of muscle mass (D'Souza et al., 2015; D'Souza et al., 2016; Inaba et al., 2018; Abbott and Giordano, 2003). Satellite cells constitute a small population of cells that are primarily responsible for skeletal muscle maintenance and repair (Hawke and Garry, 2001). In response to stimuli such as muscle injury, SCs become activated and then proliferate extensively, self-renew their population, and differentiate into mature new myofibers (Hawke and Garry, 2001). Satellite cells exist in two states in the skeletal muscle: an inactive (quiescent) state and an activated state. Satellite cells in both states express a unique marker, Pax7 (Lepper et al., 2011), whereas only activated SCs express MyoD, which is often referred to as the master regulator of myogenesis and is the key transcriptional factor responsible for converting non-muscle cell types into muscles (i.e., differentiation) (Tapscott, 2005).

Accumulating evidence indicates that chronic inflammation that accompanies most lifestyle-related diseases (Furman et al., 2019) may be a major factor responsible for reduced SC population and activity. Importantly, this dysfunction of SCs is what eventually promotes loss of muscle mass in these conditions (McKenna and Fry, 2017; Perandini et al., 2018). Because chronic inflammation is closely associated with NAFLD (Furman et al., 2019), we hypothesized that NAFLD negatively affects SC quantity and/or functionality and muscle regeneration.

This study investigated the effects of NAFLD on skeletal muscle regeneration in mice with NAFLD induced by a choline-deficient diet (CDD), with a major focus on the muscle SC population. The present study is the first to demonstrate that muscle wasting in NAFLD can be attributed to a decrease in muscle SC content and function. This observation provides evidence for the delay in muscle regeneration among mice with NAFLD.

3.2. Materials and methods

3.2.1 Animals and diets

All animal experimental protocols and procedures were approved by the Hiroshima University Animal Committee, and the mice were maintained according to Hiroshima

University guidelines for the care and use of laboratory animals (Ethical approval No. C18-15-4). Four-week-old male CD-1 (ICR) mice were purchased from Charles River Japan, Hino, Japan. Mice were fed with a commercial standard chow diet (MF, Oriental Yeast, Tokyo, Japan) for 1 wk. At 5 wk of age, mice were fed with either a choline-deficient diet for 4 wk (NAFLD group; n = 8) or a 0.2% choline-containing diet for 4 wk (control [CONT] group; n = 8). The composition of the diets has been reported in a previous study (Mitsumoto et al., 2017). At 9 wk of age, after 4 wk of the CONT or NAFLD diet treatment, all animals from each CONT and NAFLD diet group were divided into two subgroups (4 mice per group): a muscle injury group by cardiotoxin (CTX) injection (injured groups were named as CTX-CONT and CTX-NAFLD groups) for muscle regeneration analysis or a non–muscle injury group (uninjured groups were named as CONT and NAFLD groups) for single myofiber isolation and mRNA extraction. All mice were housed in standard metal cages in a room with controlled temperature and humidity under a 12:12 h light:dark cycle. All mice had free access to the group diet and water.

3.2.2. Skeletal muscle injury and tissue and blood collection

Skeletal muscle injury was induced via intramuscular injection of 10 μM CTX (Latoxan, Valence, France; 100 μL per muscle) on the left tibialis anterior (TA) and left gastrocnemius (GAS) of both the CTX-CONT and the CTX-NAFLD groups as previously described (Nissar et al., 2012). At 5 d postinjury, mice were sacrificed under isofurane anesthesia (between 13:00 and 15:00 h) after removal of food (06:00 h). Blood was collected from the abdominal vein into tubes on ice. Then, serum was obtained by centrifugation at 8000 rpm for 10 min and stored at −80°C. The TA muscles from injured mice (CTX-CONT and CTX-NAFLD groups) and uninjured mice (CONT and NAFLD groups) were isolated, weighed, covered with optimum cutting temperature embedding compound, and immediately frozen in liquid nitrogen-cooled isopentane. The GAS muscles from uninjured mice were snap frozen in liquid nitrogen after measuring the net weight and were used for mRNA analysis. All tissues were stored at –80°C until analysis. In

the uninjured CONT and NAFLD mice groups, both the left and right extensor digitorum longus (EDL) muscles were harvested and used for single muscle fiber isolation.

3.2.3. Serum biochemical parameters

Serum alanine transaminase and aspartate transaminase levels were determined using a Beckman Coulter AU480 analyzer (Beckman Coulter, Krefeld, Germany)—an automated chemistry instrument for turbidimetric, spectrophotometric, and ion-selective electrode measurements—according to the manufacturer's protocol.

3.2.4. Immunofluorescence staining of muscle sections

The frozen TA sections (6 μm thick) from the uninjured CONT and NAFLD groups were fixed for 20 min with 4% paraformaldehyde at room temperature (RT, approximately 25 ± 5°C), permeabilized with 0.2% Triton-X100 (Sigma-Aldrich, Saint Louis, Missouri 63103 USA) in Phosphate-buffered saline (PBS) containing 2% bovine serum albumin (Sigma), 0.1% sodium azide, 5% fetal bovine serum, and 5% normal goat serum for 1 h at RT, and then transferred to a blocking solution from the M.O.M. kit (Vector Laboratories Inc., USA) for 1 h at RT. Muscle sections were then incubated with primary antibodies (mouse anti-Pax7 (1:100; Developmental Studies Hybridoma Bank (DSHB), Iowa City, IA, USA) and rabbit antilaminin (1:500; Abcam ab11575, Cambridge, MA) at 4°C overnight followed by incubation with a secondary antibody (goat antimouse IgG1 Alexa-594 [1:1000; Invitrogen A-21125], Carlsbad, CA) and Fluorescein (FITC)-AffiniPure goat antirabbit IgG (1:500; Jackson ImmunoResearch 111-095-003, West Grove, PA) at RT for 1 h. Nuclei were counterstained with DAPI (4′,6-diamidino-2-phenylindole) for 10 min at RT.

3.2.5 Single myofiber isolation, immunostaining, and culture

The EDL muscles obtained from groups of uninjured CONT and NAFLD mice were digested by 0.2% collagenase I in Dulbecco's modified Eagle medium (DMEM) (Invitrogen), as previously described (Nissar et al., 2012). Then, the isolated single fibers were either fixed

immediately with 4% paraformaldehyde for 5 min or cultured for 24 h and 48 h in DMEM supplemented with 10% (v/v) horse serum, 100 μg/mL streptomycin, and 0.5% (v/v) chick embryo extract at 37°C in 5% CO_2. After the 24 h and 48 h culture, all single fibers from all experimental groups were fixed with 4% paraformaldehyde for 5 min and subjected to immunostaining. Fixed single myofibers were then permeabilized with 0.5% Triton-X 100 in PBS for 30 min at RT, blocked (PBS with 1.5% normal goat serum and 1.5% normal horse serum) for 30 min at RT, and then stained with primary antibodies (mouse anti-Pax7 [DSHB]) at 1:1, rabbit anti-MyoD (Santa Cruz Biotechnology M-318, Dallas, TX, USA at 1:100) at 4°C overnight. Subsequently, the myofibers were stained with appropriate secondary antibodies at RT for 1 h. Secondary antibodies used were FluoroLinkCy3-labeled goat antimouse IgG (1:1000; GE Health care PA43002, Jackson ImmunoResearch) for Pax7 (red) and Fluorescein isothiocyanate (FITC)-labeled goat antirabbit IgG (1:500; Jackson ImmunoResearch) for MyoD (green). After immunostaining, myofibers were counterstained with 1 μg/mL DAPI (blue) for 5 min at RT.

3.2.6 Skeletal muscle histology

Following standard procedures, the TA muscle of all treatment groups (injured and uninjured) and extensor digitorum longus (EDL) muscle of uninjured group embedded in optimum cutting temperature embedding compound were transversely cryosectioned (8 μm) and stained with hematoxylin and eosin to access the differences in muscle morphology between mice cohorts at rest and 5 d postinjury. On average, approximately 90 fibers were analyzed per muscle section. The image analysis provided essential information about fiber morphology, fiber size, and the presence of myopathic makers (such as centrally located nuclei, pale cytoplasm, and necrotic fibers) as previously established (Krause et al., 2011).

3.2.7. Microscopy and image analysis

An Olympus IX81 Inverted wide microscope was used to capture all the images, and Nikon Elements software was used to analyze them. The analysis included quantification of SC numbers ($Pax7^{+}/DAPI^{+}$), SCs differentiation ($MyoD^{+}/Pax7^{-}/DAPI^{+}$), and SC

proliferation ($MyoD^+/Pax7^+/DAPI^+$) on single myofibers and average myofiber size in TA muscle sections.

3.2.8. RNA analysis

Total RNA was isolated from liver tissue and GAS muscles of the uninjured CONT and NAFLD mice using the RNeasy lipid tissue kit (QIAGEN Sciences, Germantown, MD). cDNA synthesis was performed with 1 μg isolated RNA using ReverTra Ace (TOYOBO, Osaka, Japan) and random hexamers (TaKaRa Bio, Kyoto, Japan) according to the manufacturers' recommendations. For real-time quantitative polymerase chain reaction (qPCR), THUNDERBIRD SYBR qPCR Mix (TOYOBO) and StepOnePlus (Applied Biosystems, Foster City, CA) were used with conditions set as previously described (Mitsumoto et al., 2017). Specific primers were obtained from Eurofins Genomics, Tokyo, Japan (Table 1).

Table 1. Primer sequences for qPCR

Target gene	Sequence (5'-3')	
L19	Forward	GGCATAGGGAAGAGGAAGG
	Reverse	GGATGTGCTCCATGAGGATGC
TNFα	Forward	CGTCGTAGCAAACCACCAAG
	Reverse	TTGAAGAGAACCTGGGAGTAGACA
IL-1β	Forward	GAAGGGCTGCTTCCAAACCT
	Reverse	GTTGTTCATCTCGGAGCCTG
NOX2	Forward	AGCTATGAGGTGGTGATGTTAGTGG
	Reverse	TGCACAGCAAAGTGATTGGC
GPx2	Forward	TCCCTTGCAACCAGTTCG
	Reverse	ATGCTCGTTCTGCCCATTGA
Adipsin	Forward	TGTACTTCGTGGCTCTGGTG
	Reverse	CACCTGCACAGAGTCGTCAT
Mogat1	Forward	CTGGTTCTGTTTCCCGTTGT
	Reverse	TGGGTCAAGGCCATCTTAAC

3.2.9. Serum TNF-α quantification

Serum tumor necrosis factor-alpha (TNF-α) was determined using the Mouse TNF-α ELISA kit (BioLegend, California, USA, catalog: 430907) according to the manufacturer's instruction.

3.2.10. Liver lipid analysis

Hepatic fat accumulation was determined by Nile red staining. Briefly, liver cryosections (5 μm thick) were fixed with 4% PFA in PBS for 15 min. It was then washed in PBS and incubated in Nile red (Sigma,19123) and counter stained with 1 μg/mL DAPI (blue) for 15 min at room temperature. Images were taken using an Olympus BX53 microscope (Olympus, Tokyo, Japan)

3.2.11. Western blot analyses

Equal amounts of protein derived from uninjured gastrocnemius (Gas) muscle was resolved by SDS-PAGE, transferred onto a polyvinylidene difluoride (PVDF) membranes (Bio-Rad, Missisauga, Ontario), blocked with 5% skim milk at room temperature (RT) for 1 hr. Subsequently, the membranes were incubated with a primary antibody against NADPH oxidase 2 (NOX2) (Proteintech Group Inc's), Arginase 1 (Biolegend, London, UK) and GAPDH (Santa Cruz Biotechnology, Santa Cruz, CA) overnight at 4°C, followed by incubation with an appropriate secondary antibody. Proteins were then visualized with an ECL western blot detection system

3.2.12. Statistical analysis

All data were analyzed by Student's *t* test and $p < 0.05$ was considered as statistically significant (denoted appropriately in all figures). Data are expressed as means ± standard error (S.E.).

3.3. Results

3.3.1. NAFLD development

To induce NAFLD, mice were fed a CDD for 4 wk, whereas the control mice were fed a 0.2% choline-containing diet. The data showed that mice fed a CDD had a slightly greater body weight (Table 2) and developed hepatomegaly, with an approximately 50% increase in liver weight (Figure 9A) compared with the control mice.

Table 2. Mouse body weight

Groups	CON	NAFLD
Initial body weight	31.20 ± 0.78	30.33 ± 0.77
Final body weight	38.55 ± 0.87	39.6 ± 0.64
Body weight gain (g/4w)	7.35 ± 0.67*	9.28 ± 0.38*

Values are expressed as means ± S.E. (n=8). * Denotes significant difference in nonalcoholic fatty liver disease (NAFLD) compared to control (CON) assessed by *t* test $p < 0.05$.

To further investigate hepatic function and integrity, various serum biochemical parameters were evaluated. The results showed that mice fed a CDD for 4 wk had serious hepatic injury as indicated by a significant increase in blood aspartate aminotransferase and alanine transaminase levels when compared with the control mice ($P < 0.01$) (Figure 9B, C, respectively).

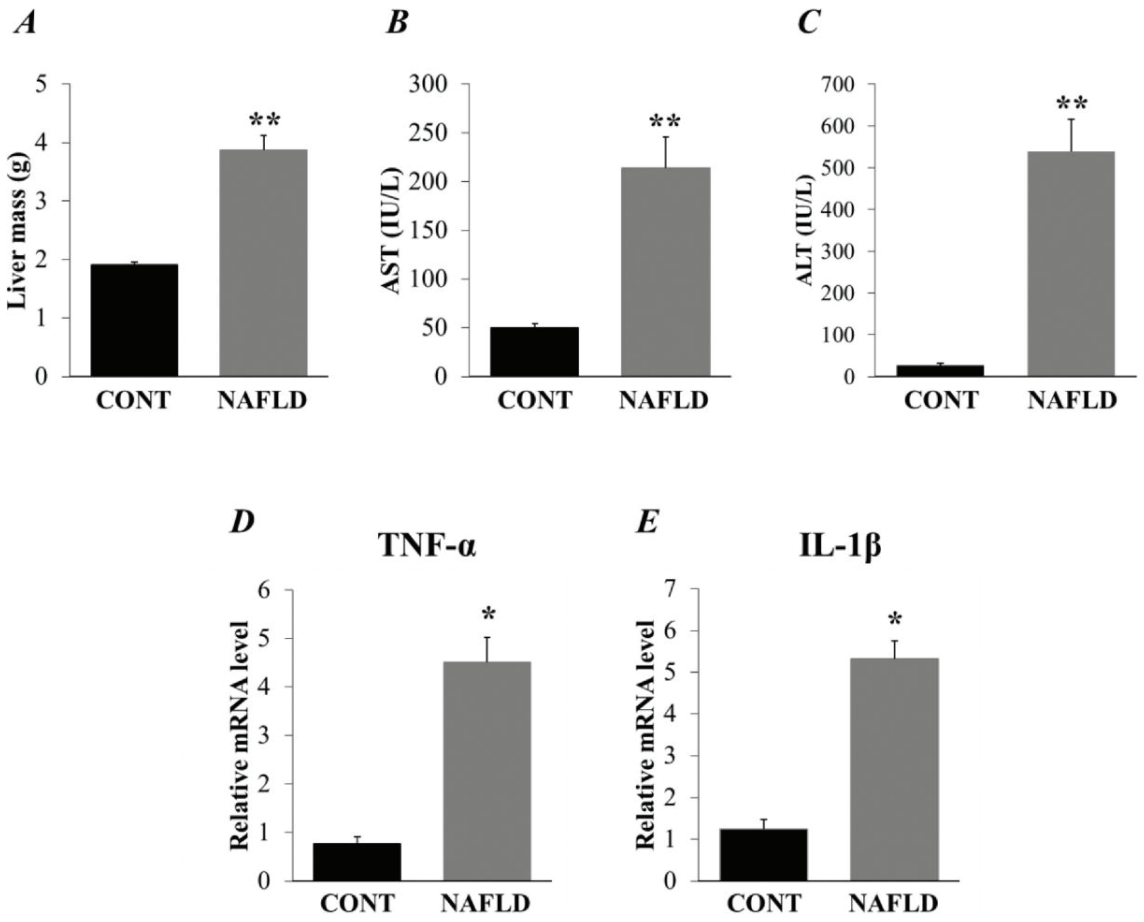

Figure 9. The pathologic analysis and assessment of mouse liver tissues after dietary treatment. Control-group mice (n = 4) (CONT) were fed with a control diet and mice in the nonalcoholic fatty liver disease (NAFLD) group (n = 4) were placed on a choline-deficient diet for 4 wk. (A) The NAFLD mice showed a significant increase in liver size compared with the CONT mice. (B-C) Serum aspartate transaminase and alanine transaminase level. (D-E) Relative hepatic mRNA expression levels of proinflammatory genes TNF-α and IL-1 β. All values are expressed as means ± SEs. * $P < 0.05$ and ** $P < 0.01$ as determined by the student *t* test.

Further evaluation of the NAFLD mice hepatocytes by Nile red fluorescence staining indicated that lipid droplet accumulation in the livers of the NAFLD mice was severely high (Figure 10A), which is consistent with previous findings (Mitsumoto et al., 2017). In fact, the expression level of adipsin and monoacylglycerol O-acyltransferase 1 (Mogat1), which are fatty liver maker genes, was severely downregulated in mice with NAFLD (Figure 10 B, C). An imbalance in cytokine production has been shown to play a key role in the

pathogenesis of NAFLD (Kugelmas et al., 2003). Therefore, mRNA expression of tumor necrosis factor α (TNF-α) and interleukin-1 β (IL-1 β) in liver tissues was evaluated using qPCR. As expected, a significant increase in the expression of TNF-α ($P < 0.05$) and IL-1 β ($P < 0.05$) was observed in the livers of NAFLD mice when compared with that in the controls (Figure 9 D, E). These results suggest that NAFLD was successfully induced after feeding mice with a CDD for 4 wk.

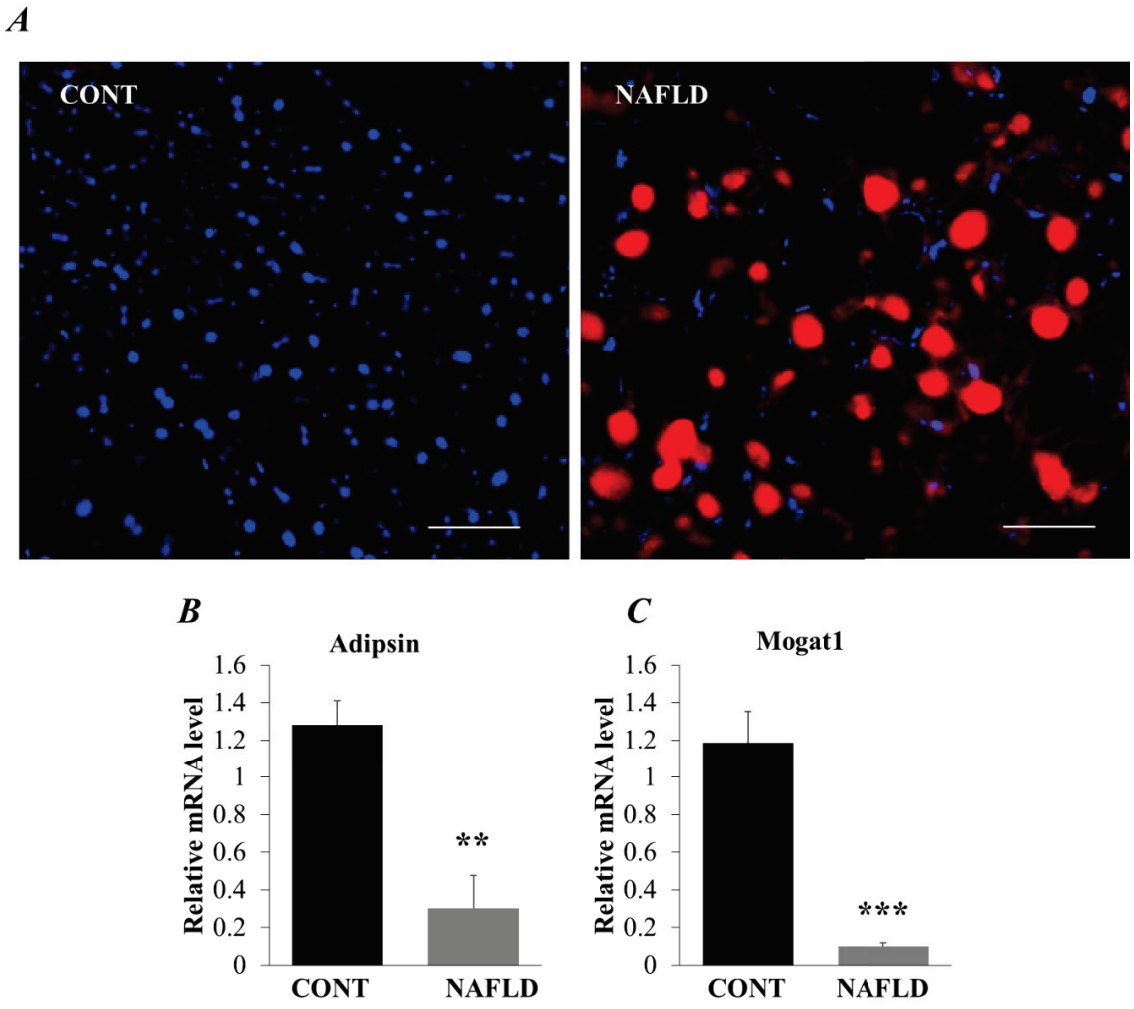

Figure 10. Lipid droplet accumulation in the livers of the NAFLD mice (A) Lipid droplet accumulation increases in NAFLD mice hepatocytes as indicated by Nile red fluorescence staining. Lipid droplets (red) / nuclei staining (blue) (B-C) Hepatic gene expression level of

adipsin and modat1 are downregulated NAFLD mice. All values are expressed as means ± SEs. * $P < 0.05$ and ** $P < 0.01$ as determined by the student *t* test.

3.3.2. Defects in muscle health among NAFLD mice

Previous studies have shown that the muscle mass of uninjured TA muscle remains unaltered after an American lifestyle-induced obesity syndrome diet (Cabrera et al., 2016). Similarly, there was no difference in the uninjured TA and GAS muscle masses between CDD-fed mice (NAFLD group) and mice fed with a 0.2% choline-containing diet (CONT group) (Figure 11A). However, a hematoxylin and eosin–stained cross-section of uninjured TA muscle revealed that the average myofiber area was significantly reduced in the NAFLD mice compared with the CONT mice ($P < 0.01$) (Figure 11 B, C).

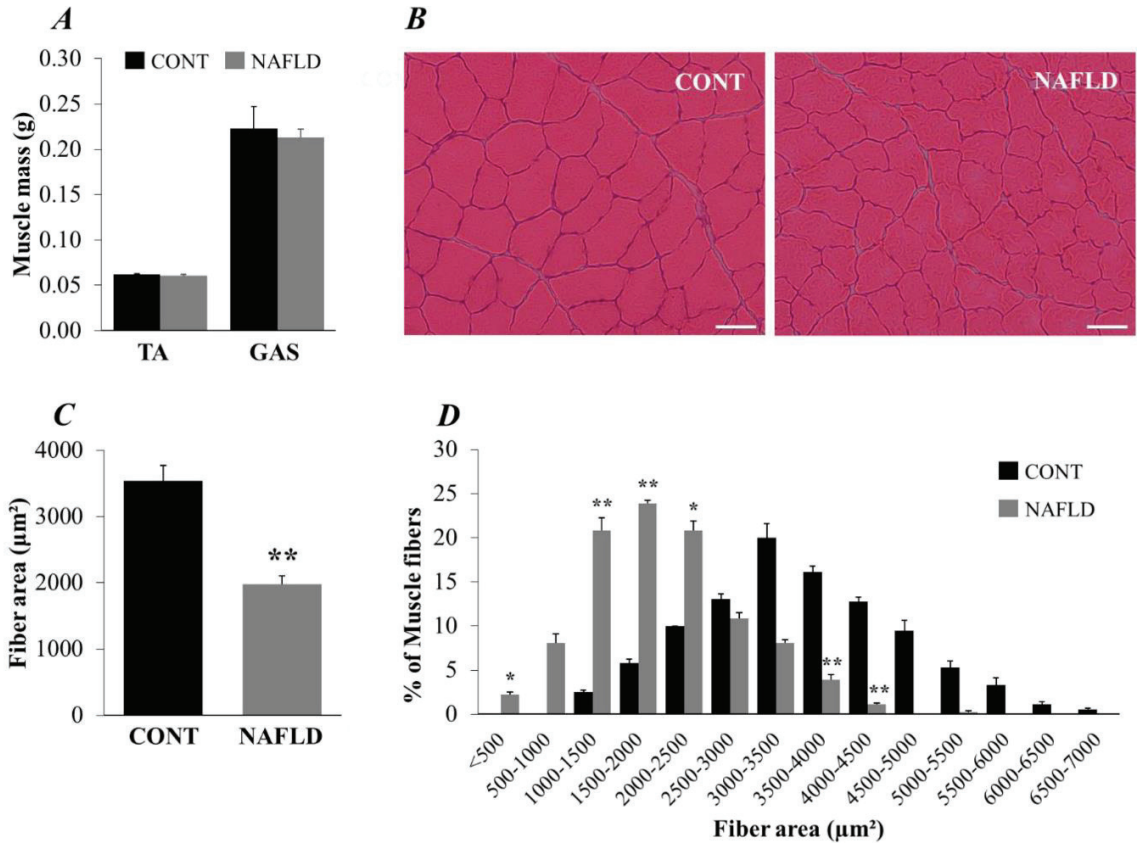

Figure 11. The muscle of a mouse with NAFLD displayed hallmarks of myopathy. (A) The muscle mass of uninjured TA and GAS muscles. (B) The H&E-stained cryosections of uninjured TA muscles illustrated muscle atrophy in muscles of mice with NAFLD. Scale bar represents 50 μm. (C) Quantification of an average myofiber cross-sectional area of an uninjured TA muscle from (B) indicated the occurrence of muscle atrophy in NAFLD mice (n = 4) compared with CONT mice (n = 4). (D) Muscle fiber diameter distribution revealed a larger percentage of smaller fibers in NAFLD mice muscles compared with those of CONT mice. An average of 90 fibers were randomly counted per muscle. All values are expressed as means ± SEs. *$P < 0.05$ and **$P < 0.01$ as determined by the Student *t* test. CONT, control; GAS, gastrocnemius; H&E, hematoxylin and eosin; NAFLD, nonalcoholic fatty liver disease; TA, tibialis anterior.

Furthermore, as depicted in Figure 11D, a significantly greater percentage of small myofibers (and a significantly smaller percentage of large myofibers) was observed in the NAFLD mice compared with that in the CONT mice. Similarly, the average myofiber area of NAFLD EDL muscle was significantly reduced ($P < 0.01$) (Figure 12A, B), and the significantly greater percentage of small myofibers was observed in NAFLD EDL muscle when compared with that in controls (Figure 12C). Taken together, these findings suggest that the muscle wasting observed in NAFLD may be attributed to a reduction in the size of individual myofibers.

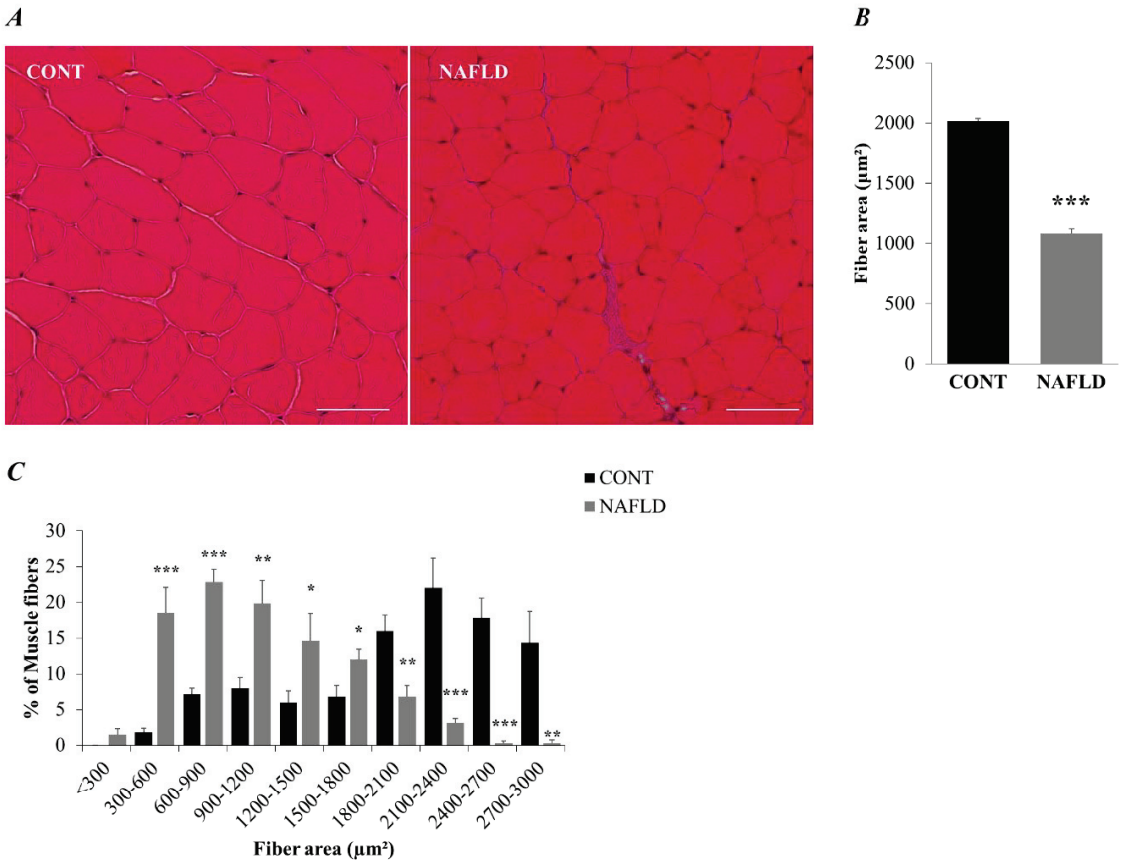

Figure 12. Myofiber atrophy was shown in NAFLD EDL muscle (A) H&E stained cryosections of uninjured EDL muscles illustrate muscle atrophy in NAFLD mice muscles. Scale bar represents 200 µm. (C) quantification of average myofiber cross-sectional area of uninjured EDL muscles from B indicated the occurrence of muscle atrophy in NAFLD mice compared with CONT. (D) Muscle fiber diameter distribution reveals a larger percentage of smaller fibers in NAFLD mice muscles compared to CONT. An average of 120 fibers were randomly counted per muscle. All values are expressed as means ± S.E. $*p < 0.05$, $**p < 0.01$, $***p < 0.001$ as determined by Student´s *t* test. n= 5 C and n=5 NAFLD). Control mice (CONT), nonalcoholic fatty liver disease mice (NAFLD), extensor digitorum longus (EDL), and hematoxylin and eosin (H&E).

3.3.3. Population of SCs in skeletal muscle of NAFLD mice

The importance of SC content in skeletal muscle health has been well established (von Maltzahn et al., 2013; McCarthy et al., 2011). Based on this fact, it was hypothesized that the reduction in individual myofiber (i.e., myofiber atrophy) observed in NAFLD TA and EDL muscle was owed to a decreased SC number. This hypothesis was tested by quantifying the

Pax7^{+} SC number on single myofibers isolated from the EDL muscle of uninjured NAFLD and CONT mice (Seale et al., 2011). The result showed that the number of Pax7^{+} SCs was significantly lower in the resting EDL muscle (quiescent state) of NAFLD mice compared with that of CONT mice ($P < 0.01$) (Figure 13A, B). To confirm that SC numbers were actually reduced in the muscles of NAFLD mice, Pax7^{+} SC numbers were also quantified in sections of uninjured TA muscle from CONT mice and NAFLD mice (Figure 13A). The numbers of Pax7^{+} SCs were reduced 4.3-fold in NAFLD TA muscle compared with CONT TA muscle (Figure 13C, D), suggesting a depletion of the SC pool in NAFLD mice.

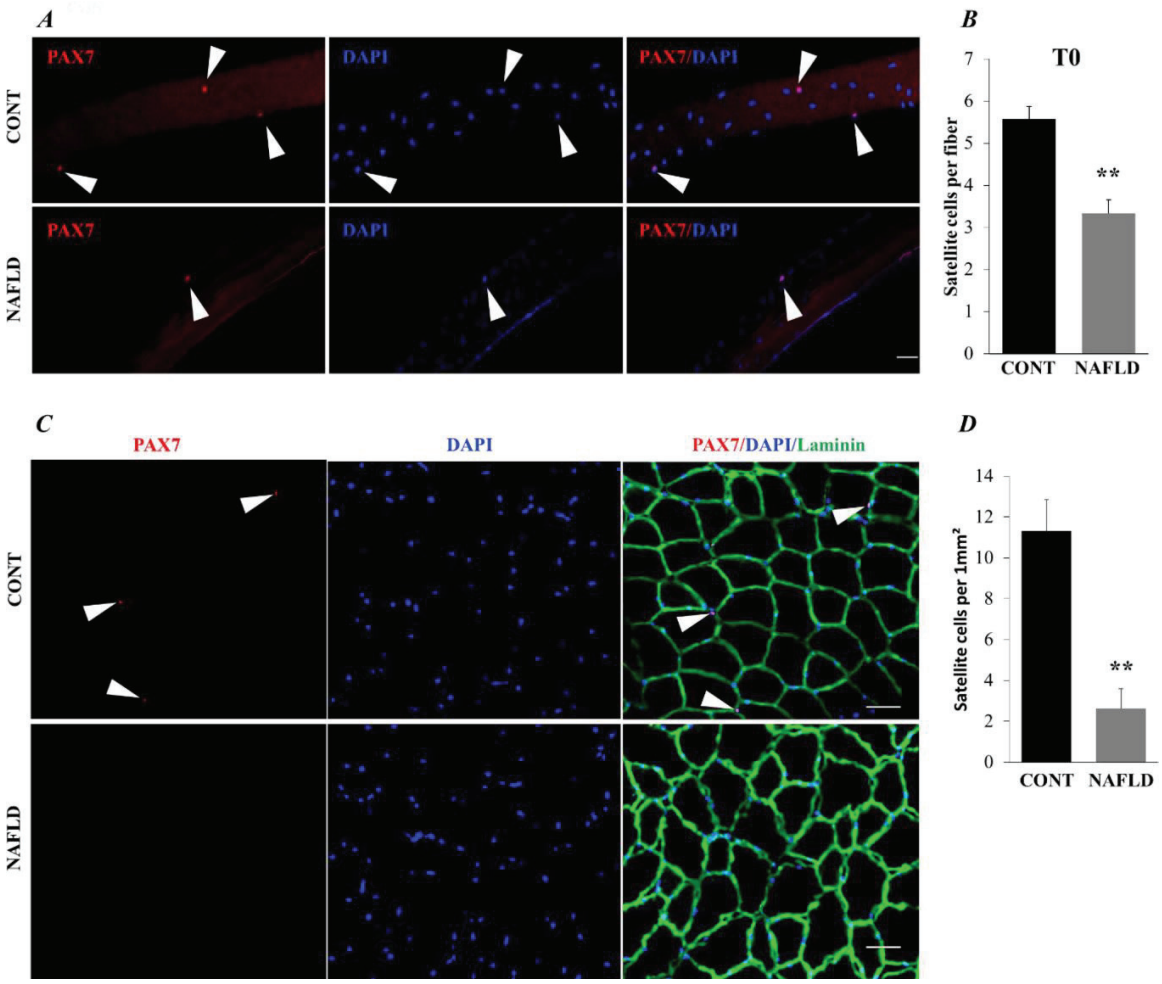

Figure 13. The content of SCs was decreased in the skeletal muscle of mice with NAFLD. (A) Representative images of quiescent SCs on freshly isolated (time, 0 h) single myofiber from EDL muscles stained for Pax7 (red) and DAP1 (blue) immunoreactivity (white arrowheads). (B) The quantification of SC numbers (via Pax 7^+ content analysis) in freshly isolated single myofibers from EDL muscles. A total of 70 single myofibers were counted per group (≥15 single myofibers from each of the 4 animals). (C) Uninjured TA muscle sections showing Pax 7^+ SC (red), basal laminin (green), and myonuclei (blue). White arrowheads mark SCs. Scale bar represents 50 μm. (D) Quantification of Pax7+ SC/1 mm^2 CSA in the TA muscle of NAFLD mice when compared with CONT mice (n = 5). All values are expressed as means ± SEs. ** $P < 0.01$, as determined by the Student *t* test. Scale bars are 50 μm. CONT, control mice; EDL, extensor digitorum longus; NAFLD, nonalcoholic fatty liver disease; SC, satellite cell; TA, tibialis anterior.

3.3.4. Impairment in muscle regeneration after injury in NAFLD mice

Depletion of SCs often results in regenerative defects (Lepper et al., 2011; von Maltzahn et al., 2013). As such, one could expect to see impairment in muscle regeneration in the muscles of NAFLD mice 5 d postinjury. To investigate this, TA muscles from both CTX-CONT and CTX-NAFLD groups were subjected to CTX injury. In response to the injury, the absolute mass of TA and GAS muscles in both animal groups remained unaltered 5 d postinjury (Figure 14A). However, histologic (hematoxylin and eosin) staining of injured CTX-CONT and CTX-NAFLD TA muscles indicated a morphologic difference between the animal cohorts at 5 d postinjury (Figure 14B). Furthermore a significant reduction ($P < 0.01$) was observed in the cross-sectional area of regenerating muscles in the CTX-NAFLD group at 5 d postinjury compared with that in the CTX-CONT group (Figure 14C). To support the hypothesis that exposure to NAFLD profoundly affects the ability of skeletal muscle to repair after injury, the muscle fiber distribution graph was plotted. There was a significantly higher percentage of small fibers in the CTX-NAFLD muscles compared with the CTX-CONT muscles (Figure 14D).

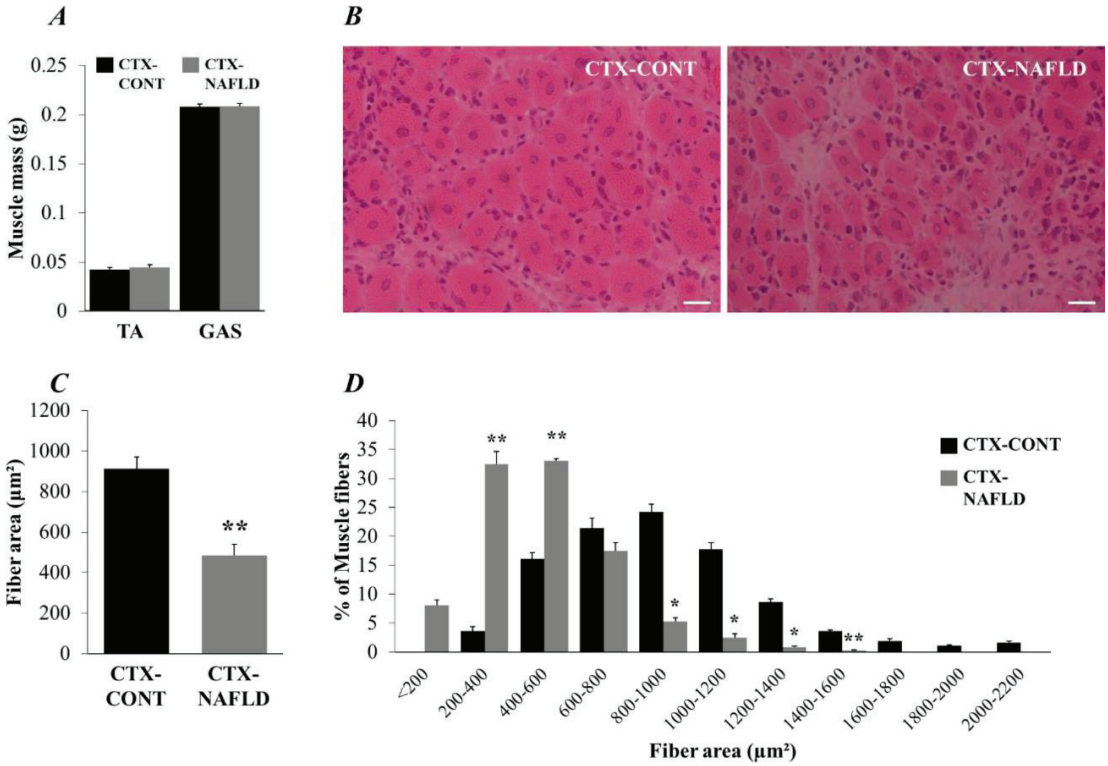

Figure 14. The NAFLD environment caused delay in muscle regeneration after 5 d postinjury. (A) The muscle mass (g) of the injured TA and GAS muscles. (B) The H&E-stained cryosections of injured TA muscles depicted delay in muscle regeneration in muscles of CTX-NAFLD mice compared with those of CTX-CONT mice. Scale bar represents 20 µm. (C) Quantification of average myofiber cross-sectional area of the regenerating (centrally nucleated) myofibers from B showed that NAFLD significantly impaired muscle regeneration. (D) Distribution of regenerating myofiber area revealed a larger percentage of smaller fibers in CTX-NAFLD mice compared with CTX-CONT mice. An average of 90 fibers were randomly counted per muscle. All values are expressed as means ± SEs. $*P < 0.05$ and $**P < 0.01$ as determined by the Student *t* test. CONT, control mice (n = 4); CTX-CONT, injured control mice; CTX-NAFLD, injured nonalcoholic fatty liver disease mice; GAS, gastrocnemius; H&E, hematoxylin and eosin; NAFLD, nonalcoholic fatty liver disease mice (n = 4); TA, tibialis anterior.

3.3.5. NAFLD and impaired SC activity

Because delayed muscle regeneration is attributed not only to SC depletion but also to abnormalities in SC function (Hawke and Garry, 2001; von Maltzahn et al., 2013), the effect of NAFLD on the activation, proliferation, and differentiation of SCs was examined.

However, the possibility that choline deficiency and not NAFLD is responsible for the depletion of the SC pool in vivo was first eliminated by culturing isolated single muscle fibers from EDL muscles in the presence of choline for 24 or 48 h. Next, the 24-h cultured single fibers were stained for nuclei and Pax7 (Figure 15A). The result showed that the number of SCs (as indicated by $Pax7^+$ myonuclei) was lower on the NAFLD muscle fibers than on the CONT muscle fibers (Figure 15B), suggesting that SCs in NAFLD possessed lower activation ability. Next, single fibers cultured for 48 h was co-stained with Pax7 and MyoD (Figure 15C) in other to examine the proliferation and differentiation characteristics of SCs in the NAFLD and CONT muscles. The result indicated that NAFLD impaired SC proliferation and differentiation as evidenced by a decrease in expression of $Pax7^+/MyoD^+$ and $Pax7^-/MyoD^+$ in the myofibers of NAFLD mice compared with those in CONT mice (Figure 15D). However, there was no difference in the expression of $Pax7^+/MyoD^-$ markers between the groups (Figure 15D). This observation suggests that the self-renewal capacity of the NAFLD muscle remained unaltered.

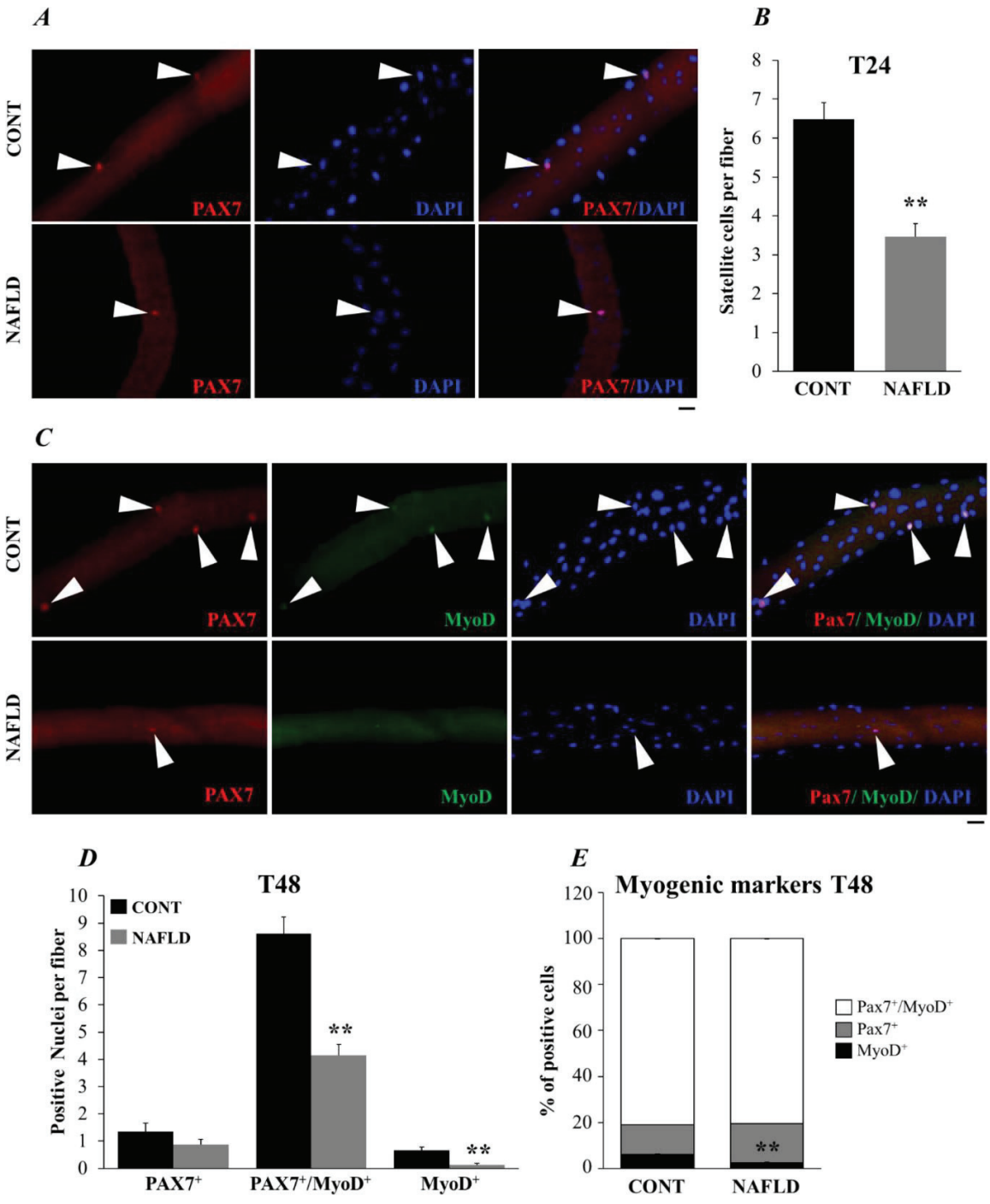

Figure 15. The function of SCs was altered in mice with NAFLD. (A) Representative image of single myofibers isolated from EDL muscles and after 24 h in cell culture stained for Pax7 (red) and DAP1 (blue) immunoreactivity (arrowheads). (B) Quantification of SC content (via

$Pax7^+$ analysis) after 24 h of culture indicated that SC activation was lowered in NAFLD mice compared with control mice. A total of 60 single myofibers were counted per group (≥15 single myofiber from each of the 4 animals). (C) Representative image of single myofibers isolated from EDL muscles and after 48 h in cell culture stained for DAPI (blue), Pax7 (red), and MyoD (green) (white arrowheads). (D) Quantification of $Pax7^+/MyoD^-$, $Pax7^+/MyoD^+$, $Pax7^-/MyoD^+$ content after 48 h indicated a reduction in the ability of NAFLD SCs to undergo expansive proliferation and differentiation compared with CONT SCs. (E) Quantification of the number of SCs expressing each myogenic marker after 48 h of cell culture, expressed as a percentage of the total number of SCs, indicated that differentiation was impaired in NAFLD mice compared with CONT mice. A total of 50 single myofibers were counted per group (≥15 single myofiber from each of the 3 animals). All values are expressed as means ± SEs. $^{**}P < 0.01$ as determined by the Student *t* test. Scale bar represents 50 μm. CONT, control; EDL, extensor digitorum longus; GAS, gastrocnemius; NAFLD, nonalcoholic fatty liver disease; SC, satellite cells; TA, tibialis anterior.

Because the number of SCs in the beginning in the NAFLD myofibers was lower compared with that in the myofibers of CONT mice, to avoid inaccurate quantification, the expression of myogenic markers was quantified as a percentage to validate the potential for expansive proliferation, self-renewal, and differentiation activities of the NAFLD SCs compared with that of CONT SCs. The result showed that there was no difference in the proliferation and self-renewal capacity of NAFLD SCs, as indicated by the percentage of $Pax7^+/MyoD^+$ and $Pax7^+$ nuclei when compared with CONT SCs. However, significantly fewer $MyoD^+$ nuclei were observed in NAFLD myofibers ($P < 0.01$) (Figure 15E). These results suggested that NAFLD did not impair SC proliferation and self-renewal ability but altered the process of differentiation instead.

3.3.6. Elevated oxidative stress and expression of arginase 1 and inflammatory cytokine in muscle of NAFLD mice

Several studies have shown that chronic inflammation induces an imbalance in reactive oxygen species (ROS) homeostasis that results in poor muscle health (Kozakowska et al., 2015; Choi et al., 2016). Interestingly, chronic inflammation is a major factor that mediates NAFLD and other extrahepatic complications. Thus, the significant increase in serum tumor necrosis factor α (TNFα) level (Table 3) and the hepatic expression of TNFα and IL-1

cytokines (Figure 9C, D) was hypothesized to induce ROS production in the muscles of NAFLD mice.

Table 3. Serum TNF-α level

Parameter	Control group (n = 5)	NAFLD group (n=6)
Serum TNF-α (pg/mL)	0.248 ± 0.087	2.162 ± 0.376*

The data are shown as the mean ± standard deviation. *$p < 0.05$. TNF-α tumor necrosis factor-alpha

This hypothesis was tested by assessing the expression of NADPH oxidase-2 (NOX2), an important enzyme involved in ROS generation (Fan et al., 2016), which is induced by proinflammatory cytokines, especially TNFα. The gene and protein expression of NOX2 from the GAS muscles of uninjured NAFLD and CONT groups was quantified using qPCR and western blotting. The result showed that both the mRNA and the protein expression level of NOX2 are significantly upregulated in the GAS muscles of the NAFLD mice compared with those of the CONT mice ($P < 0.05$) (Figure 16A, Figure 17A, B). Similarly, the expression level of glutathione peroxidase 2 (GPx2), an endogenous antioxidant enzyme responsible for scavenging ROS in cells and tissues (Ji, 2007) was quantified using qPCR. The result showed that the expression level of GPx2 was also increased in the GAS muscles of NAFLD mice compared with those of the CONT mice (Figure 16B). This result suggested that elevated oxidative stress occurs in the muscles of NAFLD mice.

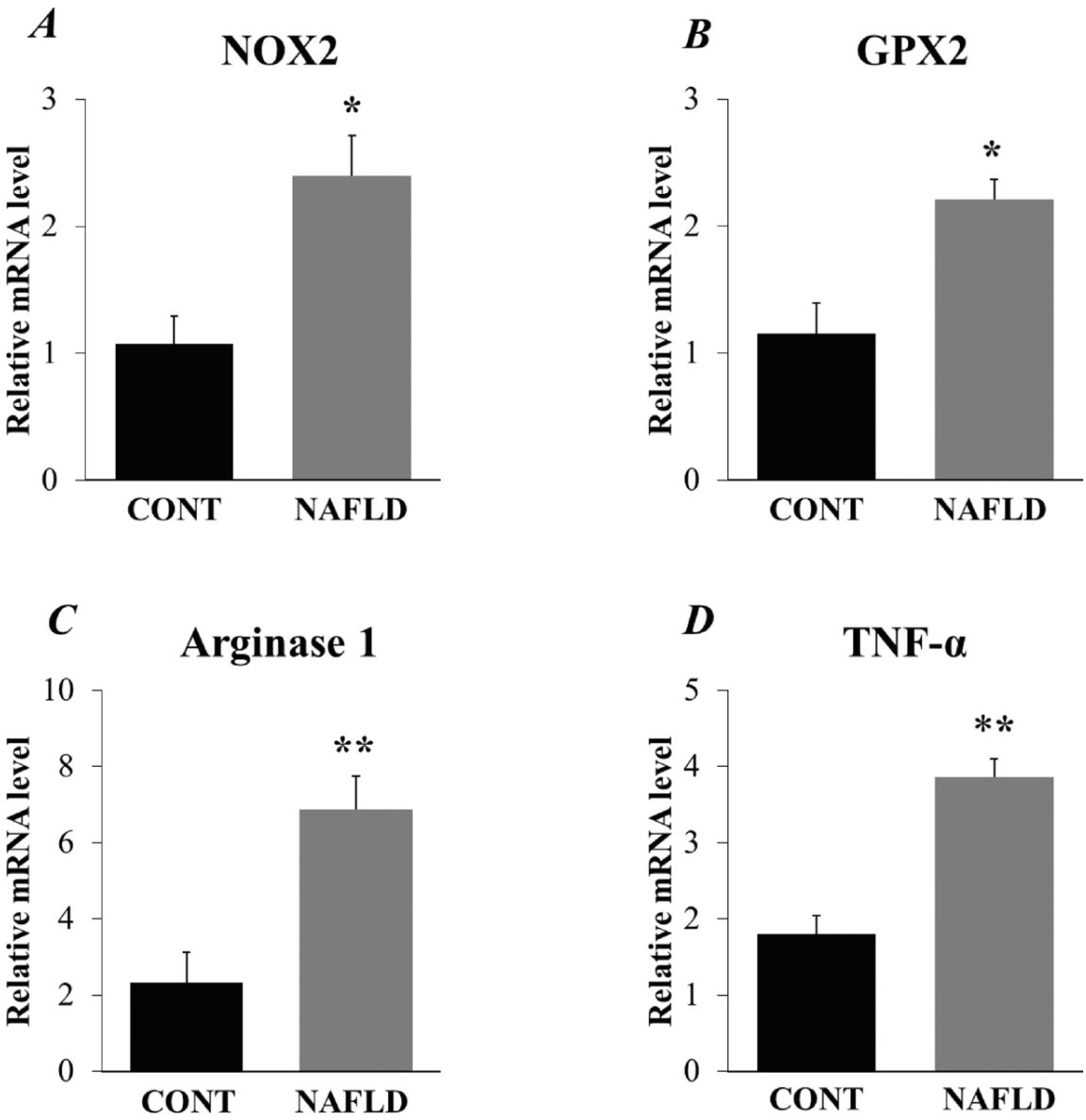

Figure 16. Oxidative stress biomarkers, arginase 1, and inflammatory cytokine gene expression were elevated in uninjured GAS muscles of mice with NAFLD. The relative mRNA expression levels of (A) NOX2, (B) GPX2, (C) arginase 1, and (D) TNFα. Target mRNA expressions were normalized to that of mouse L19 mRNA level (n = 4). All values are expressed as means ± SEs. *$P < 0.05$ and **$P < 0.01$ as determined by the Student *t* test. GAS, gastrocnemius; GPx2, glutathione peroxidase 2; NOX2, NADPH oxidase-2; TNF-α, tumor necrosis factor α

Previous studies have demonstrated that chronic oxidative stress, especially that generated by NOX2, upregulates arginase 1 expression, which in turn leads to increased ROS production (Pandya et al., 2019). Thus, the gene and protein expression of arginase 1 from GAS muscle of uninjured NAFLD mice and there corresponding CONT group was quantified. As expected, a significant increase in arginase 1 gene and protein expression was observed in NAFLD GAS muscle ($P < 0.05$) compared with that of the CONT mice (Figure 16C, Figure 17A, C). Next, because arginase 1 is known to induce not only ROS production but also the inflammatory cytokine cascade (Shosha et al., 2020) that directly impairs SC function and muscle regeneration (Chen et al., 2007), the mRNA expression of TNFα in the GAS muscle of NAFLD and CONT mice was evaluated. The result showed that the TNFα transcript level was increased in the GAS muscle of NAFLD mice when compared with that of the CONT muscle ($P < 0.01$) (Figure 16D). These data were consistent with depletion of the SC pool and decreased expression of the myogenic marker MyoD.

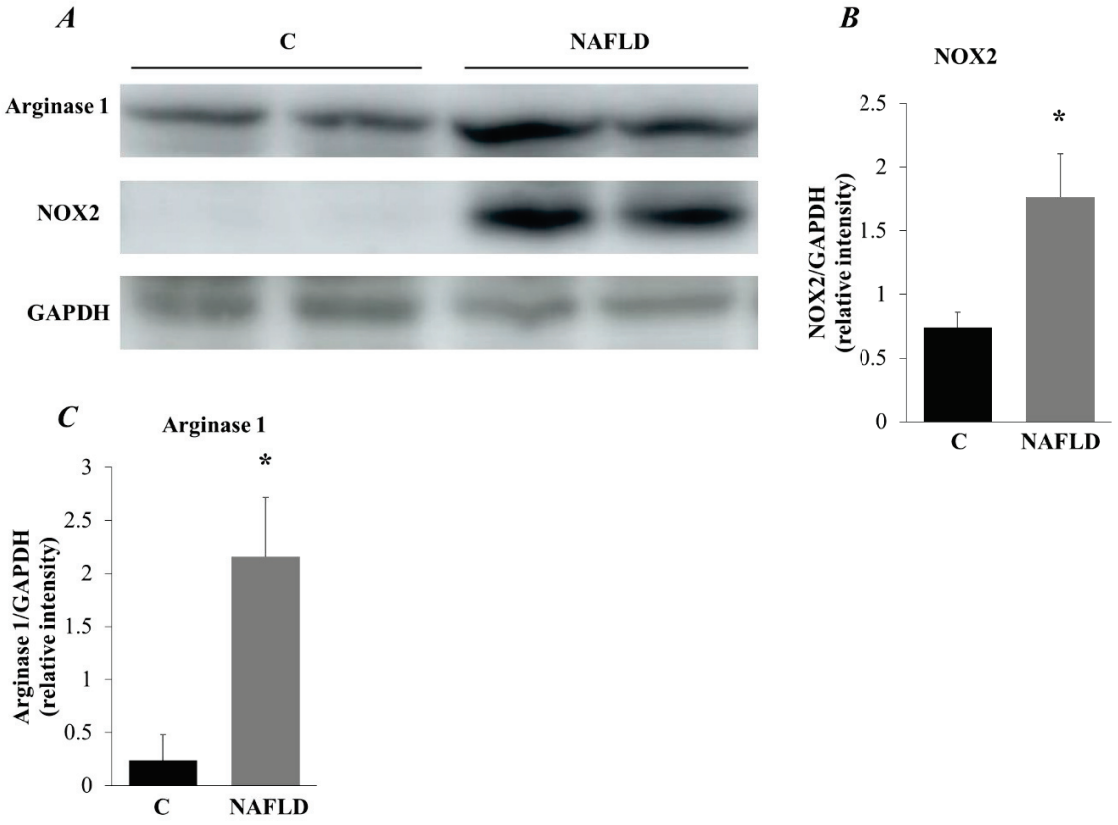

Figure 17. Representative western blot of oxidative stress marker (a) Representative image of western blots of protein extracted from C and NAFLD GAS muscle samples. Densitometry quantification of (b) NOX2 and (c) Arginase 1. Values are normalized to the expression levels of the housekeeping gene GAPDH. Results are means ± SD (n = 4-5, $^{*}p < 0.05$, $^{\#}p < 0.01$); data were analyzed using an unpaired t-test.

3.4. Discussion

Nonalcoholic fatty liver disease is a well-recognized liver disease that has recently gained considerable interest as a risk factor for other chronic diseases. Recent clinical studies have suggested that NAFLD is associated with loss of skeletal muscle mass, also known as sarcopenia (Kim et al., 2018; Pan et al., 2018). In animal experiments, a high-fat diet or westernized diet is widely used to induce NAFLD (Recena Aydos et al., 2019; Tetri et al., 2008), and several studies have been conducted to clarify the causal relationship between NAFLD and sarcopenia and its underlying mechanism (Merli and Dasarathy, 2015). However, because these diets also induce insulin resistance in the skeletal muscles (Pataky et al., 2017), the possibility that the increased insulin resistance triggered by these diets is directly responsible for the loss of skeletal muscle mass observed in mice with NAFLD cannot be ruled out. A nutritional model with a diet deficient in choline is also used in NAFLD research and characterized by an increase in triacylglycerol, steatosis, inflammation, and oxidative stress in the liver (Raubenheimer et al., 2006; Corbin and Zeisel, 2012). Here, the CDD model was applied to study the relationship between NAFLD and skeletal muscle functions. Notably this study showed for the first time that SC content and function are severely impaired in NAFLD mice and that these eventually delay muscle regeneration after injury. Furthermore, this study demonstrated that along with SC dysfunction, there was an increase in the expression level of the oxidative stress biomarker arginase 1 and inflammatory cytokines in the muscle of NAFLD mice. Further studies on the direct relationship between these deleterious agents (oxidative stress, hyperactive arginase pathway, and inflammation) and SC dysfunction in NAFLD mice may be of considerable value. This study's data strongly suggest that the NAFLD environment negatively affects skeletal muscle functions, as indicated by reduced myofiber size compared to that in the CONT group.

Importantly, this phenomenon was observed in the early stages of NAFLD, suggesting that muscle atrophy begins at the early stages of the disease, continues as the disease progresses, and eventually results in the loss of muscle mass.

Alteration in SC content and activity has been linked to a progressive decline in muscle fiber size that eventually leads to a decrease in muscle mass (Alway et al., 2014). This study showed that NAFLD mice exhibited a significant decline in SC population, as defined by a decrease in $Pax7^+$ cells in single myofibers isolated from EDL muscle in a quiescent state and TA muscle sections.

However, the use of CDD raises the question as to whether the choline deficiency or the NAFLD environment causes depletion of the SC pool. To assess whether choline deficiency or the NAFLD environment was responsible for SC decline, isolated single fibers from NAFLD mice and CON mice were cultured in the presence of choline for 24 h and 48 h, respectively. The results indicated that the SC content (defined by the number of $Pax7^+$ cells) was not restored by the exogenously added choline after 24 h of culture. This observation suggested that the NAFLD environment, and not choline deficiency, directly affected SC content. In addition, the study's findings suggested that NAFLD impaired SC function. First, SCs from the muscles of NAFLD mice exhibited a reduced capacity to be activated (as defined by the number of Pax7+ cells after 24-h culture) when compared with those of the CONT mice. Second, the commitment of SCs from NAFLD mice toward myogenic differentiation (as defined by the number of Pax7- /$MyoD^+$ cells after 48 h of culture) was impaired when compared with that from the CONT mice. However, proliferation (defined by the number of $Pax7^+$/$MyoD^+$ cells after a 48 h of culture) and self-renewal capacities (defined by the number of $Pax7^+$/$MyoD^-$ cells after 48 h of culture) of the SCs from NAFLD mice remained indistinguishable from those of the CONT mice. These findings clearly suggested that the NAFLD environment caused a decline in SC population and function (especially SC activation and differentiation).

SCs have been shown to be a major factor for maintaining skeletal muscle and repair (Hawke and Garry, 2001); thus, deficits in the content and function of this group of cells often result in negative consequences in the muscle regeneration process (Lepper et al., 2011; von

Maltzahn et al., 2013). The current study showed that the TA muscles of NAFLD mice exhibited defective muscle regeneration as defined by muscle morphology, fiber size, and distribution at 5 d postinjury. This delay in muscle regeneration may be attributed in part to alteration in SC content and activity, which was observed in this study. Thus, preservation of SC content and functions in individuals with NAFLD may be a potential strategy to prevent the loss of skeletal muscle mass that characterizes NAFLD.

Additionally, this study systematically elucidated the molecular mechanism responsible for the delay in muscle regeneration observed in NAFLD muscle and found that the expression levels of inflammatory cytokines, TNF-α and arginase 1, and oxidative stress markers including NOX2 and GPx2 were markedly increased in the GAS muscles of NAFLD mice. These deleterious agents have been shown to induce SC dysfunction and apoptosis (Perandini et al., 2018; Kozakowska et al., 2015; Choi et al., 2016; Langen et al., 2004) that consequently contribute to loss of skeletal muscle mass. Strikingly, several studies have indicated that an increase in the level of inflammatory cytokines (e.g., TNF-α and IL-1 β) contributes to the development of muscle atrophy by directly or indirectly impairing SC differentiation (Perandini et al., 2018; Langen et al., 2004). A well-studied indirect mechanism through which chronic inflammation causes progressive loss of muscle mass is by inducing the production of ROS, thereby triggering apoptosis of muscle cells (Kozakowska et al., 2015; Choi et al., 2016; Chhetri et al., 2018; Dalle et al., 2018; Powers et al., 2005). Production of ROS by inflammatory cytokines is mediated through mitochondria and NOX enzyme activation (Yang et al., 2007; Langen et al., 2002; Kim et al., 2007). Increased NOx2 expression not only elevates ROS production, but also increases arginase 1 expression (Rojas et al., 2017). Increased expression of arginase 1 in turn stimulates the production of more ROS, thereby worsening muscle degeneration (Rojas et al., 2017; De Palma et al., 2014). The increase in the expression of inflammatory cytokines in the GAS muscle of NAFLD observed in this study is interesting because chronic inflammation has been frequently reported to mediate NAFLD and extra hepatic complications (VanWagner and Rinella, 2016; Bullón-Vela et al., 2020). Thus, based on these previous findings, the increase in serum TNF-α level and hepatic expression level of

inflammatory cytokines (TNF-α and IL-1 β) found in this study was proposed to be directly responsible for the elevation of inflammatory cytokine TNF-α in the GAS muscle of NAFLD mice, which may explain the decrease in SC differentiation, as evidenced by the reduction in the myogenesis marker MyoD. Furthermore, the increase in the inflammatory cytokine was also hypothesized to trigger ROS production and subsequently increase arginase 1 expression, which in turn stimulates the production of more ROS and eventually causes the death of more SCs. Thus, it is interesting to speculate that the decline in the SC pool observed in this study may be owed to ROS-induced apoptotic insult. However, future studies are needed to validate this by directly measuring the level of ROS in the muscle of mice with NAFLD. In addition, it is crucial to elucidate whether the generated ROS triggers apoptosis or autophagy of SCs in NAFLD muscle. Finally, the role of arginase 1 in the progression of NAFLD myopathy needs to be established using an arginase 1 inhibitor.

Abstract

Muscle wasting is a common complication in patients with nonalcoholic fatty liver disease (NAFLD). In this study, we investigated the effect of NAFLD on satellite cell (SC) content and skeletal muscle repair. Male CD-1 mice fed a choline-deficient diet for 4 wk were used as an NAFLD model. Histologic and mRNA expression analyses, immunochemical staining with single muscle fibers was performed to assess the effect of NAFLD on muscle Pax7+ SCs, and muscle regeneration by intramuscular injection of cardiotoxin. The result showed that the total number of Pax7+ SCs in the extensor digitorum longus and tibialis anterior muscles of mice with NAFLD was significantly decreased when compared with that in the control group, in which the depletion of the SC pool possibly impaired muscle regeneration, as evidenced by the smaller size of the regenerating myofibers. Importantly, NAFLD was found to significantly impaired the differentiation ability of SCs, as shown by a decreased number of SCs expressing a myogenic marker, MyoD. Finally, this study indicated that molecular mechanisms underlying a decline in SC numbers may be attributed to the upregulation of proinflammatory cytokines (tumor necrosis factor α [TNFα]) and an oxidative stress marker (NADPH oxidase-2 [NOX2\) in mice with NAFLD. The findings demonstrate that a decrease in SC content in the skeletal muscle is an important factor that contributes to muscle wasting in NAFLD. Thus, preservation of the muscle SC pool is a potential therapeutic strategy to reduce NAFLD-associated muscle wasting.

Chapter 4

Experiment 2

Comparative study on molecular mechanism of diabetic myopathy in two different types of streptozotocin-induced diabetic models

4.1 Introduction

Skeletal muscle is the largest organ in the body and is a major determinant of the whole-body energy balance and basal metabolic rate (Frontera and Ochala, 2015; Pedersen and Febbraio, 2008). Muscle, due to its high regenerative potential, has a remarkable capacity for growth and repair after injury. A critical component responsible for these processes is the presence of satellite cells (SCs), which are primary muscle stem cells (Relaix and Zammit, 2012). Skeletal muscle is a highly resilient tissue that can adapt to numerous stimuli. However, numerous studies have shown that this process can be compromised in chronic disease states such as diabetes.

Muscle dysfunction is a major complication associated with diabetes (Wang et al., 2020; Vignaud et al., 2007) and can result not only in physical disability but also in metabolic disorders such as abnormal accumulation of fat and alteration in glucose metabolism (Meex et al., 2019). Unfortunately, because the number of patients with diabetes mellitus has increased in the recent years (Lin et al., 2020), it is critical to understand the molecular mechanisms underlying diabetic myopathy, which is a serious diabetic complication that is often overlooked. However, a major concern in devising innovative therapeutic strategies is obtaining a relevant animal model that can mirror this pathophysiology observed in the patients.

Currently, the streptozotocin (STZ) model is widely used to characterize diabetic myopathy in vivo as well as to examine the effect of food factors on the regulation of skeletal muscle mass (Kivelä et al., 2006; Arcaro et al., 2021; Copray et al., 2000; Fujimak et al., 2016; Jeong et al., 2013). However, recent studies have shown that at high doses, owing to its non-specific cytotoxicity, STZ can cause direct acute kidney damage in animals (Mohammed-Ali et al., 2017; Breyer et al., 2005). Due to this nonspecific cytotoxicity of STZ at high dose, it would

be difficult to ascertain whether the changes seen in STZ-induced diabetic mice skeletal muscle are due to a direct toxic action of STZ or are caused by hyperglycemia/hypoinsulinemia. In addition, in human patients, diabetic myopathy is often associated with insulin resistance; this is not commonly seen in high-STZ-induced diabetic model (Chao et al., 2018).

A high-fat diet and low-dose STZ (HFD/STZ) model was established to reduce the nonspecific cytotoxic effect of STZ; at the same time, insulin resistance was found to be more marked in this model. This model involves the administration of high-fat chow for 4 weeks followed by injection with a low dose of STZ (40–60 mg/kg) for 5 consecutive days (Chao et al., 2018; Zhang et al., 2008). To address the concerns raised regarding the use of high-dose STZ for studies on diabetic myopathy, this study aimed to compared these two STZ models (high-dose STZ model and HFD/STZ model) with the goal of obtaining the best suitable animal model that mirrors the pathology of human diabetic myopathy. The alterations in diabetic skeletal muscles in these two STZ models was evaluated using histological and gene expression analyses. The results indicate that despite the similarity in some of the parameters tested, significant differences can be observed between different diabetic models, and these unique characteristics found in each model mirror specific conditions as seen in patients. This suggests that either of the models can be selectively used in different contexts according to the purpose of studies on diabetic myopathy.

4.2. Materials and methods

4.2.1. Animals

Animal studies were performed in accordance with the protocols approved by the Hiroshima University Animal Care and Use Committee (Permit Number: C18-15-5). Male C57BL/6J mice (Charles River Japan, Hino, Japan) at postnatal week 7 were used in this study. Two types of diabetes models were used to study diabetic myopathy. For the first model, mice fed a standard laboratory chow diet (MF, Oriental Yeast, Tokyo, Japan) and given a single intraperitoneal high-dose STZ (Sigma-Aldrich, Louis, MO) (180 mg/kg dissolved in 0.1 M

citrate buffer, pH 4.5) (high-STZ group) was utilized as the test group. Similarly, the control group (CON group), was fed a standard laboratory chow diet, however, only 0.1 M citrate buffer, pH 4.5 was given to mice in this group. The mice in this first model were analyzed 4 weeks after STZ treatment. Meanwhile, for the second model, a control group fed a standard laboratory chow diet (CON group), and a test group fed a high-fat diet (HFD) (Oriental Yeast Co., Tokyo, Japan; 45% fat, 20.5% protein, and 34.8% carbohydrate) together with low-dose STZ (55 mg/kg for 5 consecutive days) (HFD/STZ group) were utilized. As a CON group, mice received vehicle injections (0.1 M citrate buffer, pH 4.5) for 5 consecutive days. Notably, the HFD/STZ group mice were initially placed on HFD for 4 weeks and in week four, they were injected with low-dose STZ; they were subsequently maintained on HFD for an additional 12 weeks after the STZ treatment. In both models, only those animals with fasting blood glucose levels ≥300 mg/ dl were considered diabetic. All mice were given free access to drinking water, and they were housed in metal cages in a room with controlled temperature (24 ± 1 °C), 50 ± 20% humidity, and a 12:12-h light-dark cycle.

4.2.2. Tissue preparation

The right and left tibialis anterior (TA), extensor digitorum longus (EDL), gastrocnemius (Gas), soleus (Sol), and quadriceps (Quad) muscles from all groups were isolated, weighed, and snap-frozen in liquid nitrogen, except for the TA muscle, which was covered with optimum cutting temperature embedding compound (OCT) and immediately frozen in liquid nitrogen-cooled isopentane. All tissues were stored at -80 °C until analysis.

4.2.3. Histological analysis

To determine the myofiber size, hematoxylin and eosin (H&E) staining was performed as established previously [17] on TA muscle cryosections (8 μm thick). Approximately 120 fibers were analyzed per muscle section.

4.2.4. Immunohistochemistry

Frozen sections of the TA muscle (6 μm thick) were fixed in 4% paraformaldehyde for 20 min at room temperature (RT, approximately 25 ± 5 °C). Then, sections were incubated with a solution consist of 2% BSA, 0.1% sodium azide, 5% fetal bovine serum, 5% normal goat serum, and 0.2% Triton-x100 for 1 h at RT, followed by an incubation with mouse IgG-blocking solution from the M.O.M kit (Vector laboratories Inc., USA) for 1 h at RT. The sections were then incubated with primary antibodies (mouse anti-Pax7 (1:100; DSHB) and rabbit anti-laminin (1:500; Abcam ab11575) overnight at 4 °C, followed by incubation with secondary antibodies (goat anti-mouse IgG1 Alexa-594 (1:1000; Invitrogen A-21125) and Fluorescein (FITC)-AffiniPure goat anti-rabbit IgG (1:500; Jackson Immuno Research 111-095-003) at RT for 1 h. Sections were subsequently counterstained with 1 μg/ml DAPI for 10 min at RT.

4.2.5. Microscopy and image analysis

All images were captured by Olympus BX53 microscope (Olympus, Tokyo, Japan) and analyzed by Nikon Elements imaging software (Nikon, Tokyo, Japan) was used to analyze them. The analysis included quantification of SC numbers (Pax7+/DAPI+) on immuno-stained TA muscle sections and average myofiber size in H&*E*-stained TA muscle sections.

4.2.6. DNA microarray assay

Total RNA from Gas muscles was isolated using the RNeasy Lipid Tissue Kit (Qiagen Sciences, Germantown, MD, USA) according to the manufacturer's protocol. Pooled RNAs were subjected to cRNA synthesis for DNA microarray analysis with 44 K whole mouse genome 60-mer oligo microarray (Agilent Technologies, Palo Alto, CA) according to our previous report (Krause et al., 2011). All fluorescence labeling, hybridization, and image processing procedures were performed according to the manufacturer's instructions. Each comparison was hybridized to two arrays employing a DyeSwap method in order to eliminate the bias between dyes because of the difference in the efficiency of hybridization between cyanine 3-CTP and cyanine 5-CTP. Files and images were exported from the Agilent Feature Extraction Program (version 9.5). The expression values were normalized and subsequently

scaled. To determine the cutoff of significant differences for differentially expressed genes the *P* values were corrected for a false discovery rate of <0.05.

4.2.7. Gene functional classification

For efficient interpretation of the differently expressed gene lists the Database for Annotation, Visualization, and Integrated Discovery (DAVID) (version 6.8) (Huang et al., 2009) was used to organize functionally related genes into biologically meaningful modules. As a precautionary measure duplication of the official gene symbols input into the analysis was avoided. Functional clusters with enrichment (EASE) score ≥ 1.3 were selected to be functionally significant.

4.2.8. Quantitative PCR

Total RNA was isolated from Gas muscles of each group using the RNeasy Lipid Tissue Kit (Qiagen Sciences, Germantown, MD, USA). ReverTra Ace (TOYOBO, Osaka, Japan) and random hexamers (TaKaRa Bio, Kyoto, Japan) were used to synthesize cDNA according to the manufacturer's instructions. Quantitative PCR was performed on an Applied Biosystems StepOnePlus™ system using THUNDERBIRD™ Next SYBR qPCR Mix (TOYOBO) with the conditions as described previously (Mitsumoto et al., 2017). The threshold cycle (CT) values were normalized to the L19 internal reference. The primers used were obtained from Eurofin Genomics (Tokyo, Japan) (Table 4).

Table 4. Primer sequences for qPCR.

Target gene	Sequence (5'-3')	
L19	Forward	GGCATAGGGAAGAGGAAGG
	Reverse	GGATGTGCTCCATGAGGATGC
Ddit4/Redd1	Forward	GTGCTGCGTCTGGACTCTC
	Reverse	CCGGTACTTAGCGTCAGGG
Perm1	Forward	GCTTGGAAAACAGTCTTGCTC
	Reverse	GATCTCGGTCTGCCACTATG
Idh2	Forward	ATCAAGGAGAAGCTCATCCTGC
	Reverse	TCTGTGGCCTTGTACTGGTCG
Pdp1	Forward	ATGCCAGCACCAACTCAACT
	Reverse	GGGTGTGTACCTCAGACGATT
C/EBPδ	Forward	GAACCCGCGGCCTTCTA
	Reverse	TGTTGAAGAGGTCGGCGA
Ccl7	Forward	CAATGCATCCACATGCTGC
	Reverse	TGGAGTTGGGGTTTTCATGTC
Col1a1	Forward	CCCAAGGAAAAGAAGCACGTC
	Reverse	ACATTAGGCGCAGGAAGGTCA
Col3a1	Forward	TGGTCCTCAGGGTGTAAAGG
	Reverse	GTCCAGCATCACCTTTTGGT
Irf7	Forward	GAAGTGAGCCTCAGCAATGC
	Reverse	GGTTCCTCGTAAACACGGTC
Fbxo32(Atrogin1)	Forward	CAGCTTCGTGAGCGACCTC
	Reverse	GGCAGTCGAGAAGTCCAGTC
ATF3	Forward	AAGAGCTGAGATTCGCCATC
	Reverse	TCTTCAGCTCCTCAATCTGG
Klf15	Forward	CTCAAAGTTTGTGCGAATTG
	Reverse	GTGCCTTGACAACTCATCTG
Ifi44	Forward	AACTGACTGCTCGCAATAATGT
	Reverse	GTAACACAGCAATGCCTCTTGT
PPARα	Forward	CGACCTGAAAGATTCGGAAA
	Reverse	GGCCTTGACCTTGTTCATGT
Trim63(MuRF1)	Forward	GTTTGACACCCTCTACGCCA
	Reverse	TGAGAGGAAGGTAGCCCCTC

4.2.9. ATP level estimation

Adenosine triphosphate (ATP) levels was evaluated in Quad muscle tissues using luciferin-luciferase assay kit (Fujifilm Wako Pure. Chemical, Tokyo, Japan). Briefly, 20 mg of Quads

tissues were weighed, lysed, and then centrifuged at 12,000 ×*g* at 4 °C for 5 min. Supernatants (20 μl) were added to 100 μl of detection working solution in a white 96-well plate. The ATP standard curve was used to calculate ATP concentration in each muscle sample.

4.2.10. Corticosterone levels measurement

Approximately 1 ml of blood was collected from each mouse at the end of each model experiment, and plasma corticosterone concentration (ng/ml) was subsequently measured using an enzyme immunoassay assay kit (Cayman Chemical Co., Ann Arbor, MI, USA) according to the manufacturer's instructions.

4.2.11. Western blot analyses

Equal amounts of protein derived from quad*riceps* (Quad) muscle was resolved by SDS-PAGE, transferred onto a polyvinylidene difluoride (PVDF) membranes (Bio-Rad, Missisauga, Ontario), nonspecific binding sites were blocked by incubation in 3% BSA or 5% skim milk, depending on the antibody at room temperature (RT) for 1 hr. Subsequently, the membranes were incubated with the following primary antibodies: anti-Fbx-32 (ab168372, Abcam, Cambridge, UK), anti-MuRF-1 (sc-398608, Santa Cruz Biotechnology, Santa Cruz, CA), anti-α-tubulin (FUJIFILM Wako Pure Chemical Corporation, Osaka Japan) anti-TFAM (2148), anti-P70S6K (9202S), and anti-p-P70S6K (9206S) were provided by Cell Signaling Technology (Boston, MA, USA) overnight at 4°C, followed by incubation with an appropriate secondary antibody for 1 hr at RT. Proteins were then visualized with an ECL western blot detection system

4.2.12. Statistical analysis

All data are expressed as the mean ± S.E. The differences in level of significance between the compared groups were determined using the Student's *t*-test. $P < 0.05$ was considered as statistically significant (denoted appropriately in all figures).

4.3. Results

4.3.1. Body weights and fasting blood glucose levels in STZ models

In both STZ models, body weights were significantly reduced compared with control mice; however, weight loss in the high-STZ model between the induction of diabetes at week 0 and week 4 was significantly higher than that in the HFD/STZ model which was analyzed at the end of 12 weeks after diabetic induction (Figure 18A-D). In addition, as shown in Figure 18E and F, the fasting blood glucose levels in both STZ models gradually increased throughout the experimental period; however, the fasting blood glucose level was significantly higher in the high-STZ model (928.5 mg/dl at the end of week 4 after diabetic induction) than that in the HFD/STZ model (528.5 mg/dl at the end of week 12 after diabetic induction). This suggested that in the high-STZ model, rapid loss of insulin secretion (and therefore more severe hyperglycemia) was induced when compared with the HFD/STZ model. These observations are consistent with those reported in the previous studies indicating that STZ exerts a toxic effect on pancreatic beta cells in a dose-dependent manner (Lu et al., 1998; Saini et al., 1996).

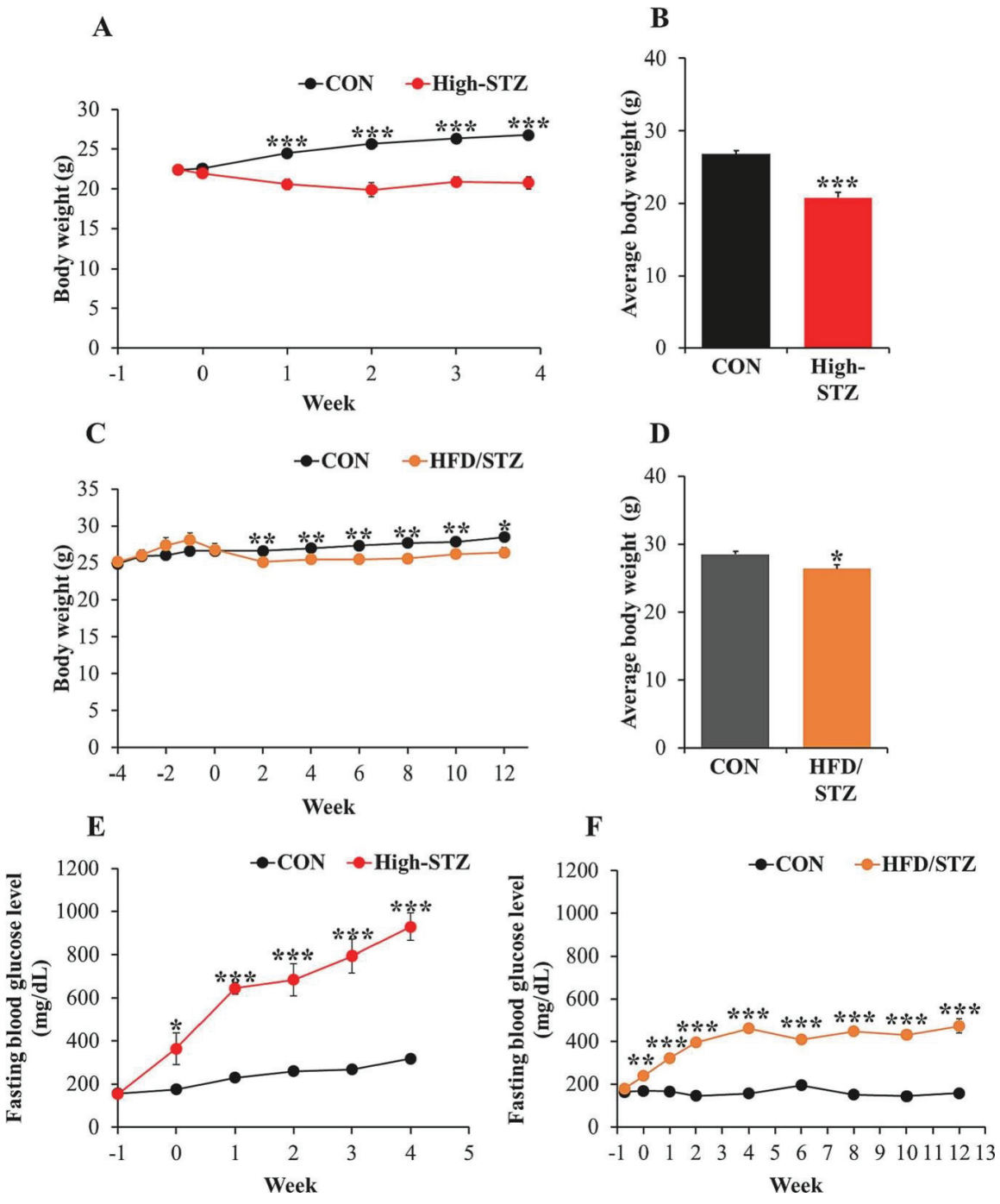

Figure 18. Pathological assessment of diabetes in High-STZ and HFD/STZ models. (A-B) Body weights of high-STZ mice decrease significantly when compared with the matched control (CON) mice. (C-D) Body weights of HFD/STZ mice decrease significantly when compared with the matched control (CON) mice. (*E*-F) Fasting blood glucose levels increase

in both experimental models. All values are expressed as means ± S.E. *$p < 0.05$, **$p < 0.01$, ***$p < 0.001$ as determined by Student's *t*-test (high-STZ $n = 5$ and its matched CON $n = 5$; HFD/STZ $n = 6$ and its matched CON n = 5).

4.3.2. Muscle mass differed between high-STZ and HFD/STZ models

As previously reported, the high-STZ model results in a loss of skeletal muscle mass (Fujimak et al., 2016; Jeong et al., 2013). The analysis of the high-STZ model showed that the muscle masses of tibialis anterior (TA), extensor digitorum longus (EDL), gastrocnemius (Gas), soleus (Sol), and quadriceps (Quad) were significantly decreased when compared with the control (Figure 19A). In contrast, the HFD/STZ model exhibited a substantial change only in the Gas muscle mass when compared with the control (Figure 19B).

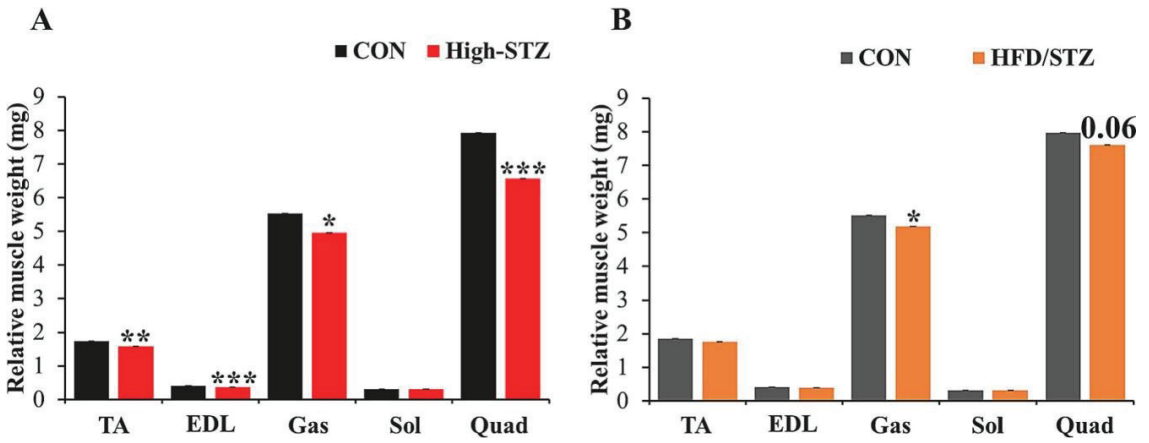

Figure 19. Relative muscle weights in High-STZ and HFD/STZ models. (A) Muscle weights in high-STZ model and (B) muscle weight in HFD/STZ model. All values are expressed as means ± S.E. *$p < 0.05$, **$p < 0.01$, ***$p < 0.001$ as determined by Student's *t*-test (high-STZ $n = 5$ and its matched CON n = 5; HFD/STZ $n = 6$ and its matched CON n = 5).

4.3.3. Myofiber size was smaller in high-STZ mice than in HFD/STZ mice

H&E staining of TA middle cross sections from the mice in both STZ models are shown in Figure 20A and B. The average muscle fiber size declined by 52% and 18% in the high-STZ and HFD/STZ models, respectively, when compared with their matched control group (Figure 20C and D). Furthermore, the changes in muscle fiber size were analyzed using the

myofiber size distribution in each model. As shown in Figure 20E and F, a significantly greater number of smaller myofibers was observed in the high-STZ model than in the HFD/STZ model when compared with their matched control mice. Taken together, these observations suggest that the high-STZ model mice show more severe diabetic myopathy than the HFD/STZ model mice.

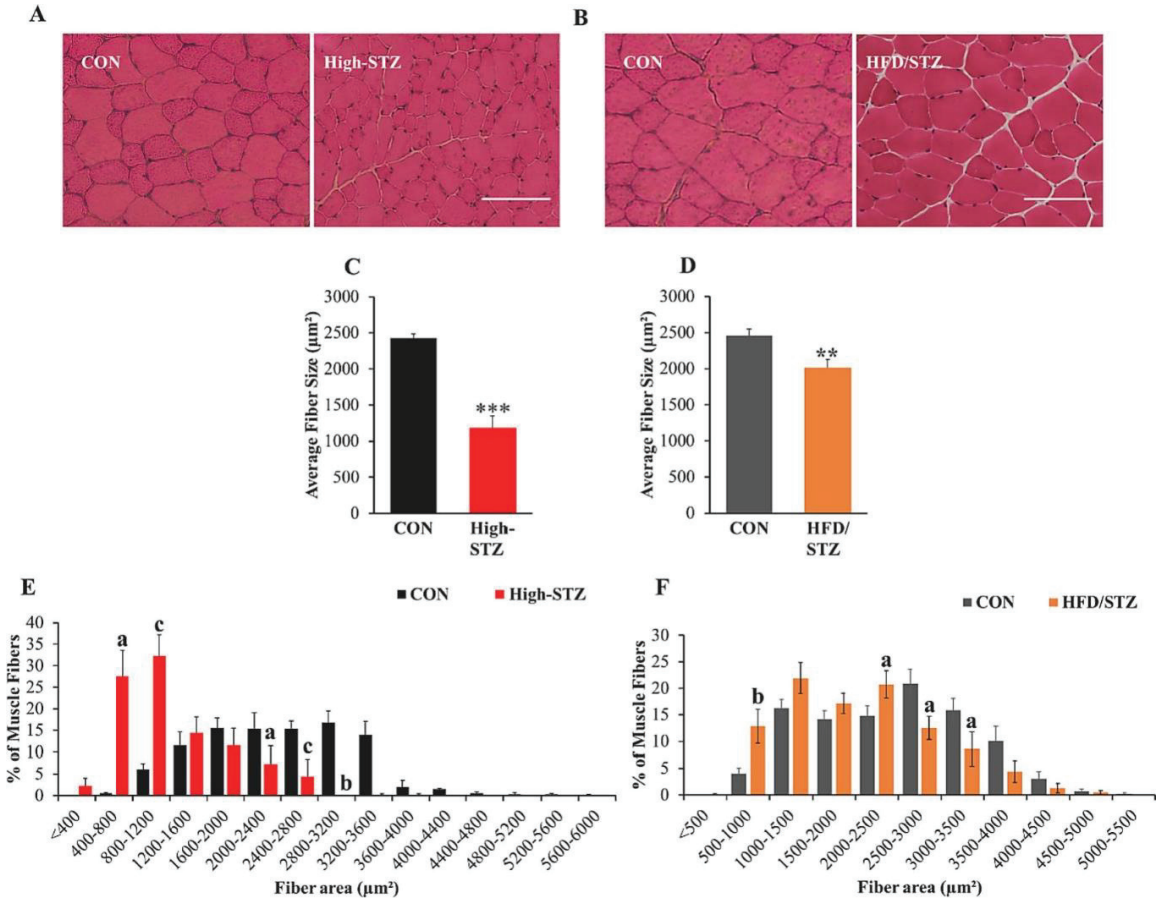

Figure 20. High dose STZ model muscles display more severe muscle fiber atrophy compared with the low dose STZ/HFD model. (A-B) Representative image of H&E stained cryosections of TA muscles obtained from the high-STZ model and the HFD/STZ model. Scale bars represent 200 µm. (C-D) Quantification of average myofiber cross-sectional area of TA muscles from both STZ models and their matched CON. (C) Muscle fiber diameter distribution in both STZ models. An average of 120 fibers was randomly counted per a muscle section. All values are expressed as means ± S.E. $^{a}/*p < 0.05$, $^{b}/**p < 0.01$, $^{c}/***p < 0.001$ as determined by Student's *t*-test (high-STZ $n = 5$ and its matched CON n = 5; HFD/STZ $n = 6$ and its matched CON n = 5). Control mice (CON), tibialis anterior (TA), and hematoxylin and eosin (H&E).

4.3.4. Loss of satellite cells was more pronounced in the high-STZ model than in the HFD/STZ model

Because alteration in SC content can have a negative impact on the muscle physiology (Wang and Rudnicki, 2012), SC numbers were quantified in sections of TA muscles obtained from both models and their corresponding controls by scoring Pax7+ immunoreactive SCs. The analysis of the result showed a dramatic decrease in the SC content in both the models. However, the decrease in the number of SCs was more severe in the high-STZ model (approximately 69% loss) than that in the HFD/STZ model (approximately 32% loss) (Figure 21A-D).

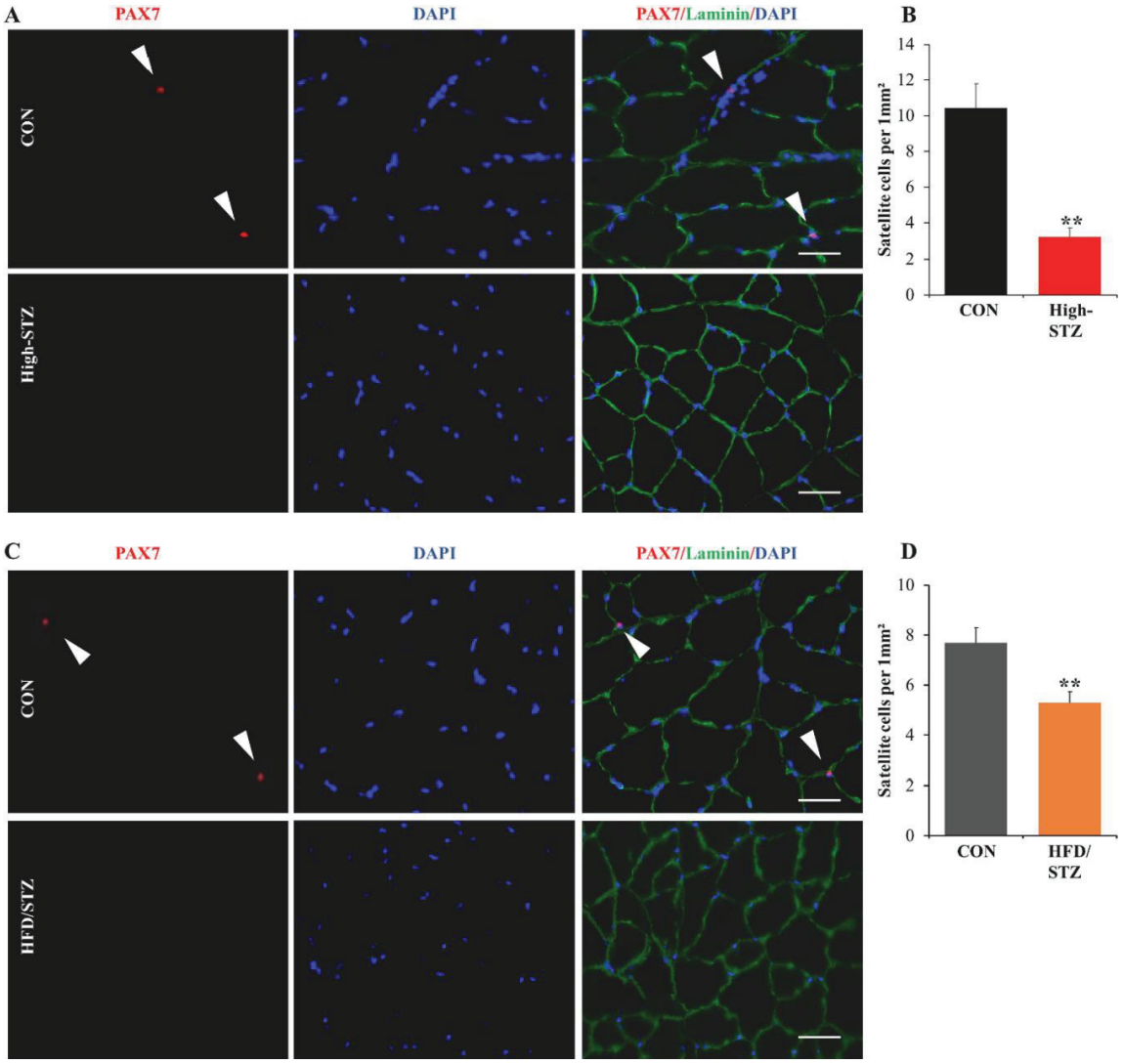

Figure 21. Satellite cell (SC) content is more reduced in the High-STZ model. (A) Representative image of SC showing laminin (green), Pax7 (red), and myonuclei (blue) in the high-STZ and its matched CON muscles. (B) Number of Pax7+ SC/1 mm^2 CSA in the TA muscle of the high-STZ mice. (C) Representative image of SC showing laminin (green), Pax7 (red) and myonuclei (blue) in the HFD/STZ and its matched CON muscles. (D) Number of Pax7+ SC/1 mm^2 CSA in the TA muscle of the HFD/STZ mice. Scale bars represent 200 μm. Statistical analysis was performed using Student's *t*-test (**$p < 0.01$); high-STZ and its matched CON ($n = 5$, n = 5, respectively), HFD/STZ and its matched ($n = 6$, n = 5, respectively). Control mice (CON), tibialis anterior (TA), cross sectional area (CSA).

4.3.5. Molecular signatures related to muscle atrophy in both the models

To understand the cascade of events that triggers muscle atrophy in each model, the gene expression profiles was characterized in order to identify differentially expressed genes in the Gas muscle from the high-STZ and HFD/STZ models using DNA microarray analyses. The microarray analysis showed that 504 genes were differentially expressed between the two STZ models, with 25 genes upregulated and 19 genes downregulated in both the models (Figure 22).

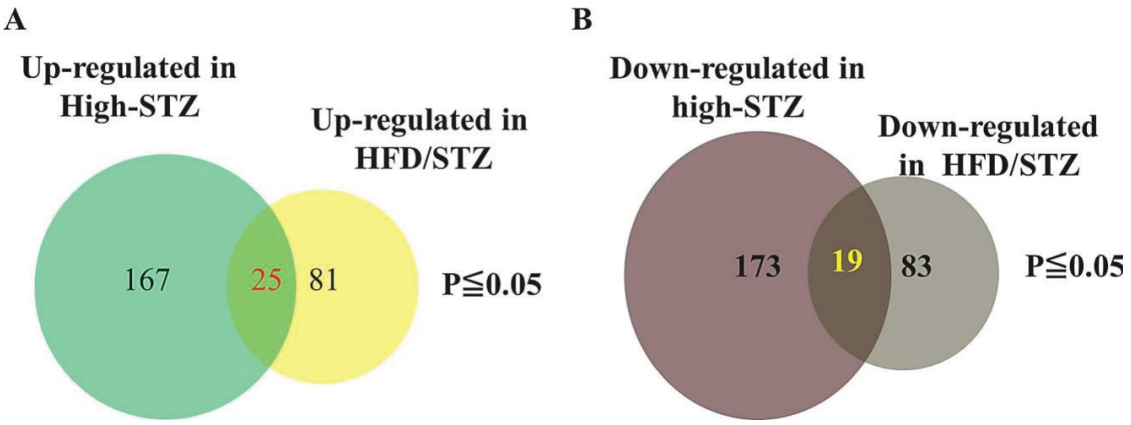

Figure 22. Venn diagram shows the number of genes that are upregulated and down-regulated in the skeletal muscle of High-STZ and HFD/STZ model. (A) Number of upregulated genes (B) Number of Down-regulated genes. *$p < 0.05$. The data are representative of two independent experiments (i.e., high-STZ model and HFD/STZ model).

These genes were classified into the following seven categories: inflammation/immune response, extracellular matrix and cell adhesion, proteolysis and response to glucocorticoids, muscle structure and regeneration, metabolism, cell signaling/cell communication, cell cycle, and apoptotic markers (Table 5, Table 6) using Database for Annotation, Visualization, and Integrated Discovery (DAVID) (version 6.8) (Huang et al., 2009).

Table 5: Selected genes differentially expressed in High-STZ skeletal muscle but not in HFD/Low STZ skeletal muscle.

Gene ID	Gene symbol	Gene description	Fold	P value
Inflammation and immune response				
NM_013654	Ccl7	chemokine (C-C motif) ligand 7	0.18	0.009
NM_011333	Ccl2	chemokine (C-C motif) ligand 2	0.15	0.000
NM_019577	Ccl24	chemokine (C-C motif) ligand 24	0.46	0.000
NM_009895	Cish	cytokine inducible SH2-containing protein	0.13	0.000
NM_021274	CXCL10	chemokine (C-X-C motif) ligand 10	0.40	0.000
NM_010696	LCP2	lymphocyte cytosolic protein 2	0.38	0.001
NM_153098	Cd109	CD109 antigen	0.14	0.000
NM_207105	H2-Ab1	histocompatibility 2, class II antigen A, beta 1	0.54	0.000
NM_009382	Thy1	thymus cell antigen 1	0.36	0.000
NM_008677	Ncf4	neutrophil cytosolic factor 4	0.48	0.000
NM_010745	Ly86	lymphocyte antigen 86	0.55	0.000
NM_027366	Ly6g6e	lymphocyte antigen 6 complex, locus G6E	0.09	0.000
NM_011210	Ptprc	protein tyrosine phosphatase, receptor type, C	0.45	0.000
NM_178611	Lair1	leukocyte-associated Ig-like receptor 1	0.39	0.000
NM_033478	Ly6g6d	lymphocyte antigen 6 complex, locus G6D	0.39	0.004
NM_027077	1700016C15Rik	RIKEN cDNA 1700016C15 gene	0.45	0.004
Extracellular matrix and cell adhesion				
NM_007742	Col1a1	collagen, type I, alpha1	0.26	0.000
NM_031163	Col2a1	collagen, type II, alpha 1	0.27	0.000
NM_009930	Col3a1	collagen, type III, alpha 1	0.34	0.000
NM_007743	Col1a2	collagen, type I, alpha 2	0.41	0.000
NM_007737	Col5a2	collagen, type V, alpha 2	0.37	0.000
NM_009928	Col15a1	collagen, type XV, alpha 1	0.47	0.000
NM_001243008	Col6a3	collagen, type VI, alpha 3	0.47	0.000
NM_033525	Npnt	Nephronectin	0.23	0.001
NM_007993	Fbn1	fibrillin 1	0.27	0.000
NM_009931	Col4a1	collagen, type IV, alpha 1	0.49	0.000
NM_010233	Fn1	fibronectin 1	0.54	0.000
Extracellular matrix degradation and response to glucocorticoid hormone				
NM_013906	Adamts8	a disintigrin-like and metallopeptidase (reprolysin type) with thrombospondin type 1 motif, 8	0.33	0.000
NM_001044384	Timp1	tissue inhibitor of mettalloproteinase 1	0.46	0.000
NM_009825	Serpinh1	serine (or cysteine) peptidase inhibitor, clade H, member 1	0.49	0.000
NM_001024139	Adamts15	a disintegrin-like and metallopeptidase (reprolysin type) with thrombospondin type 1 motif, 15	0.59	0.000
NM_023184	Klf15	Kruppel-like factor 15	2.13	0.000

Muscle structure and regeneration

NM_013602	Mt1	metallothionein 1	2.77	0.000
NM_025540	Sln	sarcolipin	2.44	0.000
NM_001314010	Igf1	insulin-like growth factor 1	0.43	0.006
NM_011056	Pde4d	Phosphodiesterase 4D, cAMP specific	2.48	0.000

Metabolism

NM_010292	Gck	glucokinase	0.47	0.000
NM_009022	Aldh1a2	aldehyde dehydrogenase family 1, subfamily A2	0.57	0.000
NM_009997	Cyp2a4	cytochrome P450, family 2, subfamily a, polypeptide 4	0.33	0.000
NM_144903	Aldob	adolase B, fructose-bisphosphate	0.34	0.000
NM_133232	Pfkfb3	6 –phosphofructo-2-kinase/fructose-2,6-biphosphatase 3	2.06	0.000
ENSMUST00000	Mrpl15	mitochondrial ribosomal protein L15	2.24	0.000
NM_008890	Pnmt	Phenylethanolamine-N-methyltransferase	2.50	0.000
NM_001077495	Pik3r1	Phosphoinositide-3-kinase regulatory subunit 1	2.64	0.000
X16314	Glul	Glutamine synthetase.	3.35	0.000
NM_007817	Cyp2f2	Cytochrome P450, family 2, subfamily f, polypeptide 2	2.49	0.000

Cell signaling and cell communications

NM_147217	Gprc5c	G protein-coupled receptor, family C, group 5, member C	0.48	0.000
NM_016769	Smad3	SMAD family member 3	0.54	0.000
NM_015814	Dkk3	dickkopf WNT signaling pathway inhibitor 3	0.36	0.000
NM_178404	Zc3h6	zinc finger CCCH type containing 6	2.03	0.000
NM_011817	Gadd45g	growth arrest and DNA-damage-inducible 45 gamma	2.65	0.001

Cell cycle and apoptotic markers

NM_007669	Cdkn1a	cyclin-dependent kinase inhibitor 1A	2.15	0.000
NM_178373	Cidec	cell death-inducing DFFA-like effector c	2.05	0.000
NM_030250768	Pdcd4	programmed cell death 4	3.51	0.000
NM_010019	Dapk2	death associated protein kinase 2	0.37	0.000
S78355	Ccnd1	cyclin D1	0.49	0.000
NM_010118	Egr2	early growth response 2	2.16	0.000
NM_001161433	Eda2r	ectodysplasin A2 receptor	2.53	0.000

NM_011817	Gadd45g	growth arrest and DNA-damage-inducible 45 gamma	2.65	0.001
ENSMUST00000	Anapc16	anaphase promoting complex subunit 16	3.19	0.000
ENSMUST00000	Prickle3	prickle planar cell polarity protein 3	3.70	0.000
ENSMUST00000	Dele1	DAP3 binding cell death enhancer 1	2.00	0.001
NM_009741	Bcl2	B cell leukemia/lymphoma 2	0.57	0.000

Fold represents the average of mRNA expression level in the gastrocnemius (Gas) muscle from the high-STZ mice relative to its matched control. The data are representative of two independent experiment.

Table 6: Selected genes differentially expressed in HFD/Low STZ skeletal muscle but not in High-STZ skeletal muscle

Gene ID	**Gene symbol**	**Gene description**	**Fold**	**P value**
Inflammation and immune response				
NM_021443	Ccl8	chemokine (C-C motif) ligand 8	6.00	0.000
NM_009139	Ccl6	chemokine (C-C motif) ligand 6	2.08	0.000
NM_011338	Ccl9	chemokine (C-C motif) ligand 9	2.23	0.000
NM_011331	Ccl12	chemokine (C-C motif) ligand 12	3.11	0.000
NM_029803	Ifi2712a	Interferon, alpha-inducible protein 27-like 2a	3.69	0.000
NM_183871	Ifi44	Interferon-induced protein 44	4.42	0.000
NM_008331	Ifit1	Interferon-induced protein with tetratricopeptide repeats 1	2.56	0.000
NM_016850	Irf7	Interferon regulatory factor 7	3.01	0.000
NM_008599	Cxcl9	chemokine (C-X-C motif) ligand 9	1.83	0.000
NM_145209	Oasl1	2'-5' oligoadenylate synthetase-like 1	5.42	0.000
NM_145227	Oas2	2'-5' oligoadenylate synthetase 2	4.49	0.000
NM_145211	Oas1a	2'-5' oligoadenylate synthetase 1A	3.39	0.000
NM_0111854	Oasl2	2'-5' oligoadenylate synthetase-like 2	3.30	0.000
NM_145153	Oas1f	2'-5' oligoadenylate synthetase 1F	2.77	0.000
NM_009780	C4b	complement component 4B	3.10	0.000
NM_008198	Cfb	complement factor B	2.27	0.000
NM_007796	Ctla2a	cytotoxic T lymphocyte-associated protein 2 alpha	2.22	0.000
NM_001077189	Fcgr2b	Fc receptor, IgG, low affinity IIb	2.08	0.000
NM_130904	Cd209d	CD209d antigen	2.03	0.000
Extracellular matrix and cell adhesion				
ENSMUST00000124337.7	Myh2	myosin, heavy polypeptide 2	0.58	0.000
NM_176922	Itga11	integrin alpha 11	1.82	0.000
NM_145467	Itgbl1	integrin, beta-like 1	1.95	0.000

Muscle structure and regeneration

NM_011724	Xirp1	xin actin-binding repeat containing 1	2.04	0.000

Metabolism

ENSMUST00000063690.3	Dhrs9	dehydrogenase/reductase (SDR family) member 9	0.14	0.000
NM_199195	Bckdhb	branched chain ketoacid dehydrogenase E1	0.50	0.000
NM_009737	Bcat2	branched chain aminotransferase 2	0.54	0.000
NM_173011	Idh2	isocitrate dehydrogenase 2	0.53	0.000
NM_019880	Mtch1	mitochondrial carrier 1	0.47	0.000
NM_175438	Aldh4a1	aldehyde dehydrogenase 4 family, member A1	0.47	0.000
NM_001033453	Pdp1	pyruvate dehyrogenase phosphatase catalytic subunit 1	0.45	0.000
NM_172961	Abat	4-aminobutyrate aminotransferase	0.34	0.000
NM_145953	Cth	cystathionase (cystathionine gamma-lyase)	0.38	0.000
NM_011144	Ppara	peroxisome proliferator activated receptor alpha	0.62	0.000
NM_025826	Acadsb	acyl-Coenzyme A dehydrogenase, short/branched chain	0.59	0.000
NM_010022	Dbt	dihydrolipoamide branched chain transacylase E2	0.59	0.000
NM_146187	Ffar2	free fatty acid receptor 2	2.37	0.000
NM_024406	Fabp4	fatty acid binding protein 4, adipocyte	2.08	0.000
NM_053119	Echs1	enoyl Coenzyme A hydratase, short chain, 1	0.63	0.000
NM_009656	Aldh2	aldehyde dehydrogenase 2	0.69	0.000
NM_007498	Atf3	activating transcription factor 3	2.48	0.000

Cell signaling and communication.

NM_201367	Gpr176	G protein-coupled receptor 176	3.95	0.001
NM_145149	Rasgrp4	RAS guanyl releasing protein 4	3.22	0.001
NM_001357573	Zranb3	zinc finger, RAN-binding domain containing 3	2.04	0.000
NM_177102	Tmem91	transmembrane protein 91	0.46	0.001
NM_175133	Gucd1	guanylyl cyclase domain containing 1	0.44	0.000
NM_010544	Ihh	Indian hedgehog (Ihh), transcript variant 1	0.30	0.001

Cell cycle and apoptotic markers

NM_030248	Cdk5rap3	CDK5 regulatory subunit associated protein 3	0.47	0.000
NM_177898	Nek5	NIMA (never in mitosis gene a)-related expressed kinase 5	0.45	0.000
NM_026282	Spc24	SPC24, NDC80 kinetochore complex component, homolog (S. cerevisiae)	0.33	0.000
NM_001163476	Gins1	GINS complex subunit 1 (Psf1 homolog)	0.37	0.000
ENSMUST00000131855.1	Eif2d	eukaryotic translation initiation factor 2D	0.17	0.000

NM_010872	Naip2	NLR family, apoptosis inhibitory protein 2	2.56	0.000
NM_027950	Osgin1	oxidative stress induced growth inhibitor 1	1.68	0.000
NM_009099	Trim30a	tripartite motif-containing 30A	2.18	0.000
S78355	Ccnd1	cyclin D1	2.02	0.000
NM_009829	Ccnd2	cyclin D2	1.94	0.000

Fold represents the average of mRNA expression level in the gastrocnemius (Gas) muscle from the HFD-STZ mice relative to its matched control. The data are representative of two independent experiment.

Further analysis of the gene expression patterns revealed the following key molecular events that distinguish these two models:

(a) Protein metabolism imbalance

One major cause of myofiber shrinkage and consequent loss of muscle mass is imbalance in the protein metabolism. Interestingly, DNA microarray data revealed that the family of genes controlling proteolytic systems was upregulated in both the models. However, these mRNAs were increased to a greater level in the high-STZ model than in the HFD/STZ model (Table 7). Hence, the transcriptomic analysis was carried out using qPCR in other to validate mRNA levels in individual mice Gas muscle from both STZ models. The mRNA levels of E3-ubiquitin-ligases genes Krüppel-like factor 15 (*KLF15*), F-box only protein 32 (*Fbxo32/Atrogin1*), CCAAT/enhancer binding protein δ (*C/EBPδ*), and Tripartite Motif Containing 63 (*Trim63*/*MuRF1*), which are reported to modulate muscle atrophy protein degradation, were found to be highly upregulated in the high-STZ model. In particular, *KLF15* and *Fbxo32* mRNA levels, which were reportedly upregulated in human muscle with type 1 diabetes (O'Neill et al., 2019), were only increased in the high-STZ model (Figure 23A-D). In addition, Fbxo32/Atrogin1 and Trim63/MuRF1 protein levels from Quad muscle were examined by Western blotting and were found to be significantly upregulated in the high-STZ model (Figure 24). On the other hand, the Ddit4/REDD1, which was shown to inhibit protein synthesis by impairing mTOR activity (Shimizu et al., 2011; Tirado-Hurtado et al., 2018), was also found to be remarkably upregulated (approximately 5–7 folds) in the high-STZ model than in the HFD/STZ model (Figure 23E). Furthermore,

this study showed a decrease in the phosphorylated form of P70 S6Kinase (p-P70S6k) (Figure 25), suggesting that mTOR activity was suppressed in the muscle of high-STZ model. Interestingly, a drastic downregulation of extracellular matrix genes, especially those belonging to the collagen family (Figure 23F and G) was observed only in the high-STZ model.

Table 7. Representative genes that are expressed in both models (P≦0.05).

Gene symbol	Gene description	Fold in High STZ	Fold in HFD/Low STZ
Muscle structure and regeneration			
Irs1	insulin receptor substrate 1	2.02	2.62
Myoz2	myozenin 2	2.28	2.44
Response to glucocorticoid hormone			
Trim63	tripartite motif-containing 63	4.73	2.79
Cebpd	CCAAT/enhancer binding protein (C/EBP), delta	5.78	2.07
Ddit4	DNA-damage-inducible transcript 4	10.00	2.89
Fbxo32	F-box protein 32	2.47	1.49
Cell signaling and cell communication			
S100a9	S100 calcium binding protein A9	2.65	6.62
S100a8	S100 calcium binding protein A8	3.00	18.62
Tmx2	thioredoxin-related transmembrane protein 2	0.43	0.36
Prkg1	protein kinase, cGMP-dependent, type I	0.35	0.43
Ramp1	receptor (calcitonin) activity modifying protein 1	0.43	0.48
Grk3	G protein-coupled receptor kinase 3	0.54	0.48
Frzb	frizzled-related protein	0.34	0.21
Extracellular matrix/cell adhesion			
Itgb6	integrin beta 6	0.28	0.45
Thbs4	thrombospondin 4	0.36	0.47
Actr3b	ARP3 actin-related protein 3B	0.38	0.49
Fndc5	fibronectin type III domain containing 5	0.49	0.59
Col24a1	collagen, type XXIV, alpha 1	0.49	0.58

Actr3b	ARP3 actin-related protein 3B	0.38	0.49

DNA microarray analysis was repeated with Cy3 and Cy5 dyes reversed (a dye swap). Fold change in high-STZ represents the average of mRNA expression level in the gastrocnemius (Gas) muscle from the high-STZ mice relative to its matched control. Fold change in HFD/STZ represents the average of mRNA expression level in the gastrocnemius (Gas) muscle from the HFD/STZ mice relative to its matched control.

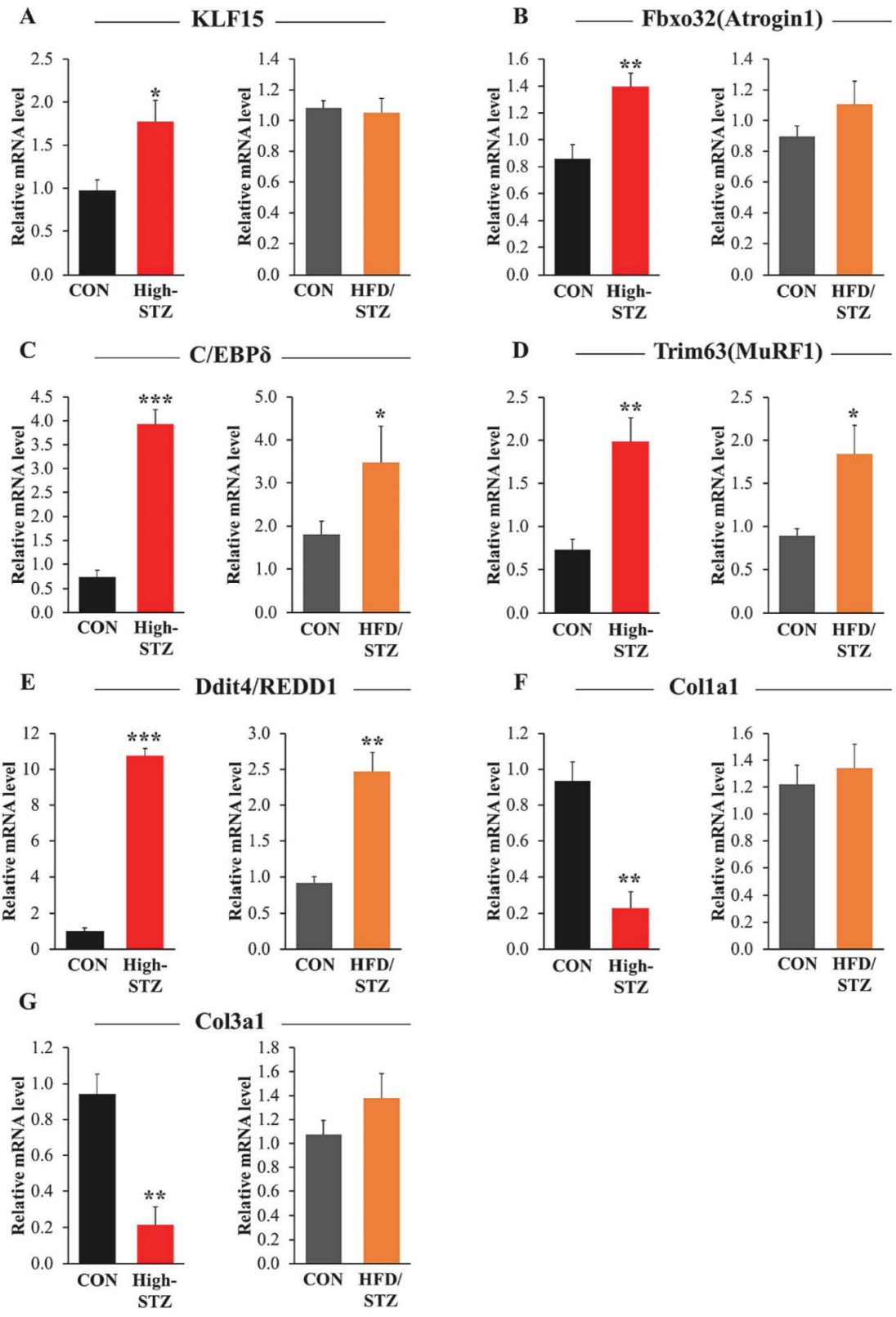
A
KLF15
Relative mRNA level
CON
High-STZ
HFD/STZ
B
Fbxo32(Atrogin1)
C
C/EBPδ
D
Trim63(MuRF1)
E
Ddit4/REDD1
F
Col1a1
G
Col3a1

Figure 23. Proteolytic pathways are severely altered in High-STZ model. (A-G) Total RNAs in gastrocnemius (Gas) muscle from the high-STZ (n = 5) and HFD/STZ (n = 6) models were isolated. The relative mRNA expression level of each gene was determined by quantitative PCR and normalized to L19 mRNA level and are presented as means ± S.E. *$p < 0.05$, **$p < 0.01$, ***$p < 0.001$. The data are representative of two independent experiments.

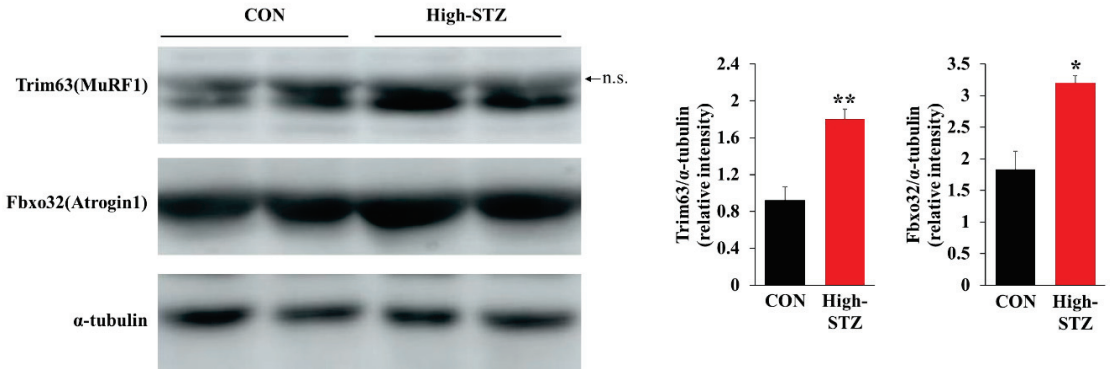

Figure 24. Western blot shows increase expression of protein degradation genes (MuRF1/Trim63, Fbxo32/atrogin-1) in high-STZ model n.s. denotes (non-specific band)

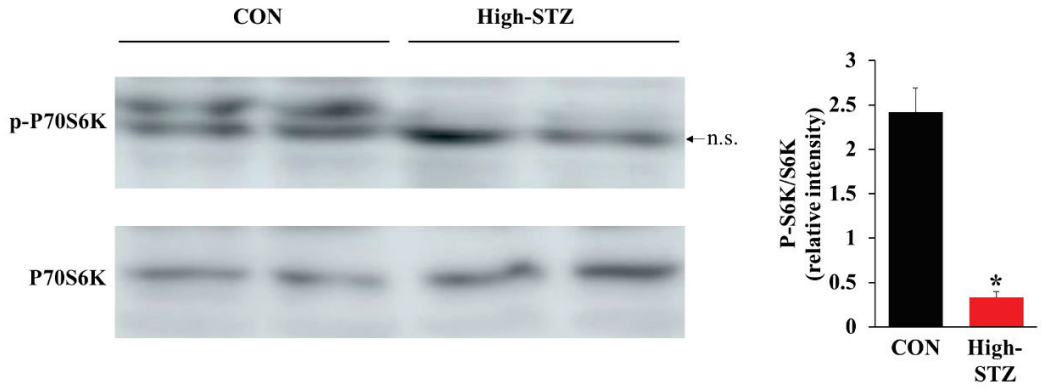

Figure 25. Western blot shows that protein synthesis was inhibited significantly in High-STZ model as indicated by phosphorylated-P70 S6 kinase (p-P70S6K). n.s. denotes (non-specific band)

Several studies have shown that alterations in protein metabolism genes can be directly stimulated by glucocorticoids (GCs) (Schakman et al., 2008; Schakman et al., 2013). Hence, the blood glucocorticoids level was quantified in each model. The result showed that there

was a significant increase in glucocorticoid levels in the high-STZ model but not in the HFD/STZ model (Figure 26). These results suggest that glucocorticoids are involved in protein metabolism imbalance, which ultimately leads to muscle atrophy in the high-STZ diabetic model.

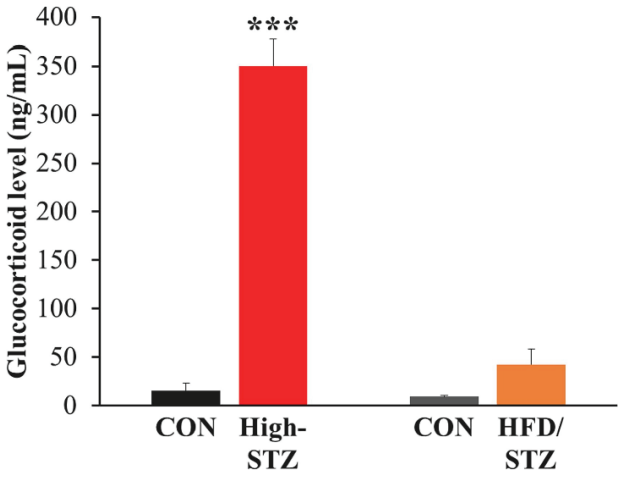

Figure 26. Glucocorticoid level is excessively high ***$p < 0.001$ in the plasma of high-STZ model when compared with its matched control. Meanwhile glucocorticoid level of HFD/STZ is not statistically significant. The data (means ± S.E.) are representative of two independent experiments. (High-STZ $n = 5$ and its matched CON n = 5; HFD/STZ $n = 6$ and its matched CON n = 5).

(b) Chronic inflammation and immune response

Because DNA microarray data indicated a large difference in inflammation and immune response between both STZ models Table 5, Table 6, the mRNA levels of some inflammatory genes in both STZ models was examined using qPCR. In the high-STZ model, inflammation and immune response genes were suppressed, as shown in Tables 5, suggesting that the decline in the expression of inflammation and immune response genes in the high-STZ model could be functionally linked to elevated GC levels, which has been well studied as an endogenous anti-inflammatory molecule (De Bosscher et al., 2009). Interestingly, qPCR data showed that interferon regulatory factor 7 (Irf7) mRNA was significantly increased specifically in the HFD/STZ model (Figure 27A). Irf7 is a member of the interferon

regulatory transcription factor family and plays a role in the transcriptional activation of virus-inducible cellular genes, including type I interferon genes. In fact, our study showed that IFN-inducible genes, such as *Ifi44* and *Ifit1*, and many types of 2′,5′-oligoadenylate synthetase (OAS) genes were upregulated in the HFD/STZ model (Table 6, Figure 27B). OAS genes reportedly respond to pathogen-associated molecular patterns to induce the degradation of cellular RNAs. Previous reports have shown that the IFN pathway contributes to myogenesis inhibition (Aljabban et al., 2020; Rizzo et al., 2018), suggesting that these IFN-inducible genes are involved in the pathology of diabetic myopathy in the HFD/STZ model. On the other hand, many types of chemokine mRNAs were upregulated in the HFD/STZ model (Table 6; Figure 27C). Previous reports have shown that CCL7 and CCL8 play important roles not only in immune cell migration, but also in the inhibition of myogenic progenitor cell fusion, which in turn leads to the prevention of myotube formation (Blanc et al., 2020). These observations suggest that the robust upregulation of inflammation and immune response genes is responsible for impaired myogenesis, which is indicated by a reduction in muscle fiber size seen in the HF/STZ diabetic model.

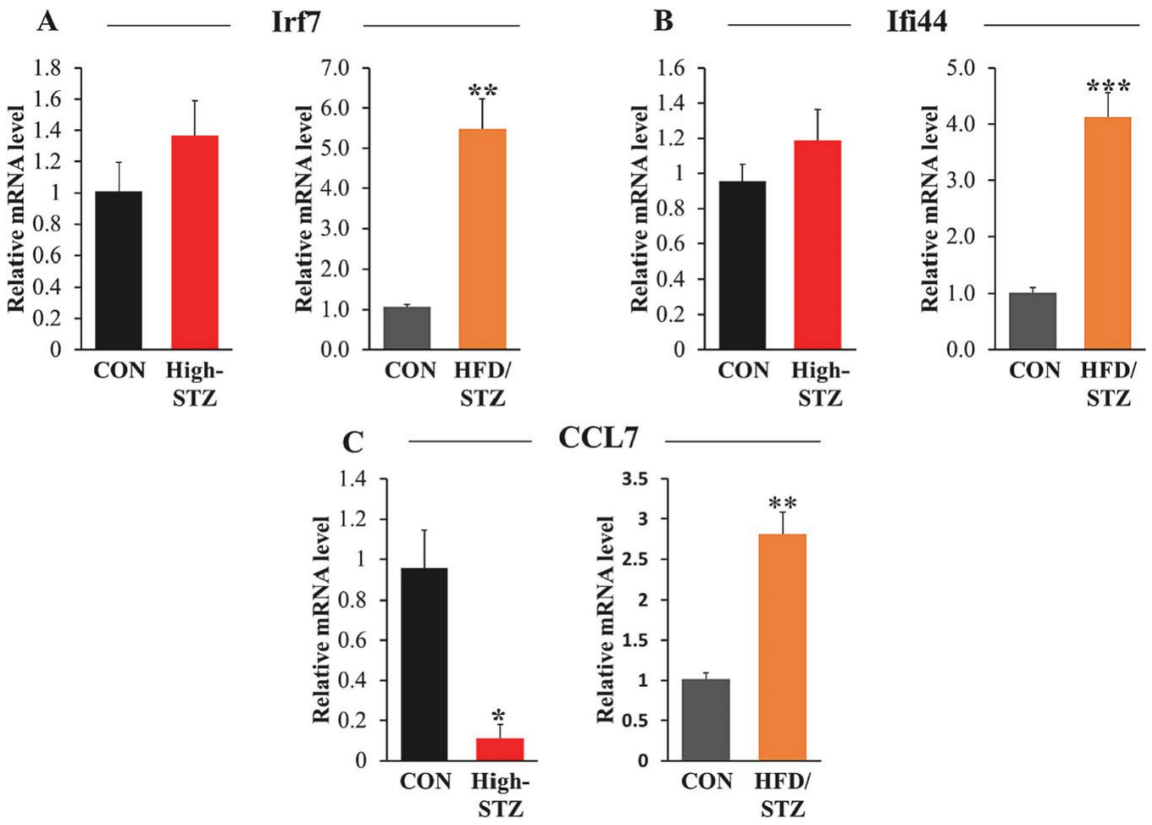

Figure 27. Chronic inflammation dominates the molecular cue of HFD/STZ model skeletal muscle. (A-C) Total RNAs in gastrocnemius (Gas) muscle from the high-STZ ($n = 5$) and HFD/STZ ($n = 6$) models were isolated. The relative mRNA expression level of each gene was determined by quantitative PCR and normalized to L19 mRNA level and are presented as means ± S.E. *$p < 0.05$, **$p < 0.01$, ***$p < 0.001$. The data are representative of two independent experiments.

(c) Energy metabolism and ATP synthesis

Impairment of mitochondrial functions to produce ATP is a key feature of muscle atrophy in a large variety of clinical conditions (Miller et al., 2019; Romanello et al., 2010; Max, 1972; Min et al., 2011). In this study, the ATP levels in the quadriceps muscle tissues from both STZ models was quantified. The result indicated that ATP levels decreased to greater extent in the HFD/STZ model than in the high-STZ model (Figure 28A). Next, the mRNA levels of genes related to these mitochondrial functions was analyzed. The result showed that peroxisome proliferator-activated receptor (*Pparα*), pyruvate dehydrogenase phosphatase catalytic subunit 1 (*Pdp1*), and isocitrate dehydrogenase 2 (*Idh2*) mRNAs were

significantly downregulated in the gastrocnemius muscle of the HFD/STZ model but not in that of the high-STZ model (Figure 28B-D). Next, the expression of activating transcription factor 3 (*ATF3*), an upstream regulator of PPARα was evaluated, and the result showed that *ATF3* was highly expressed in the HFD/STZ model but not in the high-STZ model (Figure 28E).

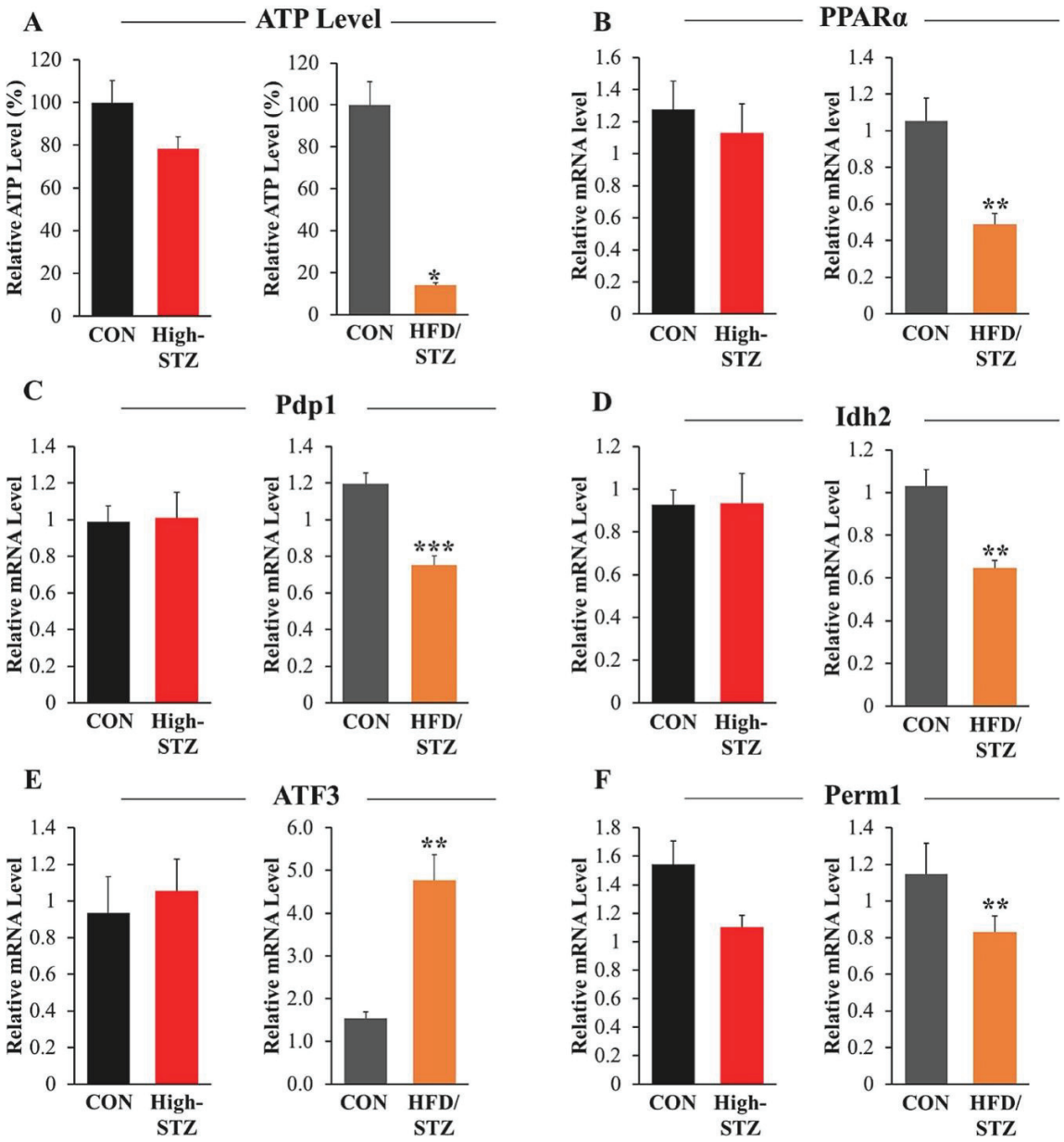

Figure 28. Energy level is decreased in HFD/STZ model skeletal muscle. (A)Decrease in ATP level is more pronounced (*$p < 0.05$) in Quad muscle tissues from HFD/STZ ($n = 6$) than in high-STZ ($n = 5$). (B-F) Total RNAs in gastrocnemius (Gas) muscle from the high-STZ (n = 5) and HFD/STZ (n = 6) models were isolated. The relative mRNA expression level of each gene was determined by quantitative PCR and normalized to L19 mRNA level and are presented as means ± S.E. *$p < 0.05$, **$p < 0.01$, ***$p < 0.001$. The data are representative of two independent experiments. Control mice (CON), gastrocnemius (Gas), and quadriceps (Quad). The data are representative of two independent experiments.

These results suggest that fatty acid oxidation was reduced in the skeletal muscle of the HFD/STZ model. Mitochondrial biogenesis and oxidative metabolism play critical roles in the generation and constant supply of ATP (Cho et al., 2013). Because this process is reported to be controlled by genes such as PGC-1- and ERR-induced regulator in muscle 1 (Perm1) and mitochondrial transcription factor A (TFAM) (Cho et al., 2016; Duguez et al., 2002), the study further showed that the *Perm1* mRNA levels were decreased in both STZ models (Figure 28F). Downregulation of *Perm1* mRNA expression might be partially related to decreased ATP levels in the gastrocnemius muscle of HFD/STZ model mice. In addition, TFAM protein level was shown to be significantly downregulated in the muscles of the HFD/STZ model (Figure 29).

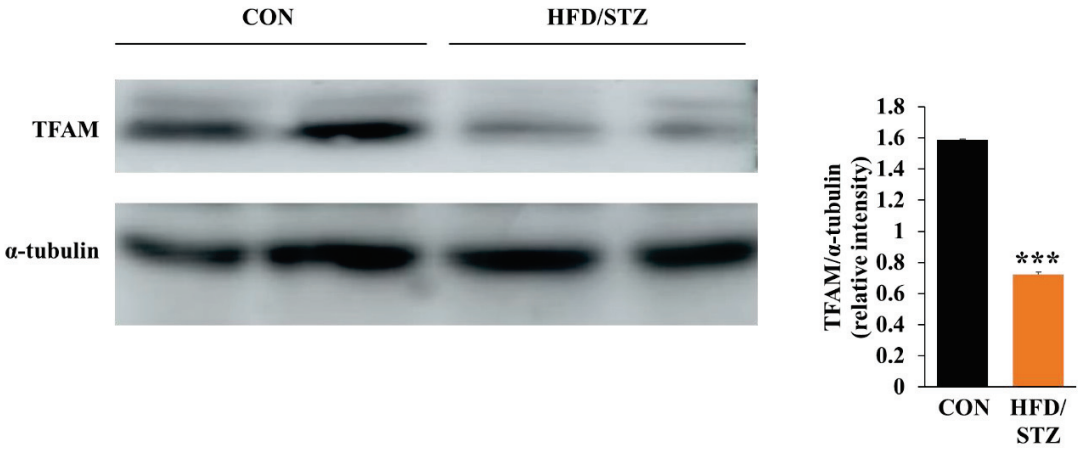

Figure 29. Representative western blot shows that mitochondria activity was significantly altered in HFD/STZ model as indicated by mitochondrial transcription factor A (TFAM)

4.4. Discussion

Although the STZ-induced diabetic animal model is a common method used to study diabetic myopathy (Kivelä et al., 2006; Arcaro et al., 2021; Copray et al., 2000; Fujimak et al., 2016; Jeong et al., 2013), however, recent reports have shown that STZ can directly exert detrimental side effects besides pancreatic toxicity (Mohammed-Ali et al., 2017; Breyer et al., 2005). Therefore, due to the nonspecific cytotoxic effect of high-dose STZ, another model induced by a high-fat diet and low-dose streptozotocin (HFD/STZ) was established to avoid the nonspecific cytotoxic effects of STZ. These two experimental models have been used arbitrarily to study diabetic myopathy; however, STZ treatment was recently shown to impair body weight gain and negatively affect muscle fiber growth independent of hyperglycemia/hypoinsulinemia, suggesting the importance of basic research to clarify pathological differences between the two diabetic STZ models. Therefore, this study was conducted to gain a clear understanding of the molecular mechanisms responsible for diabetic myopathy in these two models by characterization of muscle atrophy in vivo as well as to identify genes that are differentially expressed in the skeletal muscle of both these models with respect to human diabetic myopathy.

The current study showed that both models exhibited detrimental effects on the skeletal muscles; however, the pathophysiological and molecular mechanisms underlying this complication varied significantly between the two models. Importantly, compared with skeletal muscles from HFD/STZ mice, the mice induced with high-dose STZ was found to showed (1) a two-fold decrease in average myofiber size, (2) a clear downregulation of inflammatory/immune-related genes, (3) downregulation of extracellular matrix protein levels, especially the ones belonging to the collagenous family, and (4) increased proteolysis and a two-fold decrease in satellite cell (SC) content. This study strongly suggests that a remarkable increase in the endogenous corticosteroid level in high-dose STZ-induced mice compared with HFD/STZ mice plays an important role in the observable differences seen between both the models. In rodents, corticosterone is a principal endogenous glucocorticoid (GC) and is responsible for the survival of mammals under stressful conditions such as perceived danger (Braun and Marks, 2015); however, chronic

exposure to GCs to induce muscle wasting is well studied (Braun and Marks, 2015; Sato et al., 2017). The glucocorticoid-glucocorticoid receptor (GR) system elicits muscle atrophy partially through unbalanced protein synthesis and protein degradation (Braun and Marks, 2015; Sato et al., 2017; Kumar and Thompson, 2005). In this study, glucocorticoid-GR target genes responsible for increased protein degradation (KLF15, atrogin-1/Fbxo32, and MuRF1/Trim63) and suppression of protein synthesis (Ddit4/REDD1) were shown to be significantly upregulated in the skeletal muscles of high-STZ model mice when compared with those from HFD/STZ mice. Previous study has reported Ddit4Redd1 as an inhibitor of skeletal muscle protein synthesis by reducing mTOR activity (DeYoung et al., 2008). The current study also showed that mTOR system is negatively regulated in high-STZ model as demonstrated by decrease in phosphorylated form of P70 S6Kinase (p-P70S6K) (Figure 25). Additionally, the transcription factor CCAAT/enhancer binding protein delta (C/EBPδ) expression, which has been shown to be induced in dexamethasone-treated L6 muscle cells (Yang et al., 2005; Peris-Moreno et al., 2020), was found to be dramatically increased (5–6 folds) in the skeletal muscles of high-dose STZ mice in vivo. Increased C/EBPδ expression has been shown to activate E3 ubiquitin ligase promoter (MuRF1/Trim63) in C2C12 cells (Peris-Moreno et al., 2020), which eventually leads to protein degradation via the ubiquitin–proteasome pathway.

With regard to inflammation, in this study, the high-STZ model showed a downregulation of inflammatory/immune-related genes. Because GC is well recognized as an effective anti-inflammatory molecule (De Bosscher and Haegeman, 2009), the decrease in pro-inflammatory molecular cues is likely due to the excessive exposure to GCs in high-STZ mice. Inflammation plays a divergent role in skeletal muscle growth and recovery. A transient increase in pro-inflammatory cytokines following skeletal muscle injury triggers a pro-myogenic signaling cascade that mediates proper skeletal muscle repair, remodelling, and maintenance. In addition, previous reports have shown that SCs play a crucial role in the muscle maintenance and repair (Lepper et al., 2011; Hawke and Garry, 2001). In this study, SC content reduction was observed to be more pronounced in the high-STZ model than that in the HFD/STZ model. Further experiments are needed to analyze whether the suppression

of proinflammatory factor expression and decreased SC content seen in the high-STZ model can cause a delay in muscle repair, maintenance, and growth.

Consistent with the findings of previous studies (Choi et al., 2021; Hu et al., 2009), the present study showed that a remarkable increase in endogenous corticosteroid levels is a key factor in characterizing diabetic myopathy in high-dose STZ mice. The mechanism underlying the increase in glucocorticoid levels seen in STZ-induced diabetic mice can be explained as the released glucocorticoids in turn result in more glucose liberation through gluconeogenesis, glycogenolysis, and lipolysis (Peckett et al., 2011; Kuo et al., 2015). Chronic hyperglycemia, along with insulin depletion, has been shown to trigger oxidative stress, which eventually sends signals to the hypothalamic-pituitary-adrenal axis to induce the release of glucocorticoids from the adrenal gland. In fact, in the present study, we observed a remarkable increase in glucose concentration in the high-STZ model compared with the HFD/STZ model. Notably, enhanced glucocorticoid secretion seen in the high-STZ diabetic mouse model is similar to that observed in patients with diabetes. Several studies have reported that intracellular glucocorticoid (cortisol) levels are amplified in patients with type 2 diabetes, and unfortunately, this has been associated with several diabetic complications and deteriorated metabolic control (Rosenstock et al., 2010; Chiodini et al., 2007; Oltmanns et al., 2006). Interestingly, potent ligands of peroxisome proliferator-activated receptor (PPAR) γ, such as thiazolidinediones, can partially improve glucose metabolism in type 2 diabetes by inhibiting 11-β-hydroxysteroid dehydrogenase 1, which can convert inactive cortisone into active cortisol (Rosenstock et al., 2010). Since elevated glucocorticoid level in the high-STZ model is a key parameter that closely mirrors the pathogenesis of human type 2 diabetes, we propose that the high-STZ diabetic model is suitable not only for the study of the negative impact of glucocorticoids on the skeletal muscles but also for the evaluation of the pharmacological effects of glucocorticoid inhibitors on the skeletal muscle pathology. Previous studies have shown that STZ also induces alterations in gene expression in other tissues including kidney, liver, and lung (Dhahbi et al., 2003; Wada et al., 2001; van Lunteren et al., 2014). For instance, STZ aggravates diabetes pathology with increased expression of liver gluconeogenic enzymes

(glucose 6-phosphatase and phosphoenolpyruvate carboxykinase) (Dhahbi et al., 2003; Nocito et al., 2012; van Alkhalidy et al., 2018), which eventually triggers the physiological signal of glucocorticoid that activates protein degradation in skeletal muscle. Furthermore, STZ is well-studied to induce not only renal inflammation but also a metabolic switch in renal tubules from lipid oxidation to anaerobic glycolysis partially mediated by hypoxia-inducible factor 1α, resulting in metabolic acidosis (Cai et al., 2020; Lin et al., 2011; Wesson et al., 2020). Interestingly, the metabolic acidosis has been shown to accelerate muscle protein degradation and suppress muscle protein synthesis (Mitch et al., 1994; Caso et al., 2004; Crie and Wildenthal, 1980). However, further studies are needed to clarify the crosstalk between STZ-induced genetic alteration in muscles and other organs in the high-STZ model in order to address the complex pathogenesis of diabetic myopathy.

On the other hand, recent evidence has shown that mitochondrial dysfunction and a compromised ability to produce ATP play key roles in muscle atrophy (Romanello et al., 2010; Max, 1972; Min et al., 2011). Although this study showed obvious mitochondrial dysfunction, as indicated by decreased ATP levels in the quadriceps muscle in both STZ models, the HFD/STZ model showed a more severe phenotype. This decrease in ATP production seen in HFD/STZ model is consistent with previous study (Li et al., 2014), suggesting that mitochondrial dysfunction plays a critical role in driving muscle atrophy in HFD/STZ model. The currently observed decrease in ATP production in HFD/STZ could be due to the overexpression of the activating transcription factor 3 (*ATF3*), an upstream regulator of PPARα. *ATF3* has been shown to dramatically downregulate PPARα (Kim et al., 2017), thereby leading to a decrease in fatty acid β-oxidation in the mitochondria and eventually reducing the ATP levels. The upregulation of ATF3 expression in the HFD/STZ model has been attributed to long-term high-fat diet (HFD) feeding, which is known to promote systemic inflammation that eventually leads to insulin resistance (Choi et al., 2015). In fact, ATF3 was shown to be upregulated in insulin-resistant human patients (Kim et al., 2017). In addition, the current study showed that several genes controlling mitochondrial biogenesis (perm1), oxidative metabolism, and the TCA cycle (Pdp1, Idh2) were downregulated in the gastrocnemius muscles of HFD/STZ mice. In fact, downregulation of

the mitochondrial transcription factor A (TFAM) protein expression (Figure 29) a critical regulator of mitochondria biogenesis (Duguez et al., 2002) has suggested the alteration in mitochondria functions. The fact that mitochondrial dysfunction is evident in the skeletal muscles of patients with all forms of diabetes mellitus (Kelley et al., 2002; Monaco et al., 2018), taken together with the observations regarding decreased ATP level, the HFD/STZ model can be considered a useful model to study the perturbation of mitochondrial function in the skeletal muscles with the onset of hyperglycemia.

Abstract

Streptozotocin (STZ)-induced diabetic animal models have been widely used to study diabetic myopathy; however, non-specific cytotoxic effects of high-dose STZ have been discussed. The purpose of this study was to compare diabetic myopathy in a high-STZ model with another well-established STZ model with reduced cytotoxicity (high-fat diet (HFD) and low-dose STZ) and to identify mechanistic insights underlying diabetic myopathy in STZ models that can mimic perturbations observed in human patients with diabetic myopathy. Male C57BL6 mice were injected with a single high dose of STZ (180 mg/kg, High-STZ) or were given HFD plus low-dose STZ injection (STZ, 55 mg/kg/day, five consecutive days, HFD/STZ). Diabetic myopathy was characterized by histological and immunochemical analyses and conducted gene expression analysis. The high-STZ model showed a significant reduction in tibialis anterior myofiber size along with decreased satellite cell content and downregulation of inflammation response and collagen gene expression. Interestingly, blood corticosteroid levels were significantly increased in the high-STZ model, which was possibly related to lowered inflammation response-related gene expression. Further analyses using the HFD/STZ model showed downregulation of gene expression related to mitochondrial functions accompanied by a significant decrease in ATP levels in the muscles. The high-STZ model is suitable for studies regarding not only severe diabetic myopathy with excessive blood glucose but also negative impact of glucocorticoids on skeletal muscles. In contrast, the HFD/STZ model is characterized by higher immune responses and lower ATP production, which also reflects the pathologies observed in human diabetic patients.

Chapter 5

Experiment 3

Serum Amyloid A3 Promoter-Driven Luciferase Activity Enables Visualization of Diabetic Kidney Disease

5.1 Introduction

Diabetic nephropathy (DN), also referred to as diabetic kidney disease, is the progressive development of renal insufficiency induced by the diabetic milieu (Thomas et al., 2015). Approximately 40% of patients diagnosed with either type 1 or type 2 diabetes develop DN, and this number is projected to increase dramatically with the increasing trend of diabetes worldwide (Hussain et al., 2021; Su et al., 2021). Currently, DN research relies on traditional diagnostic techniques, such as the histological assessment of collagen deposition and quantification of serum/urine biomarkers (e.g., creatinine, blood urea nitrogen (BUN), albumin, and cytokines) to confirm kidney disorders (Su et al., 2021). Although these markers have provided essential insight into DN progression in human patients, there are problems of low sensitivity and missing early injury responses in diabetic kidneys. In addition, these traditional serum/urine biomarkers are often affected by other factors such as age, muscle mass, protein diet, and intake of certain drugs (Wasung et al., 2015; Griffin et al., 2019). Thus, new biomarkers that are suitable for capturing the characteristics of early kidney injury and can easily obtain reliable data are being searched and are expected to provide essential insight into DN progression. Accumulating evidence has shown that chronic renal inflammation and fibrosis are hallmark pathological features of DN (Thomas et al., 2015; Navarro-González et al., 2011; Matoba et al., 2019; Moreno et al., 2018; Qian et al., 2008). Thus, the assessment of renal inflammation and fibrosis using non-invasive tests will become more important in diagnosing DN at an earlier stage and efficiently analyzing new therapeutic agents and functional foods. In vivo imaging is a promising technology for the non-invasive monitoring of disease progression within living animals and/or for examining the efficacy of emerging therapeutic strategies with the same individual mice in real-time (Gross et al., 2009; Wessels et al., 2007). Non-invasive and high-resolution bioluminescence imaging tools for studying biological processes and quantitatively monitoring disease progression are now

being developed and have attracted attention in various research fields (Gross et al., 2009). Previous studies have successfully applied the serum amyloid A3 (Saa3) gene promoter-luciferase (luc) reporter to non-invasively monitor low-grade inflammation in the white fat tissues of obese mice fed with a high-fat diet and in a dietary adenine-induced tubulointerstitial injury model (Sanada et al., 2016; Kumrungsee et al., 2019). Here, since Saa3 expression was significantly upregulated in diabetic kidneys in two different streptozotocin-induced DN models without direct cytotoxicity to the kidneys, the novel in vivo Saa3-promoter bioluminescence imaging technique was employed to monitor renal pathology in these two DN models. Furthermore, mRNA expression analyses were performed to confirm whether the bioluminescence signal reflected the degree of kidney damage from hyperglycemia. The present study suggests that novel in vivo bioluminescence imaging could be useful in the non-invasive visualization of pathophysiological changes in the kidney that characterize DN in real-time.

5.2. Materials and Methods

5.2.1. Experimental Animals

Seven-week-old male C57BL/6J mice (Charles River Japan, Hino, Japan) and Saa3-promoter luc mice were used in this study. All mice were housed in a temperature-controlled (24 ± 1 °C) room with a 12 h/12 h light/dark cycle. The mice had free access to food and water. All animal experiments were approved by the Hiroshima University Animal Care and Use Committee (Permit Number: C18-15-5).

5.2.2. Diabetic Nephropathy Animal Models

Saa3-promoter transgenic mice (Saa3-promoter luc mice) carrying mouse Saa3 promoter regions (−314/+50) upstream of full-length luciferase cDNA were obtained and maintained as previously described (Sanada et al., 2016; Kumrungsee et al., 2019). Both the male C57BL/6J (WT) mice and Saa3-promoter luc mice were used to develop two streptozotocin (STZ)-induced DN models. For the first STZ-induced DN model, all mice were divided into two groups: the control group and the DN group. The control group was fed a standard

laboratory chow diet, and the DN group was fed a high-fat diet (HFD) (Oriental Yeast Co., Tokyo, Japan; 45% fat, 20.5% protein, and 34.8% carbohydrate) together with low-dose STZ (55 mg/kg for 5 consecutive days) (HFD/multiple-dose STZ-induced DN group). Notably, the HFD/multiple-dose STZ-induced DN mouse group was initially fed HFD for 4 weeks before being injected with low-dose STZ. Animals in the first model were analyzed 12 weeks after low-dose STZ treatment. For the second model of STZ-induced DN, all mice were divided into three groups: the control group, the DN group, and the insulin-treated DN group. Diabetes was induced via intraperitoneal (i.p.) injections of streptozotocin (STZ, Sigma-Aldrich, St Louis, MO, USA) at 125 mg/kg/day for 2 consecutive days (two moderate-dose STZ-induced DN group). Mice in the control group were administered citrate buffer alone. All mice were maintained on a standard laboratory chow diet (Oriental Yeast, Tokyo, Japan) and analyzed four weeks after two moderate-dose STZ treatments. In this model, only the mice with fasting blood glucose levels of ≥300 mg dL^{-1} after STZ injection were used for further studies.

5.2.3. DNA Microarray

Microarray analyses were performed as previously described (Sanada et al., 2016). Briefly, total RNA was extracted from the renal tissues of WT mice in both models of STZ-induced DN using the RNeasy lipid tissue kit (Qiagen Sciences, Germantown, MD, USA). The RNA samples were subjected to cRNA synthesis for DNA microarray analysis (44 K whole mouse genome 60-mer oligo microarray, Agilent Technologies, Palo Alto, CA, USA). Fluorescence labeling, hybridization, and image processing were performed according to the manufacturer's instructions. Statistical analysis of the gene expression data was performed using the Agilent Feature Extraction software (version 9.5) (Santa Clara, CA, USA).

5.2.4. RT-PCR

One microgram of total RNA isolated from the renal tissues of WT mice induced by HFD/multiple low-dose STZ and Saa3-promoter luc mice induced with two moderate doses of STZ was reverse transcribed into cDNA using ReverTra Ace (TOYOBO, Osaka, Japan) and random hexamers (TaKaRa Bio, Kyoto, Japan), according to the manufacturer's

instructions. Quantitative PCR reactions were then performed on StepOnePlusTM (Applied Biosystems, Foster City, CA, USA) using THUNDERBIRD SYBR qPCR Mix reagents (TOYOBO) under previously described conditions (Kumrungsee et al., 2019). The primers used for the PCR analysis are listed in Table 8. The expression level of the target gene was normalized to that of the housekeeping gene L19. The relative gene expression was calculated using the comparative Ct ($2^{-\Delta\Delta Ct}$) method.

Table 8. Primer sequences for qPCR

Target gene	Sequence (5'-3')	
L19	Forward	GGCATAGGGAAGAGGAAGG
	Reverse	GGATGTGCTCCATGAGGATGC
Saa3	Forward	AAGGGTCTAGAGACATGTGG
	Reverse	ACTTCTGAACAGCCTCTCTG
EMR1 (Adgre1)	Forward	ATTGTGGAAGCATCCGAGAC
	Reverse	GTAGGAATCCCGCAATGATG
TNFα	Forward	CGTCGTAGCAAACCACCAAG
	Reverse	TTGAAGAGAACCTGGGAGTAGACA
Mpeg1	Forward	GCTTGCCTCTGCATTTCTTC
	Reverse	TCTTCTGCTCCAGGTTTTGG
CEBPβ	Forward	GAAGACGGTGGACAAGCTGA
	Reverse	TGCTCCACCTTCTTCTGCAG
Ccl2 (MCP-1)	Forward	GGTCCCTGTCATGCTTCTGG
	Reverse	CCTTCTTGGGGTCAGCACAG
Col1a1	Forward	CCCAAGGAAAAGAAGCACGTC
	Reverse	ACATTAGGCGCAGGAAGGTCA
NOX2	Forward	AGCTATGAGGTGGTGATGTTAGTGG
	Reverse	TGCACAGCAAAGTGATTGGC
TGFβ	Forward	GGCACCATCCATGACATGAA
	Reverse	TTCTCTGTGGAGCTGAAGCAAT

5.2.5. In Vivo Bioluminescent Imaging

In vivo bioluminescence imaging was performed as previously described (Sanada et al., 2016; Kumrungsee et al., 2019). Briefly, before acquiring images, 150 mg/kg body weight D-luciferin (Promega, Madison, WI, USA) was administered intraperitoneally to all Saa3 promoter-luc mice in both models five minutes after substrate administration using the NightOWL II Imaging Systems LB983 (Berthold Technologies, Bad Wildbad, Germany).

For each mouse, the signal intensity was quantified as the sum of all detected photon counts per second and was presented as counts/s (cps). All images were adjusted to the same scale as the minimum and maximum luminescent intensities for any given analysis.

5.2.6. Histological Analysis

Renal tissues from Saa3-promoter luc mice induced with two moderate doses of STZ were fixed in 4% formalin solution and embedded in paraffin, and 5 mm-thick sections were prepared. The sections were then processed for hematoxylin and eosin (H&E) staining to determine the overall histology according to standard procedures (Fischer et al., 2008).

5.2.7. Measurement of Plasma BUN Level

The Plasma BUN levels of Saa3-promoter luc mice induced with two moderate doses of STZ were determined using a Beckman Coulter AU480 analyzer (Beckman Coulter, Krefeld, Germany), which is an automated chemistry instrument for turbidimetric, spectrophotometric, and ion-selective electrode measurements.

5.2.8. Statistical Analysis

Data are presented as means ± S.E. Differences in significance levels between the compared groups were determined by a Student's *t*-test or one-way ANOVA followed by Dunnett's test. Results were considered statistically significant at $p < 0.05$ (denoted appropriately in all figures).

5.3 Results

5.3.1. Gene Expression Patterns of Saa3 and Other Fibro-Inflammatory Markers Are Altered with DN Development

To examine the molecular signature that can characterize an early stage of DN in streptozotocin (STZ)-induced DN models, DNA microarray analyses of kidneys from two STZ-induced DN models using C57BL/6 mice was performed. In the first model, DN was induced by a combination of a high-fat diet and multiple low-dose STZ injections, which is a well-established DN model without renal cytotoxicity induced by STZ treatment. In general, high doses of STZ have a non-specific cytotoxic effect that has been shown to cause acute

kidney damage in mice and rats (Mohammed-Ali et al., 2017; Breyer et al., 2005). A high-dose STZ injection often makes it difficult to interpret any observations of nephropathy because hyperglycemia-induced renal injuries are confused with acute renal cytotoxicity caused by STZ treatment. To solve this problem, previous studies have developed two moderate-dose STZ injections (2 × 125 mg/kg per day STZ) to establish diabetes in C57BL/6 mice. These injections led to a mild resistance to STZ, suggesting that renal damage in this STZ model is not related to the acute tubular cytotoxicity seen in those undergoing continuous insulin administration to prevent renal pathology (Chow et al., 2006). Therefore, this STZ-induced DN model was adopted as the second model in this study. In these two STZ models, the expression of 221 genes was found to be similarly altered, with 194 genes upregulated and 27 genes downregulated in both DN models (Figure 30A,B). Functional classification of the genes indicated that numerous genes were associated with inflammation and fibrosis, whereas other genes with robust induction were associated with senescence and apoptosis (Table 9).

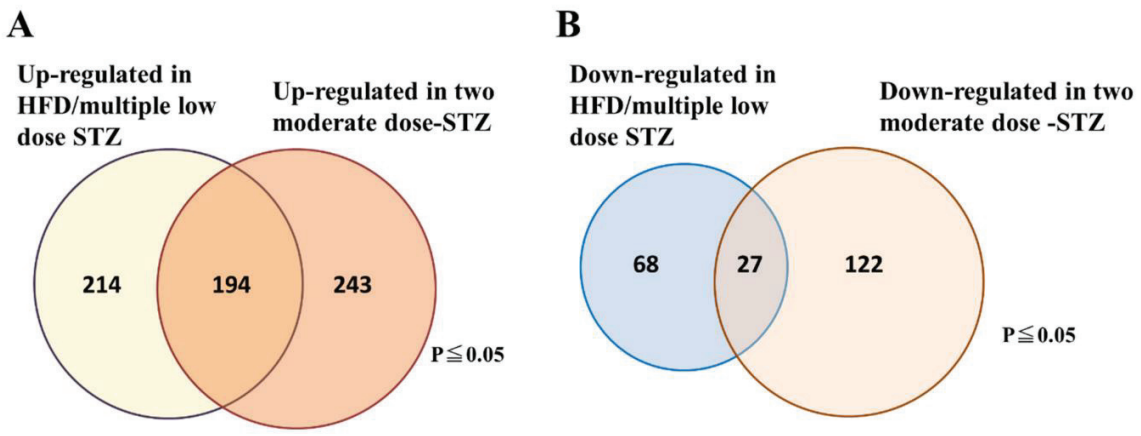

Figure 30. Venn diagram showing the number of genes that are significantly altered in the kidney tissues of the two STZ-induced DN models. (**A**) Number of upregulated genes. (**B**) Number of down-regulated genes. The data are representative of two independent experiments (i.e., HFD/multiple low-dose STZ-induced DN model, and two-moderate-dose STZ-induced DN model).

Table 9. Representative upregulated genes in both models (P≦0.05)

Gene symbol	Gene description	Fold in HFD/multiple low dose STZ-induced DN	Fold in two moderate dose of STZ-induced DN
Inflammation and immune response			
Ccl7	chemokine (C-C motif) ligand 7	9.574039	9.217479
C3	complement component 3	8.327707	4.031031
Cxcl1	chemokine (C-X-C motif) ligand 1	6.028408	2.963837
Cxcl13	chemokine (C-X-C motif) ligand 13	5.072761	3.72621
Ccl2	chemokine (C-C motif) ligand 2	4.682991	3.691467
Saa3	**serum amyloid A 3**	**4.672902**	**6.258944**
Cxcl10	chemokine (C-X-C motif) ligand 10	4.575526	4.245991
Ifi27l2a	interferon, alpha-inducible protein 27 like 2A	4.447981	1.734672
Ccl8	chemokine (C-C motif) ligand 8	4.205488	5.870678
Irf7	interferon regulatory factor 7	4.169002	1.808386
Sftpd	surfactant associated protein D	3.842778	13.99204
Saa2	serum amyloid A 2	3.943488	3.027871
Saa1	serum amyloid A 1	3.793996	5.724124
Oasl1	2'-5' oligoadenylate synthetase-like 1	3.693298	2.967476
Il1f6	interleukin 1 family, member 6	3.66638	8.421683
Oas1a	2'-5' oligoadenylate synthetase 1A	3.600839	1.863472
Ifi27	interferon, alpha-inducible protein 27	3.531166	1.931101
Ccl12	chemokine (C-C motif) ligand 12	3.505163	1.501425
Oas1f	2'-5' oligoadenylate synthetase 1F	3.341254	2.059616
Ccl3	chemokine (C-C motif) ligand 3	3.173982	1.943716
Ifit2	interferon-induced protein with tetratricopeptide repeats 2	3.050948	2.526029
Tlr2	toll-like receptor 2	2.904005	2.274702
Saa4	serum amyloid A 4	2.895843	3.129856
Tnfrsf1b	tumor necrosis factor receptor superfamily, member 1b	2.867243	1.884817
Il1rn	interleukin 1 receptor antagonist	2.845497	11.50394
B2m	beta-2 microglobulin	2.764915	2.042961
Ccl9	chemokine (C-C motif) ligand 9	2.569088	2.086461
Ifit1	interferon-induced protein with tetratricopeptide repeats 1	2.549512	2.338023
Gbp6	guanylate binding protein 6	2.507217	2.243522
Oas1d	2'-5' oligoadenylate synthetase 1D	2.450365	4.784481
C4b	complement component 4B	2.341939	1.869533
Ltc4s	leukotriene C4 synthase	2.319262	2.76853
Ccl5	chemokine (C-C motif) ligand 5	2.187073	2.618136
Mpeg1	macrophage expressed gene 1	1.578476	1.573929
Cebpb	CCAAT/enhancer binding protein (C/EBP), beta	1.359475	1.4479
Adgre1	adhesion G protein-coupled receptor E1	2.153661	1.875181
Fibrosis marker			

Col1a1	collagen, type I, alpha 1	2.310429	1.693605
Col3a1	collagen, type III, alpha 1	2.502312	1.759468
Col17a1	collagen, type XVII, alpha 1	2.513545	3.554807
Col2a1	collagen, type II, alpha 1	2.175582	1.597034
Col12a1	collagen, type XII, alpha 1	2.267022	2.13584
Tnc	tenascin C	2.086402	2.060019
Areg	amphiregulin	2.019209	8.973495
Itgav	integrin alpha V	5.06626	1.698287
Fn1	fibronectin 1	3.310534	2.894176
Timp1	tissue inhibitor of metalloproteinase 1	4.663239	3.013232
Mmp2	matrix metallopeptidase 2	2.306857	2.725541
Mmp3	matrix metallopeptidase 3	5.077015	3.464077
Fbn1	fibrillin 1	2.416774	2.539984
Atf3	activating transcription factor 3	2.70798	2.450881
Lox	lysyl oxidase	2.338978	2.056122
Cdkn1a	cyclin-dependent kinase inhibitor 1A (P21)	12.22656	15.15294
Cellular senescence and apoptosis			
Rprm	reprimo, TP53 dependent G2 arrest mediator candidate	1.24722	1.464673
Trp53inp1	transformation related protein 53 inducible nuclear protein 1	2.166779	3.87006
Tnfrsf10b	tumor necrosis factor receptor superfamily, member 10b	1.61846	4.647243
Cdkn1a	cyclin-dependent kinase inhibitor 1A (P21)	12.22656	15.15294
Ddias	DNA damage-induced apoptosis suppressor	3.199755	3.719237
Bcl2a1b	B cell leukemia/lymphoma 2 related protein A1b	1.821307	1.762403
Casp12	caspase 12	1.43227	1.75586
Aen	apoptosis enhancing nuclease	1.431768	1.663771
Casp4	caspase 4	1.565824	1.574686
Naip1	NLR family, apoptosis inhibitory protein 1	4.493729	2.603691
Bcl2a1c	B cell leukemia/lymphoma 2 related protein A1c	2.053632	1.65847
Bak1	BCL2-antagonist/killer 1	1.496008	1.508511
Bbc3	BCL2 binding component 3	2.231172	2.756859
Top2a	topoisomerase (DNA) II alpha	11.37113	3.924414
Bub1	BUB1, mitotic checkpoint serine/threonine kinase	8.765067	4.726943
Bub1b	BUB1B, mitotic checkpoint serine/threonine kinase	4.764913	1.862009
Chek1	checkpoint kinase 1	1.984729	3.368414
Mad2l1	mitotic checkpoint component Mad2	1.955027	1.971135

Furthermore, a transcriptomic analysis of fibro-inflammatory marker genes Tumour Necrosis Factor alpha (*TNFα*), Transforming growth factor beta (*TGFβ*), Collagen, type I, alpha1 (*Col1a1*), chemokine (C-C motif) ligand 2 (*Ccl2*), serum amyloid A3 (*SAA3*), EGF-like module-containing mucin-like hormone receptor-like 1 (*EMR1*), and NADPH oxidase 2 (*NOX2*) was performed using qPCR on renal tissues from the HFD/multiple low-dose STZ model. The results showed that the expression of these fibro-inflammatory markers was highly upregulated in the HFD/multiple low-dose STZ model. (Figure 31A–G). In particular, Saa*3* mRNA expression was significantly upregulated in the renal tissue of the HFD/multiple low-dose STZ-induced DN model (5-fold increase), as validated through qPCR (Figure 31A). Interestingly, previous studies have shown that Saa3 plays an active role in inflammatory disorders, and an increase in its expression is accompanied by a concomitant increase in inflammatory biomarker genes in the renal tissue of patients with DKD and corresponding diabetic mouse models (Ye and Sun, 2015; Anderberg et al., 2015; Dieter et al., 2016). These findings strongly suggest that Saa3 promoter activity is a useful biomarker for monitoring renal pathology in DN.

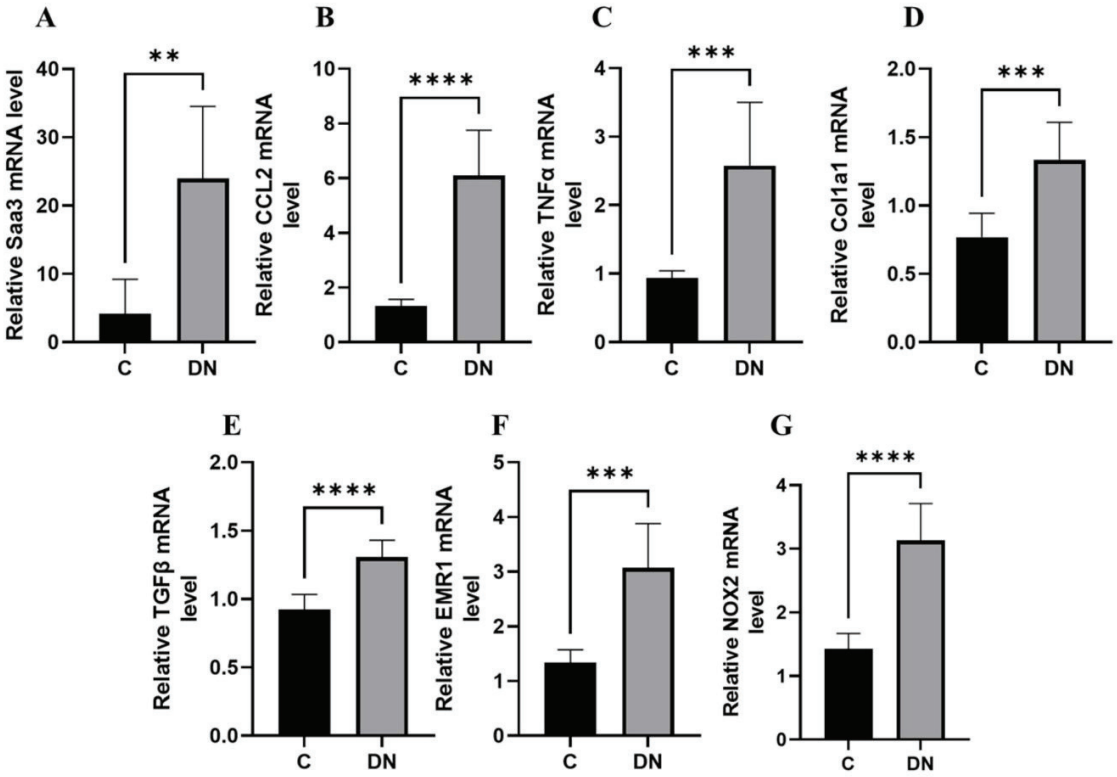

Figure 31. Renal fibro-inflammatory markers are upregulated in HFD/multiple low-dose STZ-induced DN model (A–G) Total RNAs in kidney tissues from the HFD/multiple low-dose STZ-induced DN model ($n = 9$) were isolated. The relative mRNA expression level of each gene was determined by quantitative PCR and normalized to L19 mRNA level and are presented as means ± S.E. ** $p < 0.01$, *** $p < 0.001$, **** $p < 0.0001$. The data are representative of two independent experiments. DN = Diabetic Nephropathy, C = Control.

5.3.2. Non-Invasive High-Resolution Bioluminescence Imaging Detected Diabetes Kidney Disease in the HFD/Multiple Low-Dose STZ-Induced DN Model

To monitor diabetic kidney disease in the HFD/multiple low-dose STZ-induced DN model, in vivo bioluminescence imaging with Saa3 promoter-luciferase transgenic mice (Saa3 promoter-luc mice) was performed eight weeks after diabetic induction. As shown in Figure 32A, the bioluminescent signal from the renal tissues in HFD/multiple low-dose STZ mice was stronger (from violet for the least intense to red for the most intense) when compared to the normal kidney from control mice. To verify if the visualized bioluminescence signal was specifically generated from the injured kidney in HFD/multiple low-dose STZ mice, in vivo

bioluminescence analysis was performed after opening the stomachs of Saa3 promoter-luc mice. The results showed that the Saa3-mediated bioluminescent signal was specifically detected in the injured kidney (white arrow), and not in the adjacent organs in the HFD/multiple low-dose STZ-induced DN model, whereas the uninjured kidneys and other organs of the control mice showed no bioluminescent signal (Fig. 32B).

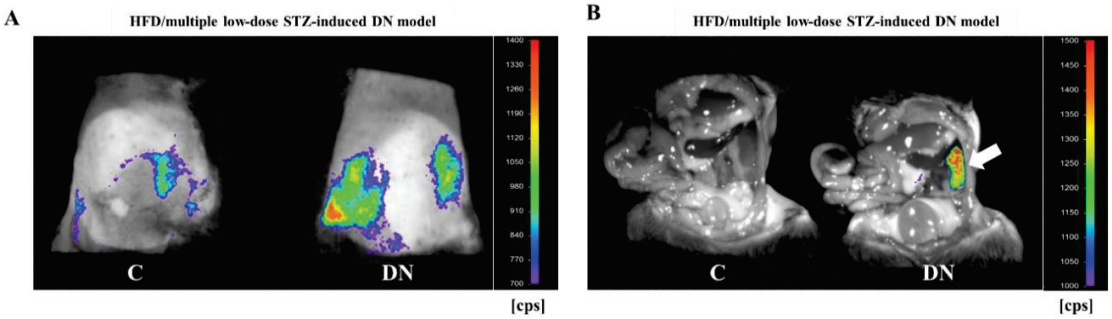

Figure 32. Visualization of renal pathology in HFD/multiple low-dose STZ-induced DN using Saa3 promoter-luc mice. (A) In vivo bioluminescence imaging from the back of Saa3 promoter-luc mice shows a strong intensity of bioluminescent signal (from violet for least intense to red for most intense), reflecting kidney injury. (B) Bioluminescent analysis of mouse organs exposed to bioluminescent imaging confirmed that the intense bioluminescent signal generated was specifically from the diabetic induced injured kidney (the white arrow), and not from the adjacent organs of the Saa3 promoter-luc mice that were induced with HFD/multiple low-dose STZ. DN = Diabetic Nephropathy, C = Control.

5.3.3. Histological, Biochemical, and Molecular Validation of In Vivo Bioluminescence Signals from the Renal Tissues of Two-Moderate-Dose STZ-Induced DN Model

To investigate whether the Saa3-mediated bioluminescence signal was also able to detect the DN status of STZ-induced DN model at a moderate dose (2 × 125 mg/kg), Saa3 promoter-luc mice were subjected to bioluminescence imaging after four weeks of diabetic induction. As shown in Figure 33A, the bioluminescence signal from diabetes-induced kidney injury in moderate-dose STZ-induced mice was extremely strong; meanwhile, there was no bioluminescent signal in the control group, reflecting an uninjured kidney. Quantitative analysis of bioluminescence intensity from two moderate-dose STZ-induced mouse kidneys showed a 2.5-fold increase in luciferase activity compared to the control (Figure 33B).

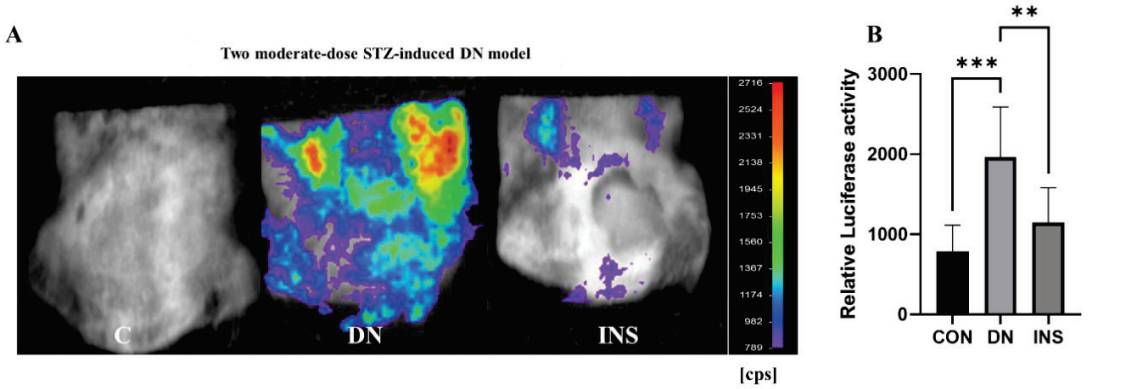

Figure 33. Bioluminescence imaging reveals renal pathology and therapeutic response of insulin in two-moderate-dose STZ-induced DN model using Saa3 promoter-luc mice. (**A**) The in vivo bioluminescence imaging from the back of Saa3 promoter-luc mice shows intense bioluminescence signal from the kidney tissues and how insulin treatment decreased the signal intensity, reflecting less severe injury in kidney of the insulin-treated mouse induced with two moderate-dose STZ injections ($n = 5$). (**B**) Quantitative data ($n = 6$). Data are presented as means ± S.E. ** $p < 0.01$, *** $p < 0.001$ as determined by ANOVA followed by Dunnett's test. DN = Diabetic Nephropathy, C = Control, INS = Insulin treatment.

Interestingly, the bioluminescence signal was significantly reduced in moderate-dose STZ-induced mice after insulin treatment (Figure 33A,B), thereby suggesting the reliability of using the Saa3 promoter-luc mouse kidney in monitoring DN progression and exploring therapeutic agents and functional foods.

Moreover, to validate the in vivo bioluminescent results, the renal tissues of the same Saa3 promoter-luc mice induced with moderate-dose STZ and their corresponding control groups, which were subjected to in vivo bioluminescence imaging were screened. Histological assessment of diabetes-induced injured renal tissues revealed that glomerular hypertrophy, glomerular hypercellularity, brush border disruption, and interstitial hemorrhage were significantly increased. Notably, the histological renal injury parameters in moderate-dose STZ mice were ameliorated by insulin treatment (Figure 34A,B). Furthermore, since our microarray data (Table 9) have implicated inflammation and fibrosis as common cardinal pathogenetic mechanisms that promote diabetic nephropathy, transcriptomic analysis of the fibro-inflammatory marker genes (TNFα, TGFβ, *Col1a1, Ccl2, Saa3,* CCAAT/ enhancer

binding protein β (*C/EBP β*), *EMR1,* Macrophage-expressed gene 1 (*Mpeg1*), and *NOX2*) in the tissues of the same kidney was performed. The results showed that the mRNA expression levels of *TNFα, TGFβ, Col1a1*, *Ccl2, Saa3, C/EBP β, EMR1, NOX2,* and *Mpeg1* were significantly upregulated (Figure 34C–K). Notably, the mRNA expression levels of *TNFα, CCL2, Emr1, TGFβ,* and *Col1a1* were positively correlated with in vivo luciferase activity ($r = 0.927$, $p < 0.05$; $r = 0.821$, $p = 0.08$; $r = 0.978$, $p < 0.01$; $r = 0.897$, $p < 0.05$; $r = 0.819$, $p = 0.08$, respectively (Figure 35A-E). These results further suggested that Saa3-luciferase mice can be applied as a non-invasive model to monitor fibro-inflammation the key molecular driver of diabetic nephropathy

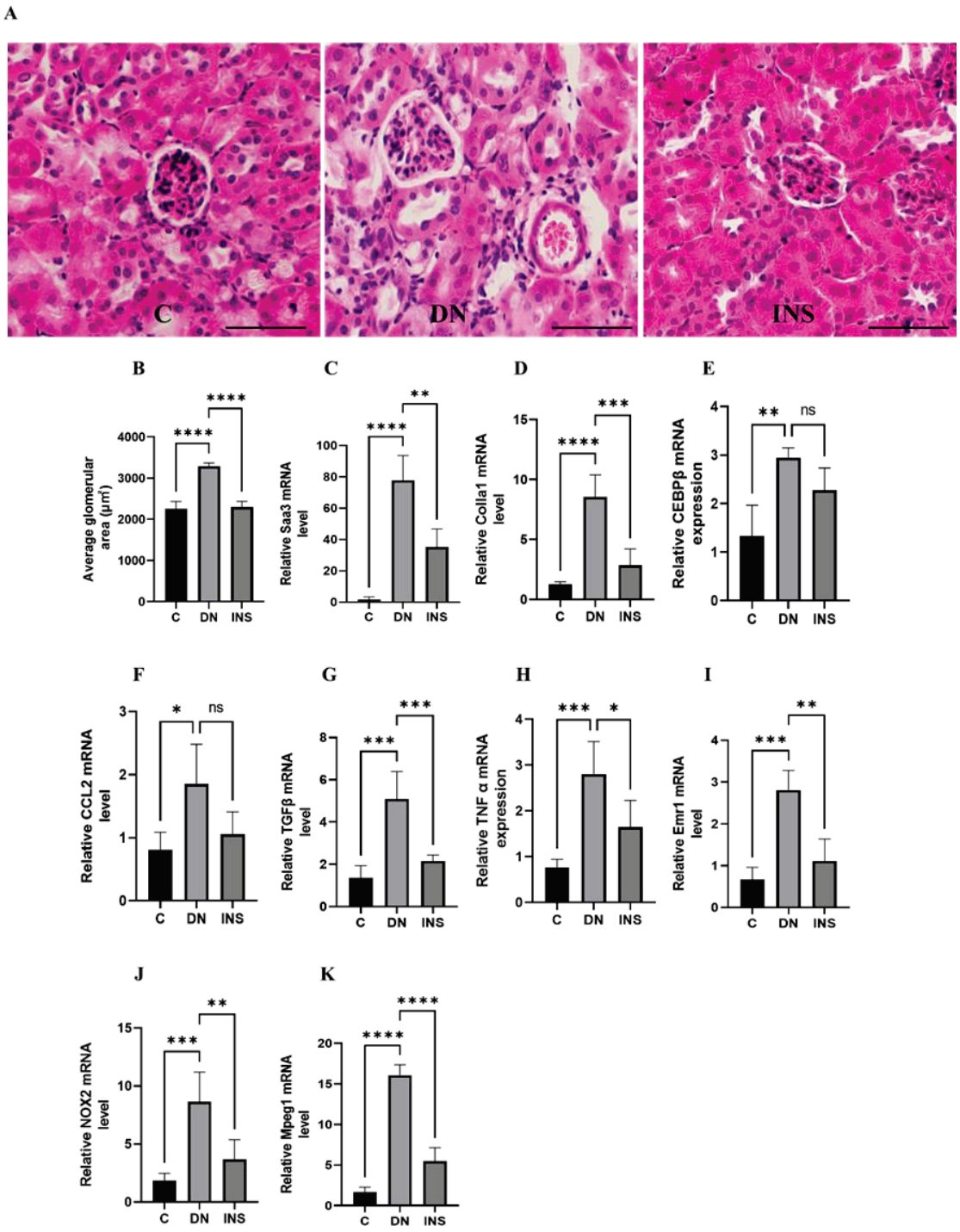

Figure 34**.** Validation of bioluminescence signals of Saa3 promoter-luc mice with traditional diagnostic techniques and ameliorative effect of insulin therapy on renal fibro-inflammatory cues in two-moderate-dose STZ-induced DN model. (**A**) Representative image of the kidney

histological staining with H&E reagents. Glomerular hypertrophy, glomerular hypercellularity (G), brush border disruption (asterisks), and interstitial hemorrhage (arrow) were significantly increased in renal tissue of DN mice. Scale bar = 200 μm. (**B**) Quantification of average glomerular size (n = 5). (**C**–**K**) Kidney gene expression analysis of fibro-inflammatory markers in two-moderate-dose STZ-induced DN model (n = 5). The relative mRNA expression level of each gene was determined by quantitative PCR and normalized to L19 mRNA level and are presented as means ± S.E. * $p < 0.05$, ** $p < 0.01$, *** $p < 0.001$, **** $p < 0.0001$ as determined by ANOVA followed by Dunnett's test; ns: statistically not significant. DN = Diabetic Nephropathy, C = Control, INS = Insulin treatment.

Interestingly, despite the robust induction of fibro-inflammatory markers in the moderate-dose STZ model, insulin treatment significantly reduced the expression of kidney fibro-inflammatory markers (Figure 34C–K).

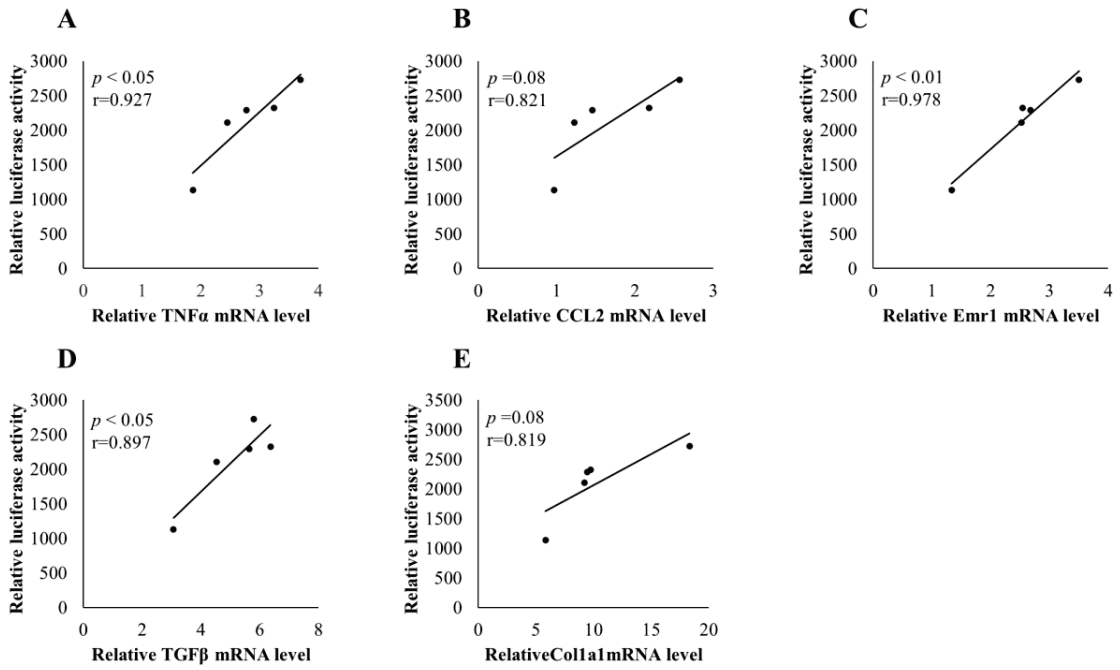

Figure 35. Positive correlation between luciferase activity and mRNA expression levels of TNFα, CCL2, Emr1, TGFβ, and Colla1 in two moderate-dose STZ-induced DN model. (n = 5). The relative mRNA expression levels of TNFα, CCL2, Emr1, TGFβ, and Colla1 in kidney tissue were determined by quantitative PCR and normalized to L19 mRNA level (n = 5). Meanwhile the in vivo luciferase activities were determined by quantitative analysis of bioluminescence intensity from two moderate dose STZ-induced mouse kidneys (n=5). Pearson's correlation coefficient showed a positive correlation between luciferase activity

(promoter activity) and mRNA expression levels of TNFα (A), CCL2 (B), Emr1 (C), TGFβ (D), and Colla1(E) in kidney tissue.

Biochemical analysis of the plasma BUN concentration was also found to be significantly increased in moderate-dose STZ-induced DN Saa3 promoter-luc mice as compared to their corresponding control group. However, insulin treatment decreased the plasma BUN concentration (Fig. 36). Taken together with our histological and molecular findings, these results indicate that diabetes-induced kidney injury mediated by fibro-inflammatory cues can be successfully monitored using non-invasive Saa3-promoter bioluminescence imaging.

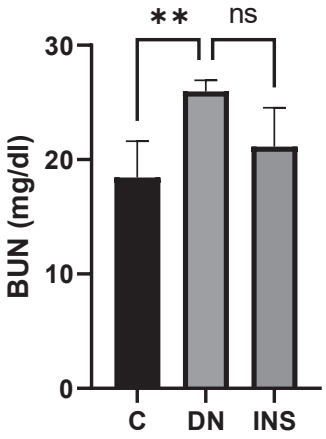

Fig. 36. Elevated plasma BUN level in two-moderate-dose STZ-induced DN model was suppressed by insulin treatment (n = 5). Data are presented as means ± S.E. ** $p < 0.01$ as determined by ANOVA followed by Dunnett's test. DN = Diabetic Nephropathy, C = Control, INS = Insulin treatment.

5.4. Discussion

Diabetic nephropathy (DN) is a common microvascular complication of diabetes and a major cause of end-stage renal disease worldwide (Hussain et al., 2021; Chawla et al., 2016). Traditional techniques, such as the histological assessment of collagen deposition and quantification of serum/urine biomarkers (e.g., creatinine, blood urea nitrogen (BUN), albumin, and cytokines), are the most commonly used to diagnose kidney disorders (Su et

al., 2021). Although these markers have provided essential insight regarding renal functions in human patients and animals, signals of early responses of renal pathologies are often missed by these traditional methods of monitoring renal functions. Serum creatinine and BUN are easy to measure using specific assays; however, these markers are often influenced by various factors, such as diet and other tissue functions (Wasung et al., 2015; Griffin et al., 2019). Despite their shortcomings, the demand for early diagnostic markers is expected to increase in human patients and animal experiments. This study attempted to identify the molecular signature of the renal inflammatory responses induced by the diabetic milieu using two types of STZ-induced DN models. STZ is widely used as a diabetogenic agent in rodent models of DN (Brosius et al., 2017; Breyer et al., 2005; Tesch and Allen, 2007). Since STZ is an analog of glucose, it is efficiently taken up by pancreatic beta cells via the glucose transporter Glut2 and causes DNA damage and beta-cell death (Brosius et al., 2017; Breyer et al., 2005; Tesch and Allen, 2007). However, because STZ treatment is toxic to other tissues, such as the kidney, numerous studies have attempted to clarify its undesirable side effects on other tissues, particularly by high-dose treatment with STZ (Brosius et al., 2017; Breyer et al., 2005; Tesch and Allen, 2007; Brouwers et al., 2013). In this study, to eliminate the detrimental toxicity to the kidney, two types of STZ models, HFD/multiple low-dose STZ injections and two moderate-dose STZ injections that can promote DN development by inducing hyperglycemia were used. Next, the comparative transcriptome analyses of damaged kidneys from both STZ models were performed. Consistent with previous studies (Anderberg et al., 2015; Niewczas et al., 2019; Usui et al., 2007; Guha et al., 2007; Okuma et al., 2021; Xu et al., 2021), these data indicate significant increases in fibrosis and inflammatory marker mRNA levels in both STZ-induced DN models. In this study, we finally utilized the Saa3-promoter activity as a sensitive and specific tool for detecting and visualizing renal pathology induced by diabetic fibro-inflammatory cues in real-time via non-invasive in vivo bioluminescence imaging. This study suggests that this novel bioluminescence imaging tool can be used not only to detect DN status in the two well-established STZ-induced models of DN but also to monitor therapeutic responses in the same individual mice.

Fibro-inflammatory cues are the cardinal molecular signals that drive DN pathogenesis and progression (Thomas et al., 2015; Navarro-González et al., 2011; Matoba et al., 2019; Moreno et al., 2018; Qian et al., 2008; Zheng et al., 2021; Meek et al., 2013). Notably, several studies have shown that serum amyloid A (Saa) is a key potential mediator of danger signals that influence inflammatory processes in several chronic inflammatory diseases, such as rheumatoid arthritis, atherosclerosis, obesity, and kidney diseases (Ye and Sun, 2015; Eklund et al., 2012; Sorić Hosman et al., 2021; Chami et al., 2019; den Hartigh et al., 2014). The Saa3 protein, one of the subtypes of the Saa family, was originally characterized as an acute-phase protein (Thaler et al., 2015). For example, Saa3 is highly expressed in adipose tissue in obese mice, which thus possibly plays a role in monocyte chemotaxis, providing a mechanism for macrophage accumulation that occurs during obesity development (den Hartigh et al., 2014). In addition, Saa can mediate a cascade of inflammatory events via interactions with multiple receptors, including Toll-like receptor 2 (TLR2), TLR4, scavenger receptor class B type 1 (SR-B1), and receptor for advanced glycation end-product (RAGE) (Ye and Sun, 2015). However, the pathological relationship between Saa3 and diabetes-induced renal fibro-inflammation has not been fully elucidated. Various inflammatory stimuli, such as TNF-α, CCL-2, IL-1β, and IL-6, which drive chronic renal inflammation in diabetic kidney disease, have been shown to stimulate Saa3 production in mice (Dieter et al., 2019). Interestingly, a recent report suggested that the accumulation of advanced glycation end-products (AGEs) in a hyperglycemic environment can increase Saa3 mRNA expression in podocytes, which are located around the capillaries of the glomerulus and further contribute to the production of pro-inflammatory cytokines through increased Saa3 expression (Anderberg et al., 2015; Goldin et al., 2006; Chen et al., 2010). These results suggested a mechanistic pathway for the induction of renal inflammation under diabetic conditions in mice. Notably, the elevated levels of the Saa family seen in the two different STZ models are similar to those observed in the kidneys of human patients with DN (Anderberg et al., 2015; Dieter et al., 2016). Taken together, these findings suggest that Saa3 plays an important role in inflammatory and fibrotic disorders in DN, and monitoring Saa3 promoter activity in renal tissues may be useful for the evaluation of diabetic kidney disease.

As described above, inflammation and fibrosis are essential factors that can promote both the pathogenesis and progression of DN. Despite the growing trend of this life-threatening disease, non-invasive screening, and monitoring tools for diabetes-induced fibro-inflammation in renal tissues in vivo are limited. Further experiments are needed to determine whether the in vivo bioluminescence signal in these two STZ-induced DN models is directly associated with increased fibro-inflammatory signals from diabetes-induced renal injury and to identify factors related to increased renal Saa3 mRNA expression during DN development. These factors are more important in driving Saa3 promoter activity in Saa3-luc mice by analyzing the causal relationship with glomerular hypertrophy observed using fibro-inflammatory markers (TNFα, TGFβ, Col1a1, Ccl2, EMR1, Nox2, and Mpeg1), which are known to cause progressive renal injuries in both animal models and human patients. Owing to the low sensitivity of these traditional serum/urine biomarkers, they tend to miss early injury responses in the diabetic kidneys of mice. This novel in vivo bioluminescence imaging is expected to serve as an important pre-clinical tool with animal studies, and will be useful for the non-invasive, real-time monitoring of the effectiveness of drugs or food factors for DN progression.

Abstract

The early detection of diabetic nephropathy (DN) in mice is necessary for the development of drugs and functional foods. The purpose of this study was to identify genes that are significantly upregulated in the early stage of DN progression and develop a novel model to non-invasively monitor disease progression within living animals using in vivo imaging technology. Streptozotocin (STZ) treatment has been widely used as a DN model; however, it also exhibits direct cytotoxicity to the kidneys. As it is important to distinguish between DN-related and STZ-induced nephropathy, in this study, we compared renal responses induced by the diabetic milieu with two types of STZ models: multiple low-dose STZ injections with a high-fat diet and two moderate-dose STZ injections to induce DN. The result showed that 221 genes whose expression was significantly altered during DN development in both models and identified serum amyloid A3 (*Saa3*) as a candidate gene. Next, the Saa3 promoter-driven luciferase reporter (Saa3-promoter luc mice) was applied to performed in vivo bioluminescent imaging to monitor the progression of renal pathology in the two STZ models. In this study, to further exclude the possibility that the in vivo bioluminescence signal is related to renal cytotoxicity by STZ treatment, insulin was injected into Saa3-promoter luc mice and showed that insulin treatment could downregulate renal inflammatory responses with a decreased signal intensity of in vivo bioluminescence imaging. These results strongly suggest that Saa3 promoter activity is a potent non-invasive indicator that can be used to monitor DN progression and explore therapeutic agents and functional foods.

Chapter 6

General Discussion and Conclusion

Skeletal muscle being the largest organ in the body is integral not only for the control of locomotion but also fundamental for breathing, energy expenditure, as well as whole body metabolic control by regulating blood glucose, amino acids, and lipids homeostasis and for maintaining a high quality of life (Sartori et al., 2021). Given the extensive role skeletal muscle play in life, one can understand that loss of skeletal muscle mass which is often refer to as muscle wasting or muscle atrophy will lead to serious consequences. In fact, it is general knowledge that skeletal muscle wasting compromises not only the quality of life but also increases morbidity, and mortality. Unfortunately, loss of muscle mass happens to everyone as we age. Furthermore, sedentary lifestyle and chronic pathological conditions associated with aging also contribute to this debilitating condition. Therefore, if we are to improve the quality and longevity of life it is important to prevent or attenuate such loss of muscle mass. Despite the great effort scientists have made, the absence of effective therapy to counteract atrophy muscle indicated that our understanding of the molecular mechanisms underlying muscle wasting is limited. Non-alcoholic fatty liver disease (NAFLD), and diabetes mellitus (DM) disease models were used for research on muscle wasting, because skeletal muscle disorders are clinically discussed for these two metabolic disease states (Pacifico et al., 2019; Choe et al., 2018; Cruz et al., 2019 D'Souza et al., 2013). Additionally, other salient complications such as chronic kidney disease could also exacerbate muscle wasting in NAFLD and DM patients thereby reducing their chances of survival. Regrettably, the lack of diagnostic tool that could detect renal disease in NAFLD and DM has impeded the development of effective therapeutic strategies that could be used to prevent/manage these secondary complication (i.e chronic kidney disease) at early stage. Thus, the aim of this thesis was: (1) to develop a relevant animal model that can be used to study muscle wasting associated with NAFLD and DM; (2) gain a clear understanding of the molecular mechanism underlying muscle wasting in each model, and (3) develop a novel diagnostic tool that can be used to detect diabetic nephropathy at early stage.

Skeletal muscle has a remarkable capacity for growth and repair following injury (Relaix et al., 2021). The ability of skeletal muscle to undergo constant repair and regeneration is largely dependent on primary muscle stem cells termed satellite cells (SCs) (Relaix et al., 2021). The impairment in SC content, function, and subsequent attenuation of muscle regeneration seen in DM is not only unique to this study. However, this is the first study that demonstrate that SC dysfunction contribute to muscle wasting in a mouse model of NAFLD. Similar to DM, this study also shows that alteration in SC activity in NAFLD decrease the regenerative ability of NAFLD skeletal muscle. Given the critical role SC plays in skeletal muscle maintenance and plasticity, this suggests that bolstering SC content/function in individuals with NAFLD and DM may slow down muscle wasting and thus, serve as a potential therapeutic target. Interestingly, recent advances in stem cell therapies targeting diabetic skeletal muscle have shown considerable success (Cai et al., 2022; Zakrzewski et al., 2019). For instance, transplantation of human skeletal myoblast (hSkM) into limb muscles of KK mouse an animal model of type 2 DM, could ameliorate diabetic symptoms (Ye et al., 2009). In fact, several studies have shown that intramuscular or systemic administration of bone marrow derived mesenchymal stem cells (MSCs) generally improved diabetic myopathy (Teng and Huang, 2019). Since SC dysfunction is a common mechanism underlying muscle wasting in DM and NAFLD, the current progress made in using stem cell therapy to manage muscle wasting in DM could be applied in reversing muscle wasting in NAFLD and other chronic disease. To improve the efficacy of this therapeutic strategy a clear understanding of the molecular mechanism underlying SC dysfunction in both DM and NAFLD is crucial. In this study chronic inflammation and oxidative stress are common molecular factors responsible for SC dysfunction in both DM and NAFLD.

Chronic inflammation

The literature is clear that persistence chronic inflammations can disrupt normal muscle regeneration by impairing muscle SC content and function (Howard et al., 2020). Chronic elevation of tumor necrosis factor-alpha (*TNF-α*) was observed in NAFLD skeletal muscle. Also, this study added interferon-inducible genes (*Ifi44,* and *Ifit1*) to a growing list

of overexpressed proinflammatory cytokines in DM that include TNF-α, Interleukin-1-beta (IL-1β), and IL-6. These pro-inflammatory cytokines can collectively and/or independently disrupt muscle SC activity. For example, chronic increase in TNF-α have been shown to promote continuous stimulation of SC, an event that eventually prevent SC differentiation (Howard et al., 2020; Howard et al., 2020). No wonder in this study MyoD (marker of differentiation) expression is downregulated in NAFLD. Akin to TNF-α, chronic increase in IL-6 and interferon gamma (IFN-γ) have also been shown to epigenetically suppress gene related to SC differentiation (Perandini et al., 2018). Interestingly, chronic inflammation of the skeletal muscle seen in these rodent studies (NAFLD and DM models) is similar to what is observed in several human muscle wasting disorders (Boursereau et al., 2017; Koshikawa et al., 2020). Thus, one might think that therapeutic strategies aiming to eliminate chronic inflammation will undoubtedly prevent SC dysfunction thereby reversing muscle wasting. As exciting as this avenue of therapeutic strategy is, regrettably this study shows that such approach will not be effective, in fact, it would exacerbate muscle wasting outcome. As discussed in chapter 4, significant reduction of pro-inflammatory cytokine by glucocorticoid a well-known anti-inflammatory molecule resulted in more loss of SC content and severe muscle damage in high-dose STZ induced diabetic model. This data suggests that any attempt to totally abolish inflammation (pro- or anti-inflammatory molecule) could aggravate loss of muscle mass. This raises a vital question, what level of inflammation is required to maintain a normal muscle health? Although it might be difficult to estimate the exact level of pro-inflammatory or anti-inflammatory molecules required to maintain proper muscle health, however. future study can develop new strategies for reversing chronic inflammation without totally abrogating it. This method can help restore the niche and function of SC which is crucial for skeletal muscle maintenance. In addition, future studies have to elucidate the origin of the pro-inflammatory cytokine, whether is from systemic circulation or from muscle resident cells such as SCs, fibro-adipogenic progenitor cells, endothelial cells, and macrophages. This study is crucial for the development of therapeutic intervention.

Oxidative stress

Oxidative stress is caused by imbalance between reactive oxygen species (ROS) generation and antioxidant defense (Pizzino et al., 2017). A shift in pro-oxidant/antioxidant balance is a critical pathogenic factor shared by both NAFLD, and DM patients. This study demonstrated that oxidative stress is evident in skeletal muscle from the mice models of NAFLD and DM. Numerous study have also confirmed that oxidative stress is enhanced in the skeletal muscle of diabetic patient. Chronic oxidative stress could hinder muscle SC activity, expansion, viability, and lifespan via several mechanisms. For example, redox imbalance can result in DNA damage an event that could trigger SC senescence or apoptosis (Kumari and Jat, 2021; Filomeni et al., 2015; Sugihara et al., 2018). DNA microarray data of skeletal muscle from DM models presented in this study showed that the markers of cellular senescence and apoptosis are significantly elevated. This suggest that it is possible that some of the SCs are either undergoing apoptosis or senescence. Although, this study did not investigate if this same mechanism hinders SC activity in NAFLD, there is a possibility that this mechanism is responsible for SC dysfunction in NAFLD muscle. Thus, additional experimentation that will specifically test this hypothesis would further help improve our understanding of how oxidative stress drives SC dysfunction in NAFLD skeletal muscle.

Additionally, oxidative stress has been implicated in disrupting SC fate determination, whether to remain inactive (in quiescence) become activated, self-renew their population, or commit to differentiation. In fact, vettor and colleagues showed that oxidative stress can change SC fate to that of fibroadipogenic cell (Vettor et al., 2009). Whether this same process occur within DM and NAFLD skeletal muscle remain unknown. However, the rapid degradation of extracellular matrix protein and expression of fibrosis marker observed in this study and other study suggested this event might occur in DM and NAFLD muscle. Thus, with the aid of scRNA sequencing future study will investigate the effect of oxidative stress on DM and NAFLD skeletal muscle SC fate. No doubt, verification of the occurrence of SC fate reprograming in DM and NAFLD will open up new strategy for the treatment of muscle atrophy and other complications associated with a variety of regenerative tissues in disease state.

Though this study has proposed oxidative stress/inflammation mediated impairment in SC activity as a primary mechanism of muscle wasting in NAFLD and DM, an alternative scenario (which need not to be mutually exclusive) could involve impairment of protein metabolism pathway. While oxidative stress and elevated glucocorticoid level have been reported to independently promote protein degradation and suppress protein synthesis in atrophic muscle, the fact that this is occurring in high-STZ induced diabetic model of this study is a critical finding to unlocking another mechanism underlying muscle wasting in NAFLD. Oxidative stress induces protein degradation via several mechanism such as (1) induction of autophagy, and ubiquitin-proteasome system key proteins; (2) modification myofibrillar proteins to enhance proteolytic processing**;** (3) promote calpain and caspase-3 activation (Szentesi et al., 2019). The inhibitory effect of oxidative stress on protein synthesis results primarily from inhibiting translation at the level of initiation, via phosphorylation of the eIF4E repressor protein (Samluk et al., 2019). Meanwhile elevated glucocorticoid level mediate protein degradation via ubiquitin-proteasome system and autophagy lysosome system (Braun and Marks, 2015). On the other hand, glucocorticoid elicit his inhibitory effect on protein synthesis by interference with the IGF-1/PI3K/Akt/mTOR signaling pathway (Braun and Marks, 2015). The present finding indicated that the interplay between oxidative stress and elevated glucocorticoid level aggravate protein degradation and severely suppress protein synthesis in DM model. Therefore, to reverse alteration in DM skeletal muscle protein metabolism it is crucial to target not only oxidative stress but also glucocorticoid receptor. Although, the alteration in NAFLD protein metabolism pathway was not elucidated in this study, the DM data suggest that similar event might occur in the skeletal muscle of NAFLD. After-all oxidative stress also dominates the molecular cue of NAFLD. Clearly, future studies are needed to further investigate the effect of oxidative stress and glucocorticoid on NAFLD skeletal muscle protein metabolism.

Another potential approach to reverse loss of muscle mass associated with DM is to identify and treat other secondary complications of DM at their early stage. Failure to do this may blunted the gains made in restoring muscle mass. Diabetes nephropathy (DN) is one of such debilitating secondary complication. Considering the absence of diagnostic tool that

could specifically detect this condition at is early stage, chapter 5 of this thesis focus on developing a novel non-invasive diagnostic tool that could be used not only for diabetes nephropathy but also for early detection of nephrotoxicity in clinical drug development. Analysis of the microarray data of kidneys from two STZ-induced DN models provided an overview of potential biomarkers that could be used for early detection of DN in mice, ranging from fibro-inflammatory biomarkers to senescence and apoptosis biomarker. Several studies have shown that fibro-inflammatory cues are the cardinal molecular signals that drive DN pathogenesis and progression. Measurement of serum amyloid A 3 (Saa3) is an appropriate choice not only because it is a major mediator of fibro-inflammatory signal but also it originates from the site of injury. This suggest that the application of the Saa3 promoter activity for bioluminescence imaging of diabetes-induced kidney injury will no doubt eliminate the challenge of organ non-specificity. In preclinical studies the gold standard for accurate detection of kidney injury is histological examination (Giffin et al., 2009). However, the drawback of this technique is that it requires sacrificing the mice making it difficult to monitor the disease progression. Meanwhile, with the novel non-invasive approach of molecular kidney imaging developed in this study, disease staging, prognostication, monitoring of treatment responses and management of mice induced with DN, and other chronic kidney disease is visible. Non-invasive visualization of the aristolochic acid induced kidney injury also indicated that Saa3 mediated bioluminescence imaging can also be used to assess nephrotoxicity effects of drug before clinical trial. Studies have shown that only 40-60% of animal findings are predictive of toxicity in humans. These limitations have hindered the progression of potentially efficacious compounds from reaching clinical phase of drug trail. To address this limitation, future study could incorporate the novel Saa3 mediated bioluminescence imaging technique develop in this study to immortalized human proximal tubule cell line.

Overall, with regards to the aims of this thesis, our understanding of the molecular mechanisms mediating loss of muscle mass in NAFLD, and DM have improved. It is clear that the cascade of event responsible for muscle SC dysfunction in NAFLD and DM is caused by multiple factors. Furthermore, in addition to defect in SC, this study demonstrated that

alteration in protein metabolism and oxidative stress plays critical role in the deteriorations of DM and NAFLD muscle health. Thus, to adequately treat muscle atrophy associated with chronic disease it is crucial to develop drugs that will interfere simultaneously with multiple targets rather than single target. This study also presented reliable diagnostic tool for kidney disease with the ultimate aim of early detection of disease and/or drug induced kidney injury at preclinical setting.

References

Abbott, J.D. and Giordano, F.J., 2003. Stem cells and cardiovascular disease. *Journal of nuclear cardiology*, *10*(4), pp.403-412.

Accili, D. and Arden, K.C., 2004. FoxOs at the crossroads of cellular metabolism, differentiation, and transformation. *Cell*, *117*(4), pp.421-426.

Alexakis, C., Partridge, T. and Bou-Gharios, G., 2007. Implication of the satellite cell in dystrophic muscle fibrosis: a self-perpetuating mechanism of collagen overproduction. *American Journal of Physiology-Cell Physiology*, *293*(2), pp.C661-C669.

Aljabban, J., Syed, S., Syed, S., Rohr, M., Weisleder, N., McElhanon, K.E., Hasan, L., Safeer, L., Hoffman, K., Aljabban, N. and Mukhtar, M., 2020. Investigating genetic drivers of dermatomyositis pathogenesis using meta-analysis. *Heliyon*, *6*(9), p.e04866.

Alkhalidy, H., Moore, W., Wang, Y., Luo, J., McMillan, R.P., Zhen, W., Zhou, K. and Liu, D., 2018. The flavonoid kaempferol ameliorates streptozotocin-induced diabetes by suppressing hepatic glucose production. *Molecules*, *23*(9), p.2338.

Alway, S.E., Myers, M.J. and Mohamed, J.S., 2014. Regulation of satellite cell function in sarcopenia. *Frontiers in aging neuroscience*, *6*, p.246.

Anderberg, R.J., Meek, R.L., Hudkins, K.L., Cooney, S.K., Alpers, C.E., Leboeuf, R.C. and Tuttle, K.R., 2015. Serum amyloid A and inflammation in diabetic kidney disease and podocytes. *Laboratory Investigation*, *95*(3), pp.250-262.

Arcaro, C.A., Assis, R.P., Oliveira, J.O., Zanon, N.M., Paula-Gomes, S., Navegantes, L.C.C., Kettelhut, I.C., Brunetti, I.L. and Baviera, A.M., 2021. Phosphodiesterase 4 inhibition restrains muscle proteolysis in diabetic rats by activating PKA and EPAC/Akt effectors and inhibiting FoxO factors. *Life Sciences*, *278*, p.119563.

Baghdadi, M.B., Castel, D., Machado, L., Fukada, S.I., Birk, D.E., Relaix, F., Tajbakhsh, S. and Mourikis, P., 2018. Reciprocal signalling by Notch–Collagen V–CALCR retains muscle stem cells in their niche. *Nature*, *557*(7707), pp.714-718.

Baskin, K.K., Winders, B.R. and Olson, E.N., 2015. Muscle as a "mediator" of systemic metabolism. *Cell metabolism*, *21*(2), pp.237-248.

Bentzinger, C.F., Wang, Y.X., Dumont, N.A. and Rudnicki, M.A., 2013. Cellular dynamics in the muscle satellite cell niche. *EMBO reports*, *14*(12), pp.1062-1072.

Bernet, J.D., Doles, J.D., Hall, J.K., Kelly Tanaka, K., Carter, T.A. and Olwin, B.B., 2014. p38 MAPK signaling underlies a cell-autonomous loss of stem cell self-renewal in skeletal muscle of aged mice. *Nature medicine*, *20*(3), pp.265-271.

Billeter, R. and Hoppeler, H., 1992. Muscular basis of strength. *Strength and power in sport*, p.50.

Bjornson, C.R., Cheung, T.H., Liu, L., Tripathi, P.V., Steeper, K.M. and Rando, T.A., 2012. Notch signaling is necessary to maintain quiescence in adult muscle stem cells. *Stem cells*, *30*(2), pp.232-242.

Blanc, R.S., Kallenbach, J.G., Bachman, J.F., Mitchell, A., Paris, N.D. and Chakkalakal, J.V., 2020. Inhibition of inflammatory CCR2 signaling promotes aged muscle regeneration and strength recovery after injury. *Nature communications*, *11*(1), pp.1-12.

Bloemberg, D. and Quadrilatero, J., 2019. Autophagy, apoptosis, and mitochondria: molecular integration and physiological relevance in skeletal muscle. *American Journal of Physiology-Cell Physiology*, *317*(1), pp.C111-C130.

Bodine, S.C., Stitt, T.N., Gonzalez, M., Kline, W.O., Stover, G.L., Bauerlein, R., Zlotchenko, E., Scrimgeour, A., Lawrence, J.C., Glass, D.J. and Yancopoulos, G.D., 2001. Akt/mTOR pathway is a crucial regulator of skeletal muscle hypertrophy and can prevent muscle atrophy in vivo. *Nature cell biology*, *3*(11), pp.1014-1019.

Bonaldo, P. and Sandri, M., 2013. Cellular and molecular mechanisms of muscle atrophy. *Disease models & mechanisms*, *6*(1), pp.25-39.

Bonnans, C., Chou, J. and Werb, Z., 2014. Remodelling the extracellular matrix in development and disease. *Nature reviews Molecular cell biology*, *15*(12), pp.786-801.

Boursereau, R., Abou-Samra, M., Lecompte, S., Noel, L. and Brichard, S.M., 2017. New targets to alleviate skeletal muscle inflammation: role of microRNAs regulated by adiponectin. *Scientific reports*, *7*(1), pp.1-14.

Braun, T.P. and Marks, D.L., 2015. The regulation of muscle mass by endogenous glucocorticoids. *Frontiers in physiology*, *6*, p.12.

Breyer, M.D., Böttinger, E., Brosius, F.C., Coffman, T.M., Harris, R.C., Heilig, C.W. and Sharma, K., 2005. Mouse models of diabetic nephropathy. *Journal of the American Society of Nephrology*, *16*(1), pp.27-45.

Brosius, F.C., Alpers, C.E., Bottinger, E.P., Breyer, M.D., Coffman, T.M., Gurley, S.B., Harris, R.C., Kakoki, M., Kretzler, M., Leiter, E.H. and Levi, M., 2009. Mouse models of diabetic nephropathy. *Journal of the American Society of Nephrology*, *20*(12), pp.2503-2512.

Brouwers, B., Pruniau, V.P., Cauwelier, E.J., Schuit, F., Lerut, E., Ectors, N., Declercq, J. and Creemers, J.W., 2013. Phlorizin pretreatment reduces acute renal toxicity in a mouse model for diabetic nephropathy. *Journal of Biological Chemistry*, *288*(38), pp.27200-27207.

Bullón-Vela, V., Abete, I., Tur, J.A., Pintó, X., Corbella, E., Martínez-González, M.A., Toledo, E., Corella, D., Macías, M., Tinahones, F. and Fitó, M., 2020. Influence of lifestyle factors and staple foods from the Mediterranean diet on non-alcoholic fatty liver disease among older individuals with metabolic syndrome features. *Nutrition*, *71*, p.110620.

Cabrera, D., Ruiz, A., Cabello-Verrugio, C., Brandan, E., Estrada, L., Pizarro, M., Solis, N., Torres, J., Barrera, F. and Arrese, M., 2016. Diet-induced nonalcoholic fatty liver disease is associated with sarcopenia and decreased serum insulin-like growth factor-1. *Digestive diseases and sciences*, *61*(11), pp.3190-3198.

Cai, T., Ke, Q., Fang, Y., Wen, P., Chen, H., Yuan, Q., Luo, J., Zhang, Y., Sun, Q., Lv, Y. and Zen, K., 2020. Sodium–glucose cotransporter 2 inhibition suppresses HIF-1α-mediated metabolic switch from lipid oxidation to glycolysis in kidney tubule cells of diabetic mice. *Cell death & disease*, *11*(5), pp.1-17.

Cai, Z., Liu, D., Yang, Y., Xie, W., He, M., Yu, D., Wu, Y., Wang, X., Xiao, W. and Li, Y., 2022. The role and therapeutic potential of stem cells in skeletal muscle in sarcopenia. *Stem Cell Research & Therapy*, *13*(1), pp.1-12.

Caso, G., Garlick, B.A., Casella, G.A., Sasvary, D. and Garlick, P.J., 2004. Acute metabolic acidosis inhibits muscle protein synthesis in rats. *American Journal of Physiology-Endocrinology and Metabolism*, *287*(1), pp.E90-E96.

Chami, B., Hossain, F., Hambly, T.W., Cai, X., Aran, R., Fong, G., Vellajo, A., Martin, N.J., Wang, X., Dennis, J.M. and Sharma, A., 2019. Serum Amyloid a stimulates vascular and renal dysfunction in apolipoprotein e-deficient mice fed a normal chow diet. *Frontiers in immunology*, *10*, p.380.

Chao, P.C., Li, Y., Chang, C.H., Shieh, J.P., Cheng, J.T. and Cheng, K.C., 2018. Investigation of insulin resistance in the popularly used four rat models of type-2 diabetes. *Biomedicine & Pharmacotherapy*, *101*, pp.155-161.

Chatterjee, S., Khunti, K. and Davies, M.J., 2017. Type 2 diabetes. *The lancet*, *389*(10085), pp.2239-2251.

Chawla, A., Chawla, R. and Jaggi, S., 2016. Microvasular and macrovascular complications in diabetes mellitus: Distinct or continuum?. *Indian journal of endocrinology and metabolism*, *20*(4), p.546.

Chen, E.S., Song, Z., Willett, M.H., Heine, S., Yung, R.C., Liu, M.C., Groshong, S.D., Zhang, Y., Tuder, R.M. and Moller, D.R., 2010. Serum amyloid A regulates granulomatous inflammation in sarcoidosis through Toll-like receptor-2. *American journal of respiratory and critical care medicine*, *181*(4), pp.360-373.

Chen, S.E., Jin, B. and Li, Y.P., 2007. TNF-α regulates myogenesis and muscle regeneration by activating p38 MAPK. *American Journal of Physiology-Cell Physiology*, *292*(5), pp.C1660-C1671.

Chhetri, J.K., de Souto Barreto, P., Fougère, B., Rolland, Y., Vellas, B. and Cesari, M., 2018. Chronic inflammation and sarcopenia: A regenerative cell therapy perspective. *Experimental gerontology*, *103*, pp.115-123.

Chiodini, I., Adda, G., Scillitani, A., Coletti, F., Morelli, V., Di Lembo, S., Epaminonda, P., Masserini, B., Beck-Peccoz, P., Orsi, E. and Ambrosi, B., 2007. Cortisol secretion in patients with type 2 diabetes: relationship with chronic complications. *Diabetes care*, *30*(1), pp.83-88.

Cho, Y., Hazen, B.C., Gandra, P.G., Ward, S.R., Schenk, S., Russell, A.P. and Kralli, A., 2016. Perm1 enhances mitochondrial biogenesis, oxidative capacity, and fatigue resistance in adult skeletal muscle. *The FASEB Journal*, *30*(2), pp.674-687.

Cho, Y., Hazen, B.C., Russell, A.P. and Kralli, A., 2013. Peroxisome proliferator-activated receptor γ coactivator 1 (PGC-1)-and estrogen-related receptor (ERR)-induced regulator in muscle 1 (Perm1) is a tissue-specific regulator of oxidative capacity in skeletal muscle cells. *Journal of Biological Chemistry*, *288*(35), pp.25207-25218.

Choe, E.K., Kang, H.Y., Park, B., Yang, J.I. and Kim, J.S., 2018. The association between nonalcoholic fatty liver disease and CT-measured skeletal muscle mass. *Journal of Clinical Medicine*, *7*(10), p.310.

Choi, H.J., Yeon, M.H. and Jun, H.S., 2021. Schisandrae chinensis Fructus Extract Ameliorates Muscle Atrophy in Streptozotocin-Induced Diabetic Mice by Downregulation of the CREB-KLF15 and Autophagy–Lysosomal Pathways. *Cells*, *10*(9), p.2283.

Choi, M.H., Ow, J.R., Yang, N.D. and Taneja, R., 2016. Oxidative stress-mediated skeletal muscle degeneration: molecules, mechanisms, and therapies. *Oxidative Medicine and Cellular Longevity*, *2016*, pp. 1-13

Choi, M.S., Kim, Y.J., Kwon, E.Y., Ryoo, J.Y., Kim, S.R. and Jung, U.J., 2015. High-fat diet decreases energy expenditure and expression of genes controlling lipid metabolism, mitochondrial function and skeletal system development in the adipose tissue, along with increased expression of extracellular matrix remodelling-and inflammation-related genes. *British Journal of Nutrition*, *113*(6), pp.867-877.

Chow, F.Y., Nikolic-Paterson, D.J., Ozols, E., Atkins, R.C., Rollin, B.J. and Tesch, G.H., 2006. Monocyte chemoattractant protein-1 promotes the development of diabetic renal injury in streptozotocin-treated mice. *Kidney international*, *69*(1), pp.73-80.

Cleasby, M.E., Jamieson, P.M. and Atherton, P.J., 2016. Insulin resistance and sarcopenia: mechanistic links between common co-morbidities. *Journal of Endocrinology*, *229*(2), pp.R67-R81.

Cohen, S., Nathan, J.A. and Goldberg, A.L., 2015. Muscle wasting in disease: molecular mechanisms and promising therapies. *Nature reviews Drug discovery*, *14*(1), pp.58-74.

Cohen, S., Zhai, B., Gygi, S.P. and Goldberg, A.L., 2012. Ubiquitylation by Trim32 causes coupled loss of desmin, Z-bands, and thin filaments in muscle atrophy. *Journal of Cell Biology*, *198*(4), pp.575-589.

Collins, B.C., Arpke, R.W., Larson, A.A., Baumann, C.W., Xie, N., Cabelka, C.A., Nash, N.L., Juppi, H.K., Laakkonen, E.K., Sipilä, S. and Kovanen, V., 2019. Estrogen regulates the satellite cell compartment in females. *Cell reports*, *28*(2), pp.368-381.

Conboy, I.M., Conboy, M.J., Wagers, A.J., Girma, E.R., Weissman, I.L. and Rando, T.A., 2005. Rejuvenation of aged progenitor cells by exposure to a young systemic environment. *Nature*, *433*(7027), pp.760-764.

Copray, S., Liem, R., Brouwer, N., Greenhaff, P., Habens, F. and Fernyhough, P., 2000. Contraction-induced muscle fiber damage is increased in soleus muscle of streptozotocin-diabetic rats and is associated with elevated expression of brain-derived neurotrophic factor mRNA in muscle fibers and activated satellite cells. *Experimental neurology*, *161*(2), pp.597-608.

Corbin, K.D. and Zeisel, S.H., 2012. Choline metabolism provides novel insights into non-alcoholic fatty liver disease and its progression. *Current opinion in gastroenterology*, *28*(2), p.159.

Cosgrove, B.D., Gilbert, P.M., Porpiglia, E., Mourkioti, F., Lee, S.P., Corbel, S.Y., Llewellyn, M.E., Delp, S.L. and Blau, H.M., 2014. Rejuvenation of the muscle stem cell population restores strength to injured aged muscles. *Nature medicine*, *20*(3), pp.255-264.

Cotter, T.G. and Rinella, M., 2020. Nonalcoholic fatty liver disease 2020: the state of the disease. *Gastroenterology*, *158*(7), pp.1851-1864.

Crie, J.S. and Wildenthal, K., 1980. Influence of acidosis and lactate on protein degradation in adult and fetal hearts. *Journal of Molecular and Cellular Cardiology*, *12*(10), pp.1065-1074.

Cruz, J.F., Ferrari, Y.A.C., Machado, C.P., Santana, N.N., Mota, A.V.H. and Lima, S.O., 2019. Sarcopenia and severity of non-alcoholic fatty liver disease. *Arquivos de gastroenterologia*, *56*, pp.357-360.

Csapo, R., Gumpenberger, M. and Wessner, B., 2020. Skeletal muscle extracellular matrix–what do we know about its composition, regulation, and physiological roles? A narrative review. *Frontiers in Physiology*, *11*, p.253.

D'Souza, D.M., Zhou, S., Rebalka, I.A., MacDonald, B., Moradi, J., Krause, M.P., Al-Sajee, D., Punthakee, Z., Tarnopolsky, M.A. and Hawke, T.J., 2016. Decreased satellite cell number and function in humans and mice with type 1 diabetes is the result of altered notch signaling. *Diabetes*, *65*(10), pp.3053-3061.

Dalle, S., Rossmeislova, L. and Koppo, K., 2017. The role of inflammation in age-related sarcopenia. *Frontiers in physiology*, *8*, p.1045.

Day, K., Shefer, G., Richardson, J.B., Enikolopov, G. and Yablonka-Reuveni, Z., 2007. Nestin-GFP reporter expression defines the quiescent state of skeletal muscle satellite cells. *Developmental biology*, *304*(1), pp.246-259.

De Bosscher, K. and Haegeman, G., 2009. Minireview: latest perspectives on antiinflammatory actions of glucocorticoids. *Molecular endocrinology*, *23*(3), pp.281-291.

De Micheli, A.J., Laurilliard, E.J., Heinke, C.L., Ravichandran, H., Fraczek, P., Soueid-Baumgarten, S., De Vlaminck, I., Elemento, O. and Cosgrove, B.D., 2020. Single-cell analysis of the muscle stem cell hierarchy identifies heterotypic communication signals involved in skeletal muscle regeneration. *Cell reports*, *30*(10), pp.3583-3595.

De Palma, C., Morisi, F., Pambianco, S., Assi, E., Touvier, T., Russo, S., Perrotta, C., Romanello, V., Carnio, S., Cappello, V. and Pellegrino, P., 2014. Deficient nitric oxide signalling impairs skeletal muscle growth and performance: involvement of mitochondrial dysregulation. *Skeletal muscle*, *4*(1), pp.1-21.

Delli Bovi, A.P., Marciano, F., Mandato, C., Siano, M.A., Savoia, M. and Vajro, P., 2021. Oxidative stress in non-alcoholic fatty liver disease. An updated mini review. *Frontiers in Medicine*, *8*, p.165.

den Hartigh, L.J., Wang, S., Goodspeed, L., Ding, Y., Averill, M., Subramanian, S., Wietecha, T., O'Brien, K.D. and Chait, A., 2014. Deletion of serum amyloid A3 improves high fat high sucrose diet-induced adipose tissue inflammation and hyperlipidemia in female mice. *PloS one*, *9*(9), p.e108564.

DeYoung, M.P., Horak, P., Sofer, A., Sgroi, D. and Ellisen, L.W., 2008. Hypoxia regulates TSC1/2–mTOR signaling and tumor suppression through REDD1-mediated 14–3–3 shuttling. *Genes & development*, *22*(2), pp.239-251.

Dhahbi, J.M., Mote, P.L., Cao, S.X. and Spindler, S.R., 2003. Hepatic gene expression profiling of streptozotocin-induced diabetes. *Diabetes technology & therapeutics*, *5*(3), pp.411-420.

Di Malta, C., Cinque, L. and Settembre, C., 2019. Transcriptional regulation of autophagy: mechanisms and diseases. *Frontiers in cell and developmental biology*, *7*, p.114.

Dieter, B.P., McPherson, S.M., Afkarian, M., de Boer, I.H., Mehrotra, R., Short, R., Barbosa-Leiker, C., Alicic, R.Z., Meek, R.L. and Tuttle, K.R., 2016. Serum amyloid a and risk of death and end-stage renal disease in diabetic kidney disease. *Journal of diabetes and its complications*, *30*(8), pp.1467-1472.

Dieter, B.P., Meek, R.L., Anderberg, R.J., Cooney, S.K., Bergin, J.L., Zhang, H., Nair, V., Kretzler, M., Brosius, F.C. and Tuttle, K.R., 2019. Serum amyloid A and Janus kinase 2 in a mouse model of diabetic kidney disease. *PloS one*, *14*(2), p.e0211555.

DiMeglio, L.A., Evans-Molina, C. and Oram, R.A., 2018. Type 1 diabetes. *The Lancet*, *391*(10138), pp.2449-2462.

Dirks, M.L., Wall, B.T., Snijders, T., Ottenbros, C.L., Verdijk, L.B. and Van Loon, L.J., 2014. Neuromuscular electrical stimulation prevents muscle disuse atrophy during leg immobilization in humans. *Acta physiologica*, *210*(3), pp.628-641.

Dong, C., Wu, J., Chen, Y., Nie, J. and Chen, C., 2021. Activation of PI3K/AKT/mTOR pathway causes drug resistance in breast cancer. *Frontiers in Pharmacology*, *12*, p.143.

D'Souza DM, Al-Sajee D, Hawke TJ. Diabetic myopathy: impact of diabetes mellitus on skeletal muscle progenitor cells. Frontiers in physiology. 2013 Dec 20;4:379.

D'Souza, D.M., Trajcevski, K.E., Al-Sajee, D., Wang, D.C., Thomas, M., Anderson, J.E. and Hawke, T.J., 2015. Diet-induced obesity impairs muscle satellite cell activation and muscle repair through alterations in hepatocyte growth factor signaling. *Physiological reports*, *3*(8), p.e12506.

Du, H., Shih, C.H., Wosczyna, M.N., Mueller, A.A., Cho, J., Aggarwal, A., Rando, T.A. and Feldman, B.J., 2017. Macrophage-released ADAMTS1 promotes muscle stem cell activation. *Nature communications*, *8*(1), pp.1-11.

Duguez, S., Féasson, L., Denis, C. and Freyssenet, D., 2002. Mitochondrial biogenesis during skeletal muscle regeneration. *American Journal of Physiology-Endocrinology And Metabolism*, *282*(4), pp.E802-E809.

Ebert, S.M., Al-Zougbi, A., Bodine, S.C. and Adams, C.M., 2019. Skeletal muscle atrophy: discovery of mechanisms and potential therapies. *Physiology*, *34*(4), pp.232-239.

Ebner, N., Sliziuk, V., Scherbakov, N. and Sandek, A., 2015. Muscle wasting in ageing and chronic illness. *ESC heart failure*, *2*(2), pp.58-68.

Eizirik, D.L., Pasquali, L. and Cnop, M., 2020. Pancreatic β-cells in type 1 and type 2 diabetes mellitus: different pathways to failure. *Nature Reviews Endocrinology*, *16*(7), pp.349-362.

Eklund, K.K., Niemi, K. and Kovanen, P.T., 2012. Immune functions of serum amyloid A. *Critical Reviews™ in Immunology*, *32*(4).

Ennion, S., Sant'Ana Pereira, J., Sargeant, A.J., Young, A. and Goldspink, G., 1995. Characterization of human skeletal muscle fibres according to the myosin heavy chains they express. *Journal of Muscle Research & Cell Motility*, *16*(1), pp.35-43.

Fan, L.M., Cahill-Smith, S., Geng, L., Du, J., Brooks, G. and Li, J.M., 2017. Aging-associated metabolic disorder induces Nox2 activation and oxidative damage of endothelial function. *Free Radical Biology and Medicine*, *108*, pp.940-951.

Ferguson, D. and Finck, B.N., 2021. Emerging therapeutic approaches for the treatment of NAFLD and type 2 diabetes mellitus. *Nature Reviews Endocrinology*, *17*(8), pp.484-495.

Filomeni, G., De Zio, D. and Cecconi, F., 2015. Oxidative stress and autophagy: the clash between damage and metabolic needs. *Cell Death & Differentiation*, *22*(3), pp.377-388.

Fischer, A.H., Jacobson, K.A., Rose, J. and Zeller, R., 2008. Hematoxylin and eosin staining of tissue and cell sections. *Cold spring harbor protocols*, *2008*(5), pp.pdb-prot4986.

Fochi, S., Giuriato, G., De Simone, T., Gomez-Lira, M., Tamburin, S., Del Piccolo, L., Schena, F., Venturelli, M. and Romanelli, M.G., 2020. Regulation of microRNAs in satellite cell renewal, muscle function, sarcopenia and the role of exercise. *International Journal of Molecular Sciences*, *21*(18), p.6732.

Foldvari, M., Clark, M., Laviolette, L. C., Bernstein, M. A., Kaliton, D., Castaneda, C., Pu, C. T., Hausdorff, J. M., Fielding, R. A., & Singh, M. A. F. (2000). Association of muscle power with functional status in community-dwelling elderly women. The Journals of Gerontology: Series A, 55(4), M192–M199.

Foletta, V.C., White, L.J., Larsen, A.E., Léger, B. and Russell, A.P., 2011. The role and regulation of MAFbx/atrogin-1 and MuRF1 in skeletal muscle atrophy. *Pflügers Archiv-European Journal of Physiology*, *461*(3), pp.325-335.

Frontera, W.R. and Ochala, J., 2015. Skeletal muscle: a brief review of structure and function. *Calcified tissue international*, *96*(3), pp.183-195.

Fujimaki, S., Wakabayashi, T., Asashima, M., Takemasa, T. and Kuwabara, T., 2016. Treadmill running induces satellite cell activation in diabetic mice. *Biochemistry and biophysics reports*, *8*, pp.6-13.

Fukada, S.I., Yamaguchi, M., Kokubo, H., Ogawa, R., Uezumi, A., Yoneda, T., Matev, M.M., Motohashi, N., Ito, T., Zolkiewska, A. and Johnson, R.L., 2011. Hesr1 and Hesr3 are essential to generate undifferentiated quiescent satellite cells and to maintain satellite cell numbers. *Development*, *138*(21), pp.4609-4619.

Furman, D., Campisi, J., Verdin, E., Carrera-Bastos, P., Targ, S., Franceschi, C., Ferrucci, L., Gilroy, D.W., Fasano, A., Miller, G.W. and Miller, A.H., 2019. Chronic inflammation in the etiology of disease across the life span. *Nature medicine*, *25*(12), pp.1822-1832.

Galicia-Garcia, U., Benito-Vicente, A., Jebari, S., Larrea-Sebal, A., Siddiqi, H., Uribe, K.B., Ostolaza, H. and Martín, C., 2020. Pathophysiology of type 2 diabetes mellitus. *International journal of molecular sciences*, *21*(17), p.6275.

Giffin, R., Robinson, S. and Olson, S. eds., 2009. *Accelerating the development of biomarkers for drug safety: workshop summary*. National Academies Press.

Gjorgjieva, M., Sobolewski, C., Dolicka, D., de Sousa, M.C. and Foti, M., 2019. miRNAs and NAFLD: from pathophysiology to therapy. *Gut*, *68*(11), pp.2065-2079.

Goldin, A., Beckman, J.A., Schmidt, A.M. and Creager, M.A., 2006. Advanced glycation end products: sparking the development of diabetic vascular injury. *Circulation*, *114*(6), pp.597-605.

Gransee, H.M., Mantilla, C.B. and Sieck, G.C., 2012. Respiratory muscle plasticity. *Comprehensive Physiology*, *2*(2), p.1441.

Greer, E.L., Oskoui, P.R., Banko, M.R., Maniar, J.M., Gygi, M.P., Gygi, S.P. and Brunet, A., 2007. The energy sensor AMP-activated protein kinase directly regulates the mammalian FOXO3 transcription factor. *Journal of Biological Chemistry*, *282*(41), pp.30107-30119.

Griffin, B.R., Faubel, S. and Edelstein, C.L., 2019. Biomarkers of drug-induced kidney toxicity. *Therapeutic drug monitoring*, *41*(2), p.213.

Gross, S., Gammon, S.T., Moss, B.L., Rauch, D., Harding, J., Heinecke, J.W., Ratner, L. and Piwnica-Worms, D., 2009. Bioluminescence imaging of myeloperoxidase activity in vivo. *Nature medicine*, *15*(4), pp.455-461.

Grune, T., Reinheckel, T. and Davies, K.J., 1997. Degradation of oxidized proteins in mammalian cells. *The FASEB Journal*, *11*(7), pp.526-534.

Guha, M., Xu, Z.G., Tung, D., Lanting, L. and Natarajan, R., 2007. Specific down-regulation of connective tissue growth factor attenuates progression of nephropathy in mouse models of type 1 and type 2 diabetes. *The FASEB Journal*, *21*(12), pp.3355-3368.

Hawke, T.J. and Garry, D.J., 2001. Myogenic satellite cells: physiology to molecular biology. *Journal of applied physiology*, 91(2), pp 534-551

Hilber, K., Galler, S., Gohlsch, B. and Pette, D., 1999. Kinetic properties of myosin heavy chain isoforms in single fibers from human skeletal muscle. *FEBS letters*, *455*(3), pp.267-270.

Holecek, M., 2012. Muscle wasting in animal models of severe illness. *International journal of experimental pathology*, *93*(3), pp.157-171.

Howard, E.E., Pasiakos, S.M., Blesso, C.N., Fussell, M.A. and Rodriguez, N.R., 2020. Divergent roles of inflammation in skeletal muscle recovery from injury. *Frontiers in Physiology*, *11*, p.87.

Howard, E.E., Pasiakos, S.M., Fussell, M.A. and Rodriguez, N.R., 2020. Skeletal muscle disuse atrophy and the rehabilitative role of protein in recovery from musculoskeletal injury. *Advances in Nutrition*, *11*(4), pp.989-1001.

Hu, Z., Wang, H., Lee, I.H., Du, J. and Mitch, W.E., 2009. Endogenous glucocorticoids and impaired insulin signaling are both required to stimulate muscle wasting under pathophysiological conditions in mice. *The Journal of clinical investigation*, *119*(10), pp.3059-3069.

Huang, D.W., Sherman, B.T. and Lempicki, R.A., 2009. Systematic and integrative analysis of large gene lists using DAVID bioinformatics resources. *Nature protocols*, *4*(1), pp.44-57.

Hussain, S., Jamali, M.C., Habib, A., Hussain, M.S., Akhtar, M. and Najmi, A.K., 2021. Diabetic kidney disease: An overview of prevalence, risk factors, and biomarkers. *Clinical Epidemiology and Global Health*, *9*, pp.2-6.

Hyatt, H., Deminice, R., Yoshihara, T. and Powers, S.K., 2019. Mitochondrial dysfunction induces muscle atrophy during prolonged inactivity: A review of the causes and effects. *Archives of biochemistry and biophysics*, *662*, pp.49-60.

Hyatt, H.W. and Powers, S.K., 2020. Disturbances in Calcium Homeostasis Promotes Skeletal Muscle Atrophy: Lessons From Ventilator-Induced Diaphragm Wasting. *Frontiers in Physiology*, p.1615.

Hyatt, H.W. and Powers, S.K., 2021. Mitochondrial dysfunction is a common denominator linking skeletal muscle wasting due to disease, aging, and prolonged inactivity. *Antioxidants*, *10*(4), p.588.

Hyatt, H.W., Ozdemir, M., Yoshihara, T., Nguyen, B.L., Deminice, R. and Powers, S.K., 2021. Calpains play an essential role in mechanical ventilation-induced diaphragmatic weakness and mitochondrial dysfunction. *Redox Biology*, *38*, p.101802.

Inaba, S., Hinohara, A., Tachibana, M., Tsujikawa, K. and Fukada, S.I., 2018. Muscle regeneration is disrupted by cancer cachexia without loss of muscle stem cell potential. *PloS one*, *13*(10), p.e0205467.

Jejurikar, S.S. and Kuzon, W.M., 2003. Satellite cell depletion in degenerative skeletal muscle. *Apoptosis*, *8*(6), pp.573-578.

Jeong, J., Conboy, M.J. and Conboy, I.M., 2013. Pharmacological inhibition of myostatin/TGF-β receptor/pSmad3 signaling rescues muscle regenerative responses in mouse model of type 1 diabetes. *Acta Pharmacologica Sinica*, *34*(8), pp.1052-1060.

Ji, L.L., 2007. Antioxidant signaling in skeletal muscle: a brief review. *Experimental gerontology*, *42*(7), pp.582-593.

Jorgenson, K.W., Phillips, S.M. and Hornberger, T.A., 2020. Identifying the structural adaptations that drive the mechanical load-induced growth of skeletal muscle: a scoping review. *Cells*, *9*(7), p.1658.

Joseph, J. and Doles, J.D., 2021. Disease-associated metabolic alterations that impact satellite cells and muscle regeneration: perspectives and therapeutic outlook. *Nutrition & Metabolism*, *18*(1), pp.1-8.

Kelley, D.E., He, J., Menshikova, E.V. and Ritov, V.B., 2002. Dysfunction of mitochondria in human skeletal muscle in type 2 diabetes. *Diabetes*, *51*(10), pp.2944-2950.

Kim, G., Lee, S.E., Lee, Y.B., Jun, J.E., Ahn, J., Bae, J.C., Jin, S.M., Hur, K.Y., Jee, J.H., Lee, M.K. and Kim, J.H., 2018. Relationship between relative skeletal muscle mass and nonalcoholic fatty liver disease: a 7-year longitudinal study. *Hepatology*, *68*(5), pp.1755-1768.

Kim, H.E., Dalal, S.S., Young, E., Legato, M.J., Weisfeldt, M.L. and D'Armiento, J., 2000. Disruption of the myocardial extracellular matrix leads to cardiac dysfunction. *The Journal of clinical investigation*, *106*(7), pp.857-866.

Kim, J., Wang, Z., Heymsfield, S.B., Baumgartner, R.N. and Gallagher, D., 2002. Total-body skeletal muscle mass: estimation by a new dual-energy X-ray absorptiometry method. *The American journal of clinical nutrition*, *76*(2), pp.378-383.

Kim, J.Y., Park, K.J., Hwang, J.Y., Kim, G.H., Lee, D., Lee, Y.J., Song, E.H., Yoo, M.G., Kim, B.J., Suh, Y.H. and Roh, G.S., 2017. Activating transcription factor 3 is a target molecule linking hepatic steatosis to impaired glucose homeostasis. *Journal of hepatology*, *67*(2), pp.349-359.

Kim, Y.S., Morgan, M.J., Choksi, S. and Liu, Z.G., 2007. TNF-induced activation of the Nox1 NADPH oxidase and its role in the induction of necrotic cell death. *Molecular cell*, *26*(5), pp.675-687.

Kirwan, R., McCullough, D., Butler, T., Perez de Heredia, F., Davies, I.G. and Stewart, C., 2020. Sarcopenia during COVID-19 lockdown restrictions: long-term health effects of short-term muscle loss. *GeroScience*, *42*(6), pp.1547-1578.

Kitajima, Y., Yoshioka, K. and Suzuki, N., 2020. The ubiquitin–proteasome system in regulation of the skeletal muscle homeostasis and atrophy: from basic science to disorders. *The Journal of Physiological Sciences*, *70*(1), pp.1-12.

Kivelä, R., Silvennoinen, M., Touvra, A.M., Maarit Lehti, T., Kainulainen, H., Vihko, V., Kivelä, R., Silvennoinen, M., Touvra, A.M., Lehti, T.M. and Kainulainen, H., 2006. Effects of experimental type 1 diabetes and exercise training on angiogenic gene expression and capillarization in skeletal muscle. *The FASEB journal*, *20*(9), pp.1570-1572.

Koshikawa, M., Harada, M., Noyama, S., Kiyono, K., Motoike, Y., Nomura, Y., Nishimura, A., Izawa, H., Watanabe, E. and Ozaki, Y., 2020. Association between inflammation and skeletal muscle proteolysis, skeletal mass and strength in elderly heart failure patients and their prognostic implications. *BMC cardiovascular disorders*, *20*(1), pp.1-9.

Kottaisamy, C.P.D., Raj, D.S., Prasanth Kumar, V. and Sankaran, U., 2021. Experimental animal models for diabetes and its related complications—a review. *Laboratory Animal Research*, *37*(1), pp.1-14.

Kozakowska, M., Pietraszek-Gremplewicz, K., Jozkowicz, A. and Dulak, J., 2015. The role of oxidative stress in skeletal muscle injury and regeneration: focus on antioxidant enzymes. *Journal of muscle research and cell motility*, *36*(6), pp.377-393.

Krause, M.P., Moradi, J., Nissar, A.A., Riddell, M.C. and Hawke, T.J., 2011. Inhibition of plasminogen activator inhibitor-1 restores skeletal muscle regeneration in untreated type 1 diabetic mice. *Diabetes*, *60*(7), pp.1964-1972.

Kudryashova, E., Wu, J., Havton, L.A. and Spencer, M.J., 2009. Deficiency of the E3 ubiquitin ligase TRIM32 in mice leads to a myopathy with a neurogenic component. *Human molecular genetics*, *18*(7), pp.1353-1367.

Kugelmas, M., Hill, D.B., Vivian, B., Marsano, L. and McClain, C.J., 2003. Cytokines and NASH: a pilot study of the effects of lifestyle modification and vitamin E. *Hepatology*, *38*(2), pp.413-419.

Kumar, R. and Thompson, E.B., 2005. Gene regulation by the glucocorticoid receptor: structure: function relationship. *The Journal of steroid biochemistry and molecular biology*, *94*(5), pp.383-394.

Kumari, R. and Jat, P., 2021. Mechanisms of cellular senescence: cell cycle arrest and senescence associated secretory phenotype. *Frontiers in cell and developmental biology*, *9*, p.485.

Kumrungsee, T., Kariya, T., Hashimoto, K., Koyano, T., Yazawa, N., Hashimoto, T., Sanada, Y., Matsuyama, M., Sotomaru, Y., Sakurai, H. and van de Loo, F.A., 2019. The serum amyloid A3 promoter-driven luciferase reporter mice is a valuable tool to image early renal fibrosis development and shows the therapeutic effect of glucosyl-hesperidin treatment. *Scientific reports*, *9*(1), pp.1-13.

Kuo, T., McQueen, A., Chen, T.C. and Wang, J.C., 2015. Regulation of glucose homeostasis by glucocorticoids. *Glucocorticoid signaling*, pp.99-126.

Lacraz, G., Rouleau, A.J., Couture, V., Söllrald, T., Drouin, G., Veillette, N., Grandbois, M. and Grenier, G., 2015. Increased stiffness in aged skeletal muscle impairs muscle progenitor cell proliferative activity. *PloS one*, *10*(8), p.e0136217.

Lai, K.M.V., Gonzalez, M., Poueymirou, W.T., Kline, W.O., Na, E., Zlotchenko, E., Stitt, T.N., Economides, A.N., Yancopoulos, G.D. and Glass, D.J., 2004. Conditional activation of akt in adult skeletal muscle induces rapid hypertrophy. *Molecular and cellular biology*, *24*(21), pp.9295-9304.).

Langen, R.C., Schols, A.M., Kelders, M.C., Van Der Velden, J.L., Wouters, E.F. and Janssen-Heininger, Y.M., 2002. Tumor necrosis factor-α inhibits myogenesis through redox-dependent and-independent pathways. *American Journal of Physiology-Cell Physiology*, *283*(3), pp.C714-C721.

Langen, R.C., Van Der Velden, J.L., Schols, A.M., Kelders, M.C., Wouters, E.F. and Janssen-Heininger, Y.M., 2004. Tumor necrosis factor-alpha inhibits myogenic differentiation through MyoD protein destabilization. *The FASEB Journal*, *18*(2), pp.227-237.

Lazarus, J.V., Mark, H.E., Anstee, Q.M., Arab, J.P., Batterham, R.L., Castera, L., Cortez-Pinto, H., Crespo, J., Cusi, K., Dirac, M.A. and Francque, S., 2021. Advancing the global public health agenda for NAFLD: a consensus statement. *Nature Reviews Gastroenterology & Hepatology*, pp.1-18.

Lecker, S.H., Goldberg, A.L. and Mitch, W.E., 2006. Protein degradation by the ubiquitin–proteasome pathway in normal and disease states. *Journal of the American society of nephrology*, *17*(7), pp.1807-1819.

Lepper, C., Partridge, T.A. and Fan, C.M., 2011. An absolute requirement for Pax7-positive satellite cells in acute injury-induced skeletal muscle regeneration. *Development*, *138*(17), pp.3639-3646.

Li, R., Xia, J., Zhang, X.I., Gathirua-Mwangi, W.G., Guo, J., Li, Y., McKenzie, S. and Song, Y., 2018. Associations of muscle mass and strength with all-cause mortality among US older adults. *Medicine and science in sports and exercise*, *50*(3), p.458.

Li, X., Xu, Z., Jiang, Z., Sun, L., Ji, J., Miao, J., Zhang, X., Li, X., Huang, S., Wang, T. and Zhang, L., 2014. Hypoglycemic effect of catalpol on high-fat diet/streptozotocin-induced diabetic mice by increasing skeletal muscle mitochondrial biogenesis. *Acta Biochim Biophys Sin*, *46*(9), pp.738-748.

Li, Y.P., Chen, Y., Li, A.S. and Reid, M.B., 2003. Hydrogen peroxide stimulates ubiquitin-conjugating activity and expression of genes for specific E2 and E3 proteins in skeletal muscle myotubes. *American Journal of Physiology-Cell Physiology*, *285*(4), pp.C806-C812.

Lin, M.H., Chen, H.Y., Liao, T.H., Huang, T.C., Chen, C.M. and Lee, J.A., 2011. Determination of time-dependent accumulation of D-lactate in the streptozotocin-induced diabetic rat kidney by column-switching HPLC with fluorescence detection. *Journal of Chromatography B*, *879*(29), pp.3214-3219.

Lin, X., Xu, Y., Pan, X., Xu, J., Ding, Y., Sun, X., Song, X., Ren, Y. and Shan, P.F., 2020. Global, regional, and national burden and trend of diabetes in 195 countries and territories: an analysis from 1990 to 2025. *Scientific reports*, *10*(1), pp.1-11.

Liu, X., Gao, Y., Long, X., Hayashi, T., Mizuno, K., Hattori, S., Fujisaki, H., Ogura, T., Wang, D.O. and Ikejima, T., 2020. Type I collagen promotes the migration and myogenic differentiation of C2C12 myoblasts via the release of interleukin-6 mediated by FAK/NF-κB p65 activation. *Food & Function*, *11*(1), pp.328-338.

Low, S., Barnes, J.L., Zammit, P.S. and Beauchamp, J.R., 2018. Delta-like 4 activates Notch 3 to regulate self-renewal in skeletal muscle stem cells. *Stem Cells*, *36*(3), pp.458-466.

Lu, W.T., Juang, J.H., Hsu, B.R. and Huang, H.S., 1998, March. Effects of high or low dose of streptozocin on pancreatic islets in C57BL/6 and C. B17-SCID mice. In *Transplantation proceedings* (Vol. 30, No. 2, pp. 609-610).

Lukjanenko, L., Karaz, S., Stuelsatz, P., Gurriaran-Rodriguez, U., Michaud, J., Dammone, G., Sizzano, F., Mashinchian, O., Ancel, S., Migliavacca, E. and Liot, S., 2019. Aging disrupts muscle stem cell function by impairing matricellular WISP1 secretion from fibro-adipogenic progenitors. *Cell stem cell*, *24*(3), pp.433-446.

Mammucari, C., Milan, G., Romanello, V., Masiero, E., Rudolf, R., Del Piccolo, P., Burden, S.J., Di Lisi, R., Sandri, C., Zhao, J. and Goldberg, A.L., 2007. FoxO3 controls autophagy in skeletal muscle in vivo. *Cell metabolism*, *6*(6), pp.458-471.

Manning, B.D. and Cantley, L.C., 2007. AKT/PKB signaling: navigating downstream. *Cell*, *129*(7), pp.1261-1274.

Mantovani, A., Beatrice, G., Stupia, R. and Dalbeni, A., 2020. Prevalence and incidence of intra-and extrahepatic complications of NAFLD in patients with type 2 diabetes mellitus. *Hepatoma Research*, *6*, p.78.

Mashinchian, O., Pisconti, A., Le Moal, E. and Bentzinger, C.F., 2018. The muscle stem cell niche in health and disease. *Current topics in developmental biology*, *126*, pp.23-65.

Matoba, K., Takeda, Y., Nagai, Y., Kawanami, D., Utsunomiya, K. and Nishimura, R., 2019. Unraveling the role of inflammation in the pathogenesis of diabetic kidney disease. *International journal of molecular sciences*, *20*(14), p.3393.

Max, S.R., 1972. Disuse atrophy of skeletal muscle: loss of functional activity of mitochondria. *Biochemical and biophysical research communications*, *46*(3), pp.1394-1398.

McCarthy, J.J., Mula, J., Miyazaki, M., Erfani, R., Garrison, K., Farooqui, A.B., Srikuea, R., Lawson, B.A., Grimes, B., Keller, C. and Van Zant, G., 2011. Effective fiber hypertrophy in satellite cell-depleted skeletal muscle. *Development*, *138*(17), pp.3657-3666.

McKenna, C.F. and Fry, C.S., 2017. Altered satellite cell dynamics accompany skeletal muscle atrophy during chronic illness, disuse and aging. *Current opinion in clinical nutrition and metabolic care*, *20*(6), p.447.

McKinnell, I.W. and Rudnicki, M.A., 2004. Molecular mechanisms of muscle atrophy. *Cell*, *119*(7), pp.907-910.

Meek, R.L., LeBoeuf, R.C., Saha, S.A., Alpers, C.E., Hudkins, K.L., Cooney, S.K., Anderberg, R.J. and Tuttle, K.R., 2013. Glomerular cell death and inflammation with high-protein diet and diabetes. *Nephrology Dialysis Transplantation*, *28*(7), pp.1711-1720.

Meex, R.C., Blaak, E.E. and van Loon, L.J., 2019. Lipotoxicity plays a key role in the development of both insulin resistance and muscle atrophy in patients with type 2 diabetes. *Obesity Reviews*, *20*(9), pp.1205-1217.

Merli, M. and Dasarathy, S., 2015. Sarcopenia in non-alcoholic fatty liver disease: Targeting the real culprit?. *Journal of hepatology*, *63*(2), pp.309-311.

Miller, S.G., Hafen, P.S. and Brault, J.J., 2019. Increased adenine nucleotide degradation in skeletal muscle atrophy. *International Journal of Molecular Sciences*, *21*(1), p.88.

Min, K., Smuder, A.J., Kwon, O.S., Kavazis, A.N., Szeto, H.H. and Powers, S.K., 2011. Mitochondrial-targeted antioxidants protect skeletal muscle against immobilization-induced muscle atrophy. *Journal of applied physiology*, *111*(5), pp.1459-1466.

Mitch, W.E., Medina, R., Grieber, S., May, R.C., England, B.K., Price, S.R., Bailey, J.L. and Goldberg, A.L., 1994. Metabolic acidosis stimulates muscle protein degradation by activating the adenosine triphosphate-dependent pathway involving ubiquitin and proteasomes. *The Journal of clinical investigation*, *93*(5), pp.2127-2133.

Mitchell, W.K., Atherton, P.J., Williams, J., Larvin, M., Lund, J.N. and Narici, M., 2012. Sarcopenia, dynapenia, and the impact of advancing age on human skeletal muscle size and strength; a quantitative review. *Frontiers in physiology*, *3*, p.260.

Mitsumoto, K., Watanabe, R., Nakao, K., Yonenaka, H., Hashimoto, T., Kato, N., Kumrungsee, T. and Yanaka, N., 2017. Time-course microarrays reveal early activation of the immune transcriptome in a choline-deficient mouse model of liver injury. *Life Sciences*, *184*, pp.103-111.

Mohammed-Ali, Z., Carlisle, R.E., Nademi, S. and Dickhout, J.G., 2017. Animal models of kidney disease. In *Animal Models for the Study of Human Disease* (pp. 379-417). Academic Press.

Monaco, C.M., Hughes, M.C., Ramos, S.V., Varah, N.E., Lamberz, C., Rahman, F.A., McGlory, C., Tarnopolsky, M.A., Krause, M.P., Laham, R. and Hawke, T.J., 2018. Altered mitochondrial bioenergetics and ultrastructure in the skeletal muscle of young adults with type 1 diabetes. *Diabetologia*, *61*(6), pp.1411-1423.

Moreno, J.A., Gomez-Guerrero, C., Mas, S., Sanz, A.B., Lorenzo, O., Ruiz-Ortega, M., Opazo, L., Mezzano, S. and Egido, J., 2018. Targeting inflammation in diabetic nephropathy: a tale of hope. *Expert Opinion on Investigational Drugs*, *27*(11), pp.917-930.

Morley, J.E., Thomas, D.R. and Wilson, M.M.G., 2006. Cachexia: pathophysiology and clinical relevance. *The American journal of clinical nutrition*, *83*(4), pp.735-743.

Mourikis, P., Sambasivan, R., Castel, D., Rocheteau, P., Bizzarro, V. and Tajbakhsh, S., 2012. A critical requirement for notch signaling in maintenance of the quiescent skeletal muscle stem cell state. *Stem cells*, *30*(2), pp.243-252.

Muñoz-Cánoves, P., Neves, J. and Sousa-Victor, P., 2020. Understanding muscle regenerative decline with aging: new approaches to bring back youthfulness to aged stem cells. *The FEBS journal*, *287*(3), pp.406-416.

Nakayasu, E.S., Qian, W.J., Evans-Molina, C., Mirmira, R.G., Eizirik, D.L. and Metz, T.O., 2019. The role of proteomics in assessing beta-cell dysfunction and death in type 1 diabetes. *Expert review of proteomics*, *16*(7), pp.569-582.

Navarro-González, J.F., Mora-Fernández, C., De Fuentes, M.M. and García-Pérez, J., 2011. Inflammatory molecules and pathways in the pathogenesis of diabetic nephropathy. *Nature Reviews Nephrology*, *7*(6), pp.327-340.

Ng, C.C., Lee, Z.Y., Chan, W.Y., Jamaluddin, M.F., Tan, L.J., Sitaram, P.N., Ruslan, S.R. and Hasan, M.S., 2020. Low muscularity as assessed by abdominal computed tomography on intensive care unit admission is associated with mortality in a critically ill Asian population. *Journal of Parenteral and Enteral Nutrition*, *44*(3), pp.425-433.

Niewczas, M.A., Pavkov, M.E., Skupien, J., Smiles, A., Md Dom, Z.I., Wilson, J.M., Park, J., Nair, V., Schlafly, A., Saulnier, P.J. and Satake, E., 2019. A signature of circulating inflammatory proteins and development of end-stage renal disease in diabetes. *Nature medicine*, *25*(5), pp.805-813.

Nishikawa, H., Asai, A., Fukunishi, S., Nishiguchi, S. and Higuchi, K., 2021. Metabolic Syndrome and Sarcopenia. *Nutrients*, *13*(10), p.3519.

Nissar, A.A., Zemanek, B., Labatia, R., Atkinson, D.J., van der Ven, P.F., Fürst, D.O. and Hawke, T.J., 2012. Skeletal muscle regeneration is delayed by reduction in Xin expression: consequence of impaired satellite cell activation?. *American Journal of Physiology-Cell Physiology*, *302*(1), pp.C220-C227.

Nocito, L., Zafra, D., Calbo, J., Dominguez, J. and Guinovart, J.J., 2012. Tungstate reduces the expression of gluconeogenic enzymes in STZ rats.

O'Neill, B.T., Bhardwaj, G., Penniman, C.M., Krumpoch, M.T., Suarez Beltran, P.A., Klaus, K., Poro, K., Li, M., Pan, H., Dreyfuss, J.M. and Nair, K.S., 2019. FoxO transcription factors are critical regulators of diabetes-related muscle atrophy. *Diabetes*, *68*(3), pp.556-570.

Okuma, H., Mori, K., Nakamura, S., Sekine, T., Ogawa, Y. and Tsuchiya, K., 2021. Ipragliflozin Ameliorates Diabetic Nephropathy Associated with Perirenal Adipose Expansion in Mice. *International journal of molecular sciences*, *22*(14), p.7329.

Oltmanns, K.M., Dodt, B., Schultes, B., Raspe, H.H., Schweiger, U., Born, J., Fehm, H.L. and Peters, A., 2006. Cortisol correlates with metabolic disturbances in a population study of type 2 diabetic patients. *European journal of endocrinology*, *154*(2), pp.325-331.

Ono, Y., Urata, Y., Goto, S., Nakagawa, S., Humbert, P.O., Li, T.S. and Zammit, P.S., 2015. Muscle stem cell fate is controlled by the cell-polarity protein Scrib. *Cell reports*, *10*(7), pp.1135-1148.

Orlando, G., Balducci, S., Bazzucchi, I., Pugliese, G. and Sacchetti, M., 2017. The impact of type 1 diabetes and diabetic polyneuropathy on muscle strength and fatigability. *Acta diabetologica*, *54*(6), pp.543-550.

Oyabu, M., Takigawa, K., Mizutani, S., Hatazawa, Y., Fujita, M., Ohira, Y., Sugimoto, T., Suzuki, O., Tsuchiya, K., Suganami, T. and Ogawa, Y., 2022. FOXO1 cooperates with C/EBPδ and ATF4 to regulate skeletal muscle atrophy transcriptional program during fasting. *The FASEB Journal*, *36*(2), p.e22152.

Pacifico, L., Perla, F.M. and Chiesa, C., 2019. Sarcopenia and nonalcoholic fatty liver disease: a causal relationship. *Hepatobiliary surgery and nutrition*, *8*(2), p.144.

Pan, X., Han, Y., Zou, T., Zhu, G., Xu, K., Zheng, J., Zheng, M. and Cheng, X., 2018. Sarcopenia contributes to the progression of nonalcoholic fatty liver disease-related fibrosis: a meta-analysis. *Digestive Diseases*, *36*(6), pp.427-436.

Pandya, C.D., Lee, B., Toque, H.A., Mendhe, B., Bragg, R.T., Pandya, B., Atawia, R.T., Isales, C., Hamrick, M., Caldwell, R.W. and Fulzele, S., 2019. Age-dependent oxidative stress elevates arginase 1 and uncoupled nitric oxide synthesis in skeletal muscle of aged mice. *Oxidative medicine and cellular longevity*, *2019*, pp. 1-9.

Papanikolaou, K., Draganidis, D., Chatzinikolaou, A., Laschou, V.C., Georgakouli, K., Tsimeas, P., Batrakoulis, A., Deli, C.K., Jamurtas, A.Z. and Fatouros, I.G., 2019. The redox-dependent regulation of satellite cells following aseptic muscle trauma (SpEED): study protocol for a randomized controlled trial. *Trials*, *20*(1), pp.1-11.

Pataky, M.W., Wang, H., Yu, C.S., Arias, E.B., Ploutz-Snyder, R.J., Zheng, X. and Cartee, G.D., 2017. High-fat diet-induced insulin resistance in single skeletal muscle fibers is fiber type selective. *Scientific reports*, *7*(1), pp.1-11.

Peckett, A.J., Wright, D.C. and Riddell, M.C., 2011. The effects of glucocorticoids on adipose tissue lipid metabolism. *Metabolism*, *60*(11), pp.1500-1510.

Pedersen, B.K. and Febbraio, M.A., 2008. Muscle as an endocrine organ: focus on muscle-derived interleukin-6. *Physiological reviews*, *88*(4), pp.1379-1406.

Peng, S., Plank, L.D., McCall, J.L., Gillanders, L.K., McIlroy, K. and Gane, E.J., 2007. Body composition, muscle function, and energy expenditure in patients with liver cirrhosis: a comprehensive study. *The American journal of clinical nutrition*, *85*(5), pp.1257-1266.

Perandini, L.A., Chimin, P., Lutkemeyer, D.D.S. and Câmara, N.O.S., 2018. Chronic inflammation in skeletal muscle impairs satellite cells function during regeneration: can physical exercise restore the satellite cell niche?. *The FEBS journal*, *285*(11), pp.1973-1984.

Peris-Moreno, D., Taillandier, D. and Polge, C., 2020. MuRF1/TRIM63, master regulator of muscle mass. *International Journal of Molecular Sciences*, *21*(18), p.6663.

Petrilli, L.L., Spada, F., Palma, A., Reggio, A., Rosina, M., Gargioli, C., Castagnoli, L., Fuoco, C. and Cesareni, G., 2020. High-dimensional single-cell quantitative profiling of skeletal muscle cell population dynamics during regeneration. *Cells*, *9*(7), p.1723.

Pizzino, G., Irrera, N., Cucinotta, M., Pallio, G., Mannino, F., Arcoraci, V., Squadrito, F., Altavilla, D. and Bitto, A., 2017. Oxidative stress: harms and benefits for human health. *Oxidative medicine and cellular longevity*, *2017*.

Powers, S.K., Kavazis, A.N. and DeRuisseau, K.C., 2005. Mechanisms of disuse muscle atrophy: role of oxidative stress. *American Journal of Physiology-Regulatory, Integrative and Comparative Physiology*, *288*(2), pp.R337-R344.

Powers, S.K., Lynch, G.S., Murphy, K.T., Reid, M.B. and Zijdewind, I., 2016. Disease-induced skeletal muscle atrophy and fatigue. *Medicine and science in sports and exercise*, *48*(11), p.2307.

Powers, S.K., Smuder, A.J. and Criswell, D.S., 2011. Mechanistic links between oxidative stress and disuse muscle atrophy. *Antioxidants & redox signaling*, *15*(9), pp.2519-2528.

Powers, S.K., Wiggs, M.P., Duarte, J.A., Zergeroglu, A.M. and Demirel, H.A., 2012. Mitochondrial signaling contributes to disuse muscle atrophy. *American Journal of Physiology-Endocrinology and Metabolism*, *303*(1), pp.E31-E39.

Qian, Y., Feldman, E., Pennathur, S., Kretzler, M. and Brosius III, F.C., 2008. From fibrosis to sclerosis: mechanisms of glomerulosclerosis in diabetic nephropathy. *Diabetes*, *57*(6), pp.1439-1445.

Raubenheimer, P.J., Nyirenda, M.J. and Walker, B.R., 2006. A choline-deficient diet exacerbates fatty liver but attenuates insulin resistance and glucose intolerance in mice fed a high-fat diet. *Diabetes*, *55*(7), pp.2015-2020.

Rayagiri, S.S., Ranaldi, D., Raven, A., Mohamad Azhar, N.I.F., Lefebvre, O., Zammit, P.S. and Borycki, A.G., 2018. Basal lamina remodeling at the skeletal muscle stem cell niche mediates stem cell self-renewal. *Nature communications*, *9*(1), pp.1-12.

Recena Aydos, L., Aparecida do Amaral, L., Serafim de Souza, R., Jacobowski, A.C., Freitas dos Santos, E. and Rodrigues Macedo, M.L., 2019. Nonalcoholic fatty liver disease induced by high-fat diet in C57bl/6 models. *Nutrients*, *11*(12), p.3067.

Relaix, F. and Zammit, P.S., 2012. Satellite cells are essential for skeletal muscle regeneration: the cell on the edge returns centre stage. *Development*, *139*(16), pp.2845-2856.

Relaix, F., Bencze, M., Borok, M.J., Der Vartanian, A., Gattazzo, F., Mademtzoglou, D., Perez-Diaz, S., Prola, A., Reyes-Fernandez, P.C. and Rotini, A., 2021. Perspectives on skeletal muscle stem cells. *Nature Communications*, *12*(1), pp.1-11.

Renault, V., Piron-Hamelin, G., Forestier, C., DiDonna, S., Decary, S., Hentati, F., Saillant, G., Butler-Browne, G.S. and Mouly, V., 2000. Skeletal muscle regeneration and the mitotic clock. *Experimental gerontology*, *35*(6-7), pp.711-719.

Rizzo, M., Beffy, P., Del Carratore, R., Falleni, A., Pretini, V., D'Aurizio, R., Botta, A., Evangelista, M., Stoccoro, A., Coppedè, F. and Furling, D., 2018. Activation of the interferon

type I response rather than autophagy contributes to myogenesis inhibition in congenital DM1 myoblasts. *Cell death & disease*, *9*(11), pp.1-16.

Rojas, M., Lemtalsi, T., Toque, H.A., Xu, Z., Fulton, D., Caldwell, R.W. and Caldwell, R.B., 2017. NOX2-induced activation of arginase and diabetes-induced retinal endothelial cell senescence. *Antioxidants*, *6*(2), p.43.

Romanello, V. and Sandri, M., 2010. Mitochondrial biogenesis and fragmentation as regulators of muscle protein degradation. *Current hypertension reports*, *12*(6), pp.433-439.

Romanello, V., Guadagnin, E., Gomes, L., Roder, I., Sandri, C., Petersen, Y., Milan, G., Masiero, E., Del Piccolo, P., Foretz, M. and Scorrano, L., 2010. Mitochondrial fission and remodelling contributes to muscle atrophy. *The EMBO journal*, *29*(10), pp.1774-1785.

Romanello, V., Guadagnin, E., Gomes, L., Roder, I., Sandri, C., Petersen, Y., Milan, G., Masiero, E., Del Piccolo, P., Foretz, M. and Scorrano, L., 2010. Mitochondrial fission and remodelling contributes to muscle atrophy. *The EMBO journal*, *29*(10), pp.1774-1785.

Rommel, C., Bodine, S.C., Clarke, B.A., Rossman, R., Nunez, L., Stitt, T.N., Yancopoulos, G.D. and Glass, D.J., 2001. Mediation of IGF-1-induced skeletal myotube hypertrophy by PI (3) K/Akt/mTOR and PI (3) K/Akt/GSK3 pathways. *Nature cell biology*, *3*(11), pp.1009-1013.

Rosenstock, J., Banarer, S., Fonseca, V.A., Inzucchi, S.E., Sun, W., Yao, W., Hollis, G., Flores, R., Levy, R., Williams, W.V. and Seckl, J.R., 2010. The 11-β-hydroxysteroid dehydrogenase type 1 inhibitor INCB13739 improves hyperglycemia in patients with type 2 diabetes inadequately controlled by metformin monotherapy. *Diabetes care*, *33*(7), pp.1516-1522.

Rowland, L.A., Bal, N.C. and Periasamy, M., 2015. The role of skeletal-muscle-based thermogenic mechanisms in vertebrate endothermy. *Biological Reviews*, *90*(4), pp.1279-1297.

Rubio-Ruiz, M.E., Guarner-Lans, V., Pérez-Torres, I. and Soto, M.E., 2019. Mechanisms underlying metabolic syndrome-related sarcopenia and possible therapeutic measures. *International journal of molecular sciences*, *20*(3), p.647.

Ryall, J.G., Dell'Orso, S., Derfoul, A., Juan, A., Zare, H., Feng, X., Clermont, D., Koulnis, M., Gutierrez-Cruz, G., Fulco, M. and Sartorelli, V., 2015. The NAD+-dependent SIRT1 deacetylase translates a metabolic switch into regulatory epigenetics in skeletal muscle stem cells. *Cell stem cell*, *16*(2), pp.171-183.

Sabatino, A., Cuppari, L., Stenvinkel, P., Lindholm, B. and Avesani, C.M., 2021. Sarcopenia in chronic kidney disease: what have we learned so far?. *Journal of nephrology*, *34*(4), pp.1347-1372.

Sacheck, J.M., Ohtsuka, A., McLary, S.C. and Goldberg, A.L., 2004. IGF-I stimulates muscle growth by suppressing protein breakdown and expression of atrophy-related ubiquitin ligases, atrogin-1 and MuRF1. *American Journal of Physiology-Endocrinology and Metabolism*, *287*(4), pp.E591-E601.

Saini, K.S., Thompson, C., Winterford, C.M., Walker, N.I. and Cameron, D.P., 1996. Streptozotocin at low doses induces apoptosis and at high doses causes necrosis in a murine pancreatic ß cell line, INS-1. *IUBMB Life*, *39*(6), pp.1229-1236.

Saito, Y. and Chikenji, T.S., 2021. Diverse Roles of Cellular Senescence in Skeletal Muscle Inflammation, Regeneration, and Therapeutics. *Frontiers in Pharmacology*, p.2372.

Samluk, L., Urbanska, M., Kisielewska, K., Mohanraj, K., Kim, M.J., Machnicka, K., Liszewska, E., Jaworski, J. and Chacinska, A., 2019. Cytosolic translational responses differ under conditions of severe short-term and long-term mitochondrial stress. *Molecular biology of the cell*, *30*(15), pp.1864-1877.

Sanada, Y., Yamamoto, T., Satake, R., Yamashita, A., Kanai, S., Kato, N., Van De Loo, F.A., Nishimura, F., Scherer, P.E. and Yanaka, N., 2016. Serum amyloid A3 gene expression in adipocytes is an indicator of the interaction with macrophages. *Scientific reports*, *6*(1), pp.1-15.

Sanchez, A.M., Csibi, A., Raibon, A., Cornille, K., Gay, S., Bernardi, H. and Candau, R., 2012. AMPK promotes skeletal muscle autophagy through activation of forkhead FoxO3a and interaction with Ulk1. *Journal of cellular biochemistry*, *113*(2), pp.695-710.

Sandri, M., 2013. Protein breakdown in muscle wasting: role of autophagy-lysosome and ubiquitin-proteasome. *The international journal of biochemistry & cell biology*, *45*(10), pp.2121-2129.

Sandri, M., Sandri, C., Gilbert, A., Skurk, C., Calabria, E., Picard, A., Walsh, K., Schiaffino, S., Lecker, S.H. and Goldberg, A.L., 2004. Foxo transcription factors induce the atrophy-related ubiquitin ligase atrogin-1 and cause skeletal muscle atrophy. *Cell*, *117*(3), pp.399-412.

Santos, L. dos, Cyrino, E. S., Antunes, M., Santos, D. A., & Sardinha, L. B. (2017). Sarcopenia and physical independence in older adults: The independent and synergic role of muscle mass and muscle function. Journal of Cachexia, Sarcopenia and Muscle, 8(2), 245–250.

Sartori, R., Romanello, V. and Sandri, M., 2021. Mechanisms of muscle atrophy and hypertrophy: Implications in health and disease. *Nature communications*, *12*(1), pp.1-12.

Sato, A.Y., Richardson, D., Cregor, M., Davis, H.M., Au, E.D., McAndrews, K., Zimmers, T.A., Organ, J.M., Peacock, M., Plotkin, L.I. and Bellido, T., 2017. Glucocorticoids induce

bone and muscle atrophy by tissue-specific mechanisms upstream of E3 ubiquitin ligases. *Endocrinology*, *158*(3), pp.664-677.

Schakman, O., Gilson, H. and Thissen, J.P., 2008. Mechanisms of glucocorticoid-induced myopathy. *The Journal of endocrinology*, *197*(1), pp.1-10.

Schakman, O., Kalista, S., Barbé, C., Loumaye, A. and Thissen, J.P., 2013. Glucocorticoid-induced skeletal muscle atrophy. *The international journal of biochemistry & cell biology*, *45*(10), pp.2163-2172.

Scharner, J. and Zammit, P.S., 2011. The muscle satellite cell at 50: the formative years. *Skeletal muscle*, *1*(1), pp.1-13.

Schmidt, M., Schüler, S.C., Hüttner, S.S., von Eyss, B. and von Maltzahn, J., 2019. Adult stem cells at work: regenerating skeletal muscle. *Cellular and Molecular Life Sciences*, *76*(13), pp.2559-2570.

Seale, P., Sabourin, L.A., Girgis-Gabardo, A., Mansouri, A., Gruss, P. and Rudnicki, M.A., 2000. Pax7 is required for the specification of myogenic satellite cells. *Cell*, *102*(6), pp.777-786.

Seiden, D., 1976. A quantitative analysis of muscle cell changes in compensatory hypertrophy and work-induced hypertrophy. *American Journal of Anatomy*, *145*(4), pp.459-465.

Selby, N.M. and Taal, M.W., 2020. An updated overview of diabetic nephropathy: Diagnosis, prognosis, treatment goals and latest guidelines. *Diabetes, Obesity and Metabolism*, *22*, pp.3-15.

Severinsen, M.C.K. and Pedersen, B.K., 2020. Muscle–organ crosstalk: The emerging roles of myokines. *Endocrine reviews*, *41*(4), pp.594-609.

Shally, A. and McDonagh, B., 2020. The redox environment and mitochondrial dysfunction in age-related skeletal muscle atrophy. *Biogerontology*, *21*(4), pp.461-473.

Shimizu, N., Yoshikawa, N., Ito, N., Maruyama, T., Suzuki, Y., Takeda, S.I., Nakae, J., Tagata, Y., Nishitani, S., Takehana, K. and Sano, M., 2011. Crosstalk between glucocorticoid receptor and nutritional sensor mTOR in skeletal muscle. *Cell metabolism*, *13*(2), pp.170-182.

Shosha, E., Fouda, A.Y., Narayanan, S.P., Caldwell, R.W. and Caldwell, R.B., 2020. Is the arginase pathway a novel therapeutic avenue for diabetic retinopathy?. *Journal of clinical medicine*, *9*(2), p.425.

Smerdu, V.I.K.A., Karsch-Mizrachi, I.L.E.N.E., Campione, M.A.R.I.N.A., Leinwand, L.E.S.L.I.E. and Schiaffino, S.T.E.F.A.N.O., 1994. Type IIx myosin heavy chain transcripts

are expressed in type IIb fibers of human skeletal muscle. *American Journal of Physiology-Cell Physiology*, *267*(6), pp.C1723-C1728.

Smuder, A.J., Kavazis, A.N., Hudson, M.B., Nelson, W.B. and Powers, S.K., 2010. Oxidation enhances myofibrillar protein degradation via calpain and caspase-3. *Free Radical Biology and Medicine*, *49*(7), pp.1152-1160.

Smuder, A.J., Roberts, B.M., Wiggs, M.P., Kwon, O.S., Yoo, J.K., Christou, D.D., Fuller, D.D., Szeto, H.H. and Judge, A.R., 2020. Pharmacological targeting of mitochondrial function and reactive oxygen species production prevents colon 26 cancer-induced cardiorespiratory muscle weakness. *Oncotarget*, *11*(38), p.3502.

Son, J.W., Lee, S.S., Kim, S.R., Yoo, S.J., Cha, B.Y., Son, H.Y. and Cho, N.H., 2017. Low muscle mass and risk of type 2 diabetes in middle-aged and older adults: findings from the KoGES. *Diabetologia*, *60*(5), pp.865-872.

Sorić Hosman, I., Kos, I. and Lamot, L., 2021. Serum amyloid A in inflammatory rheumatic diseases: A compendious review of a renowned biomarker. *Frontiers in Immunology*, p.3952.

Sousa-Victor, P., Gutarra, S., Garcia-Prat, L., Rodriguez-Ubreva, J., Ortet, L., Ruiz-Bonilla, V., Jardi, M., Ballestar, E., Gonzalez, S., Serrano, A.L. and Perdiguero, E., 2014. Geriatric muscle stem cells switch reversible quiescence into senescence. *Nature*, *506*(7488), pp.316-321.

Stearns-Reider, K.M., D'Amore, A., Beezhold, K., Rothrauff, B., Cavalli, L., Wagner, W.R., Vorp, D.A., Tsamis, A., Shinde, S., Zhang, C. and Barchowsky, A., 2017. Aging of the skeletal muscle extracellular matrix drives a stem cell fibrogenic conversion. *Aging cell*, *16*(3), pp.518-528.

Stitt, T.N., Drujan, D., Clarke, B.A., Panaro, F., Timofeyva, Y., Kline, W.O., Gonzalez, M., Yancopoulos, G.D. and Glass, D.J., 2004. The IGF-1/PI3K/Akt pathway prevents expression of muscle atrophy-induced ubiquitin ligases by inhibiting FOXO transcription factors. *Molecular cell*, *14*(3), pp.395-403.

Su, C.H., Hsu, Y.C., Thangudu, S., Chen, W.Y., Huang, Y.T., Yu, C.C., Shih, Y.H., Wang, C.J. and Lin, C.L., 2021. Application of multiparametric MR imaging to predict the diversification of renal function in miR29a-mediated diabetic nephropathy. *Scientific reports*, *11*(1), pp.1-11.

Suetta, C., Hvid, L.G., Justesen, L., Christensen, U., Neergaard, K., Simonsen, L., Ortenblad, N., Magnusson, S.P., Kjaer, M. and Aagaard, P., 2009. Effects of aging on human skeletal muscle after immobilization and retraining. *Journal of applied physiology*, *107*(4), pp.1172-1180.

Sugihara, H., Teramoto, N., Yamanouchi, K., Matsuwaki, T. and Nishihara, M., 2018. Oxidative stress-mediated senescence in mesenchymal progenitor cells causes the loss of their fibro/adipogenic potential and abrogates myoblast fusion. *Aging (Albany NY)*, *10*(4), p.747.

Sun, H., Saeedi, P., Karuranga, S., Pinkepank, M., Ogurtsova, K., Duncan, B.B., Stein, C., Basit, A., Chan, J.C., Mbanya, J.C. and Pavkov, M.E., 2022. IDF Diabetes Atlas: Global, regional and country-level diabetes prevalence estimates for 2021 and projections for 2045. *Diabetes research and clinical practice*, *183*, p.109119.

Swain, M.S., Lystad, R.P., Henschke, N., Maher, C.G. and Kamper, S.J., 2016. Match injuries in amateur rugby union: a prospective cohort study-FICS Biennial Symposium Second Prize Research Award. *Chiropractic & manual therapies*, *24*(1), pp.1-8.

Szentesi, P., Csernoch, L., Dux, L. and Keller-Pintér, A., 2019. Changes in redox signaling in the skeletal muscle with aging. *Oxidative medicine and cellular longevity*, *2019*.

Taliento, A.E., Dallio, M., Federico, A., Prati, D. and Valenti, L., 2019. Novel insights into the genetic landscape of nonalcoholic fatty liver disease. *International journal of environmental research and public health*, *16*(15), p.2755.

Tan, B.H. and Fearon, K.C., 2008. Cachexia: prevalence and impact in medicine. *Current Opinion in Clinical Nutrition & Metabolic Care*, *11*(4), pp.400-407.

Tapscott, S.J., 2005. The circuitry of a master switch: Myod and the regulation of skeletal muscle gene transcription. 132, pp. 2685-2695

Targher, G., Corey, K.E., Byrne, C.D. and Roden, M., 2021. The complex link between NAFLD and type 2 diabetes mellitus—mechanisms and treatments. *Nature reviews Gastroenterology & hepatology*, *18*(9), pp.599-612.

Teng, S. and Huang, P., 2019. The effect of type 2 diabetes mellitus and obesity on muscle progenitor cell function. *Stem cell research & therapy*, *10*(1), pp.1-15.

Tesch, G.H. and Allen, T.J., 2007. Rodent models of streptozotocin-induced diabetic nephropathy (Methods in Renal Research). *Nephrology*, *12*(3), pp.261-266.

Tetri, L.H., Basaranoglu, M., Brunt, E.M., Yerian, L.M. and Neuschwander-Tetri, B.A., 2008. Severe NAFLD with hepatic necroinflammatory changes in mice fed trans fats and a high-fructose corn syrup equivalent. *American Journal of Physiology-Gastrointestinal and Liver Physiology*, *295*(5), pp.G987-G995.

Thaler, R., Sturmlechner, I., Spitzer, S., Riester, S.M., Rumpler, M., Zwerina, J., Klaushofer, K., Van Wijnen, A.J. and Varga, F., 2015. Acute-phase protein serum amyloid A3 is a novel

paracrine coupling factor that controls bone homeostasis. *The FASEB Journal*, *29*(4), pp.1344-1359.

Theret, M., Gsaier, L., Schaffer, B., Juban, G., Ben Larbi, S., Weiss-Gayet, M., Bultot, L., Collodet, C., Foretz, M., Desplanches, D. and Sanz, P., 2017. AMPK α1-LDH pathway regulates muscle stem cell self-renewal by controlling metabolic homeostasis. *The EMBO journal*, *36*(13), pp.1946-1962.

Thomas, M.C., Brownlee, M., Susztak, K., Sharma, K., Jandeleit-Dahm, K.A., Zoungas, S., Rossing, P., Groop, P.H. and Cooper, M.E., 2015. Diabetic kidney disease. *Nature reviews Disease primers*, *1*(1), pp.1-20.

Thomson, D.M., 2018. The role of AMPK in the regulation of skeletal muscle size, hypertrophy, and regeneration. *International journal of molecular sciences*, *19*(10), p.3125.

Tilg, H., Adolph, T.E., Dudek, M. and Knolle, P., 2021. Non-alcoholic fatty liver disease: the interplay between metabolism, microbes and immunity. *Nature Metabolism*, *3*(12), pp.1596-1607.

Tirado-Hurtado, I., Fajardo, W. and Pinto, J.A., 2018. DNA damage inducible transcript 4 gene: the switch of the metabolism as potential target in cancer. *Frontiers in oncology*, *8*, p.106.

Toth, M.J., Miller, M.S., VanBuren, P., Bedrin, N.G., LeWinter, M.M., Ades, P.A. and Palmer, B.M., 2012. Resistance training alters skeletal muscle structure and function in human heart failure: effects at the tissue, cellular and molecular levels. *The Journal of physiology*, *590*(5), pp.1243-1259.

Tranaeus, U., Heintz, E., Johnson, U., Forssblad, M. and Werner, S., 2017. Injuries in S wedish floorball: a cost analysis. *Scandinavian journal of medicine & science in sports*, *27*(5), pp.508-513.

Usui, H.K., Shikata, K., Sasaki, M., Okada, S., Matsuda, M., Shikata, Y., Ogawa, D., Kido, Y., Nagase, R., Yozai, K. and Ohga, S., 2007. Macrophage scavenger receptor-a–deficient mice are resistant against diabetic nephropathy through amelioration of microinflammation. *Diabetes*, *56*(2), pp.363-372.

van Lunteren, E., Moyer, M. and Spiegler, S., 2014. Alterations in lung gene expression in streptozotocin-induced diabetic rats. *BMC endocrine disorders*, *14*(1), pp.1-6.

VanDusen, K.W. and Larkin, L.M., 2015. Muscle–tendon interface. In *Regenerative engineering of musculoskeletal tissues and interfaces* (pp. 409-429). Woodhead Publishing.

VanWagner, L.B. and Rinella, M.E., 2016. Extrahepatic manifestations of nonalcoholic fatty liver disease. *Current hepatology reports*, *15*(2), pp.75-85.

Varga, T., Mounier, R., Patsalos, A., Gogolák, P., Peloquin, M., Horvath, A., Pap, A., Daniel, B., Nagy, G., Pintye, E. and Poliska, S., 2016. Macrophage PPARγ, a lipid activated transcription factor controls the growth factor GDF3 and skeletal muscle regeneration. *Immunity*, *45*(5), pp.1038-1051.

Vettor, R., Milan, G., Franzin, C., Sanna, M., De Coppi, P., Rizzuto, R. and Federspil, G., 2009. The origin of intermuscular adipose tissue and its pathophysiological implications. *American Journal of Physiology-Endocrinology and Metabolism*, *297*(5), pp.E987-E998.

Vignaud, A., Ramond, F., Hourde, C., Keller, A., Butler-Browne, G. and Ferry, A., 2007. Diabetes provides an unfavorable environment for muscle mass and function after muscle injury in mice. *Pathobiology*, *74*(5), pp.291-300.

von Maltzahn, J., Jones, A.E., Parks, R.J. and Rudnicki, M.A., 2013. Pax7 is critical for the normal function of satellite cells in adult skeletal muscle. *Proceedings of the National Academy of Sciences*, *110*(41), pp.16474-16479.

Wada, J., Zhang, H., Tsuchiyama, Y., Hiragushi, K., Hida, K., Shikata, K., Kanwar, Y.S. and Makino, H., 2001. Gene expression profile in streptozotocin-induced diabetic mice kidneys undergoing glomerulosclerosis. *Kidney international*, *59*(4), pp.1363-1373.

Waddell, D.S., Baehr, L.M., Van Den Brandt, J., Johnsen, S.A., Reichardt, H.M., Furlow, J.D. and Bodine, S.C., 2008. The glucocorticoid receptor and FOXO1 synergistically activate the skeletal muscle atrophy-associated MuRF1 gene. *American Journal of Physiology-Endocrinology and Metabolism*, *295*(4), pp.E785-E797.

Wang, M., Pu, D., Zhao, Y., Chen, J., Zhu, S., Lu, A., Liao, Z., Sun, Y. and Xiao, Q., 2020. Sulforaphane protects against skeletal muscle dysfunction in spontaneous type 2 diabetic db/db mice. *Life Sciences*, *255*, p.117823.

Wang, Y.X. and Rudnicki, M.A., 2012. Satellite cells, the engines of muscle repair. *Nature reviews Molecular cell biology*, *13*(2), pp.127-133.

Wasung, M.E., Chawla, L.S. and Madero, M., 2015. Biomarkers of renal function, which and when?. *Clinica chimica acta*, *438*, pp.350-357.

Wellen, K.E., Hatzivassiliou, G., Sachdeva, U.M., Bui, T.V., Cross, J.R. and Thompson, C.B., 2009. ATP-citrate lyase links cellular metabolism to histone acetylation. *Science*, *324*(5930), pp.1076-1080.

Wessels, J., Busse, A.C., Mahrt, J., Dullin, C., Grabbe, E. and Mueller, G.A., 2007. In vivo imaging in experimental preclinical tumor research–a review. *Cytometry Part A: the journal of the International Society for Analytical Cytology*, *71*(8), pp.542-549.

Wesson, D.E., Buysse, J.M. and Bushinsky, D.A., 2020. Mechanisms of metabolic acidosis–induced kidney injury in chronic kidney disease. *Journal of the American Society of Nephrology*, *31*(3), pp.469-482.

Wood, N., Straw, S., Scalabrin, M., Roberts, L.D., Witte, K.K. and Bowen, T.S., 2021. Skeletal muscle atrophy in heart failure with diabetes: from molecular mechanisms to clinical evidence. *ESC Heart Failure*, *8*(1), pp.3-15.

Wu, H., Liu, M., Chi, V.T.Q., Wang, J., Zhang, Q., Liu, L., Meng, G., Yao, Z., Bao, X., Gu, Y. and Zhang, S., 2019. Handgrip strength is inversely associated with metabolic syndrome and its separate components in middle aged and older adults: a large-scale population-based study. *Metabolism*, *93*, pp.61-67.

Xia, Q., Huang, X., Huang, J., Zheng, Y., March, M.E., Li, J. and Wei, Y., 2021. The role of autophagy in skeletal muscle diseases. *Frontiers in Physiology*, *12*.

Xu, Q., Li, B., Wang, Y., Wang, C., Feng, S., Xue, L., Chen, J. and Jiang, H., 2021. Identification of VCAN as hub gene for diabetic kidney disease immune injury using integrated bioinformatics analysis. *Frontiers in physiology*, *12*.

Yang, D., Elner, S.G., Bian, Z.M., Till, G.O., Petty, H.R. and Elner, V.M., 2007. Pro-inflammatory cytokines increase reactive oxygen species through mitochondria and NADPH oxidase in cultured RPE cells. *Experimental eye research*, *85*(4), pp.462-472.

Yang, H., Mammen, J., Wei, W., Menconi, M., Evenson, A., Fareed, M., Petkova, V. and Hasselgren, P.O., 2005. Expression and activity of C/EBPβ and δ are upregulated by dexamethasone in skeletal muscle. *Journal of cellular physiology*, *204*(1), pp.219-226.

Ye, L., Lee, K.O., Su, L.P., Toh, W.C., Haider, H.K., Law, P.K., Zhang, W., Chan, S.P. and Sim, E.K.W., 2009. Skeletal myoblast transplantation for attenuation of hyperglycaemia, hyperinsulinaemia and glucose intolerance in a mouse model of type 2 diabetes mellitus. *Diabetologia*, *52*(9), pp.1925-1934.

Ye, R.D. and Sun, L., 2015. Emerging functions of serum amyloid A in inflammation. *Journal of leukocyte biology*, *98*(6), pp.923-929.

Yoshida, T. and Delafontaine, P., 2015. Mechanisms of cachexia in chronic disease states. *The American journal of the medical sciences*, *350*(4), pp.250-256.

Zakrzewski, W., Dobrzyński, M., Szymonowicz, M. and Rybak, Z., 2019. Stem cells: past, present, and future. *Stem cell research & therapy*, *10*(1), pp.1-22.

Zammit, P.S., Heslop, L., Hudon, V., Rosenblatt, J.D., Tajbakhsh, S., Buckingham, M.E., Beauchamp, J.R. and Partridge, T.A., 2002. Kinetics of myoblast proliferation show that

resident satellite cells are competent to fully regenerate skeletal muscle fibers. *Experimental cell research*, *281*(1), pp.39-49.

Zhang, H., Ryu, D., Wu, Y., Gariani, K., Wang, X., Luan, P., D'Amico, D., Ropelle, E.R., Lutolf, M.P., Aebersold, R. and Schoonjans, K., 2016. NAD+ repletion improves mitochondrial and stem cell function and enhances life span in mice. *Science*, *352*(6292), pp.1436-1443.

Zhang, L., Chen, Q., Chen, Z., Wang, Y., Gamboa, J.L., Ikizler, T.A., Garibotto, G. and Mitch, W.E., 2020. Mechanisms regulating muscle protein synthesis in CKD. *Journal of the American Society of Nephrology*, *31*(11), pp.2573-2587.

Zhang, M., Lv, X.Y., Li, J., Xu, Z.G. and Chen, L., 2008. The characterization of high-fat diet and multiple low-dose streptozotocin induced type 2 diabetes rat model. *Experimental diabetes research*, *2008*.

Zhang, W., Liu, Y. and Zhang, H., 2021. Extracellular matrix: an important regulator of cell functions and skeletal muscle development. *Cell & bioscience*, *11*(1), pp.1-13.

Zhao, J., Brault, J.J., Schild, A., Cao, P., Sandri, M., Schiaffino, S., Lecker, S.H. and Goldberg, A.L., 2007. FoxO3 coordinately activates protein degradation by the autophagic/lysosomal and proteasomal pathways in atrophying muscle cells. *Cell metabolism*, *6*(6), pp.472-483.

Zheng, W., Guo, J. and Liu, Z.S., 2021. Effects of metabolic memory on inflammation and fibrosis associated with diabetic kidney disease: an epigenetic perspective. *Clinical epigenetics*, *13*(1), pp.1-16.

Zoja, C., Xinaris, C. and Macconi, D., 2020. Diabetic nephropathy: Novel molecular mechanisms and therapeutic targets. *Frontiers in Pharmacology*, p.2139.